Technical Report...

ADVANCED FERRIMAGNETIC MATERIALS APPLIED TO DIGITAL PHASE SHIFTERS

SECOND SEMIANNUAL REPORT

25 December 1964 to 25 June 1965

ARPA ORDER NO. 550
PROGRAM CODE NO. 4730

RADC CONTRACT NO. AF30(602)3490

Air Force Systems Command
Research and Technology Division
Rome Air Development Center
Griffiss Air Force Base, New York

Project Defender
Advanced Research Projects Agency (ARPA)
Department of Defense
Washington, D.C.

SPERRY

MICROWAVE ELECTRONICS COMPANY

CLEARWATER, FLORIDA

AD621136

TECHNICAL REPORT

ADVANCED FERRIMAGNETIC MATERIALS APPLIED

to

DIGITAL PHASE SHIFTERS

SECOND SEMIANNUAL REPORT

25 December 1964 to June 25, 1965

ARPA ORDER NO. 550

PROGRAM CODE NO. 4730

RADC CONTRACT NO. AF30(602)3490

Prepared for:

Air Force Systems Command
Research and Technology Division
Rome Air Development Center
Griffiss Air Force Base, New York

and

Project Defender
Advanced Research Projects Agency (ARPA)
Department of Defense
Washington D.C.

Title of Work: Investigation directed toward the improvement and
evaluation of ferrimagnetic materials for use in
microwave digital phase shifters at L-, S-, C-,
and X-bands.

August 1965

SPERRY MICROWAVE ELECTRONICS COMPANY
DIVISION OF SPERRY RAND CORPORATION
CLEARWATER, FLORIDA

SJ. M 220-0052-6   Copy No. 3

BLANK PAGE

TABLE OF CONTENTS

LIST OF ILLUSTRATIONS

LIST OF TABLES

1. SYNOPSIS

This is the Second Semiannual Report on this program.

A resume is presented outlining the present status of ferrite digital phase shifters including the interpretation of the influence of material characteristics on the operating dynamics of phase shifters. The importance and influence of the following material parameters are discussed: saturation magnetization, remanent magnetization, linewidth, remanence ratio, squareness, coercive field, density, grain size, dielectric constant, dielectric loss tangent, anisotropy field, peak power threshold, switching coefficient, and magnetostriction.

The experimental investigations have concentrated on the study of the control and variation of the above parameters and the evaluation of materials with known properties in rf structures.

Magnetic losses are discussed from an analytical and experimental standpoint. Investigations on magnetic losses have been conducted at S-band, and a preliminary interpretation of the data is presented.

Structural and material parameter studies have been carried out in an X-band waveguide phase shifter structure. The results of these studies are presented together with some comparison, where possible, with recent theoretical publications.

2. INTRODUCTION

2.1 BACKGROUND OF PROGRAM

Investigators in the field of microwave devices have attempted for several years to derive high performance, low cost, fast acting components which require low switching and holding power for fast scanning array applications. The development of microwave devices utilizing the square hysteresis loop properties of ferrimagnetic materials seems to be a very promising approach toward these components. These fast switching microwave devices require toroidal material geometries with the cores magnetized circumferentially. The toroidal materials are to possess excellent microwave characteristics as well as square hysteresis loops; that is, large values of remanent magnetization and low coercive fields.

One fast switching device in this category is the ferrite digital phase shifter. These devices utilize toroidal cores for phase shifting elements and are switched in very much the same fashion as computer cores. The operating characteristics of these digital phase shifters depend to a great extent on the properties and availability of acceptable ferrimagnetic materials. While the structural configurations of the rf portion of the phase shifter are still under development and many new configurations are constantly being generated, in most every case the properties of the desired ferrimagnetic materials are quite similar. Therefore, it is very important to have a number of very suitable and optimized materials for utilization in these phase shifters. It is the purpose of this program to derive a number of optimized materials for utilization in digital phase shifters operating from L through X band and to further demonstrate their usefulness by evaluation in rf structures.

2.2 PROGRAM OBJECTIVES

The objectives of this program are directed toward the improvement and evaluation of ferrite and garnet materials for use in digital phase shifters at L, S, C and X bands. Emphasis is to be placed on peak power capability exceeding 10 kilowatts and phase stability with temperature variation over the military range. Microwave digital phase shifter structures will be studied with special emphasis placed upon the materials derived in this program combined with the requirements for high switching speed, low switching power, low loss, low holding power, compact configurations, low cost per unit and high peak and average power handling capabilities. Eighty percent of the effort will be directed toward the materials study and evaluation.

BLANK PAGE

3. OPERATING DYNAMICS OF FERRITE DIGITAL PHASE SHIFTERS

3.1 GENERAL

The technology and understanding of the operating dynamics (including the influences of ferrimagnetic material parameters) of microwave ferrite digital phase shifters (FDPS) are advancing at a reasonably rapid pace. During this six months reporting period, considerable technical information has been generated both on this program and by other investigators studying ferrite digital phase shifters.

It is the purpose of this section of the report to present a resume of the present status of the understanding of the operating dynamics of FDPS. In this section information reported by others (with appropriate references) will be interwoven and interpreted with the information generated on this program since its inception. A review of the conclusions presented in the First Semi-Annual Report are in some instances repeated for completeness.

3.2 BASIC CONCEPT OF FERRITE DIGITAL PHASE SHIFTERS

The ferrite[*] digital phase shifter (FDPS) is a device which requires toroidal material geometries (cores or tubes). The toroids are magnetized circumferentially.

It is not required that the toroidal core be completely immersed in the rf field ("core" formed entirely from microwave ferrite material). Recent investigations[1] have shown that the toroid may be formed from a composite of material (microwave material inside rf structure with flux paths closed outside the area containing rf fields with computer type material).

Ferrimagnetic digital phase shifters make use of several of these toroidal "cores" of ferrimagnetic material installed along the longitudinal axis of rectangular waveguide or coax transmission line. The location is such as to cause the propagating waves to be coupled to the cores in a reciprocal or nonreciprocal manner. The toroidal cores are composed of a very high performance microwave material (at least that portion interacting with the rf field) and, to achieve reasonable digital action, must exhibit a square or near square hysteresis loop. The two remanent states of magnetization are the normal operating positions. In the digital phase shifter design, each core is supplied with a circumferential applied magnetic field which is used to switch the toroid magnetization. The difference in permeability of the two remanent states of magnetization yields a differential phase shift proportional to the core lengths and the material properties.

[*] The word "Ferrite" is used in this report to represent any ferrimagnetic material.
[1] E. Stern and W. J. Ince, "Composite Loop Phase Shifter" (To be published).

The lengths of the cores are selected in accordance with digit requirements; for example, with 360° of phase shift required, one core or tube each may be provided to yield 180°, 90°, 45°, 22.5°, 11.25° and 5.625°. The result will be a phase shifter capable of exhibiting any differential phase shift from 0° to 360° in 5.625° steps. Common terminology is to call this phase shifter a six-digit or six-bit phase shifter.

For nonreciprocal phase shifters the structure is such that a portion of a magnetized toroid will see a circular (or elliptical) polarized rf magnetic field of one sense (positive or negative) for one direction of magnetization. Switching the direction of magnetization in the toroid reverses the sense of the circular polarized icident rf magnetic field and thus produces a differential phase shift. Accordingly, for one direction of magnetization of any given toroid, a prescribed phase shift will be obtained and, for the opposite direction, a different value will be evident. The lower value can be used as a "zero" base. Since the toroidal core exhibits a nearly square hysteresis loop, a current pulse (large enough to produce a magnetic field somewhat greater than the coercive field of the material) is used to switch the magnetization after which the magnetization falls into the remanent state and holds (no holding current is required). The circumferential switching field is generated by passing a current pulse through a turn of wire which threads the core.

The material characteristics for reciprocal operation are essentially identical to the nonreciprocal case.

The operating characteristics of the FDPS are heavily dependent on the properties of the ferrimagnetic material utilized as detailed in the following sections.

3.3 MATERIAL ASPECTS OF FERRITE DIGITAL PHASE SHIFTERS

No attempt will be made to present a rigorous mathematical interpretation of the interaction characteristics of ferrimagnetic toroidal materials and rf signals. A physical interpretation will be presented to indicate the mechanisms involved.

In an unmagnetized domain-filled ferrimagnetic material (bulk sample), so-called "low field" magnetic losses* have been predicted and experimentally verified to be present out to a maximum frequency given by

$$\omega_{max} = \gamma \left[H_{anis} + 4\pi M_s \right] \qquad (1)$$

---

* A more specific discussion of magnetic loss is included in Section 3.3.3.

where

ω_{max} = maximum frequency (mHz) for low field magnetic losses (no applied fie'd)

γ = gyromagnetic ratio (mHz/oersted)

$\gamma \approx 2.8$ mHz/oersted for most materials

H_{anis} = anisotropy field (oersteds) of the material

$4\pi M_s$ = saturation magnetization (gauss) of the material

This equation has been derived by consideration of the possible internal demagnetizing field [2] of an array of magnetic domains and from Kittel's resonance equation [3]. This relationship indicates that resonance losses in the absence of an applied field (unmagnetized sample) will be observed to a maximum frequency as predicted by equation (1).

For toroidal geometr'es where a material possesses an appreciable remanence ratio (remanent magnetization of 0.5 to 0.7 of the saturation magnetization), the material will contain a few large domains and some smaller domains in unmagnetized parts of the toroid. In this situation there is no applied field in accordance with the case of low field losses discussed above. If an rf field perpendicular to the magnetization is applied the broad distribution of magnetic loss (curve A of Figure 1) is confined to a resonance peak* similar to that shown in curve B. This type of response is caused by ferrimagnetic
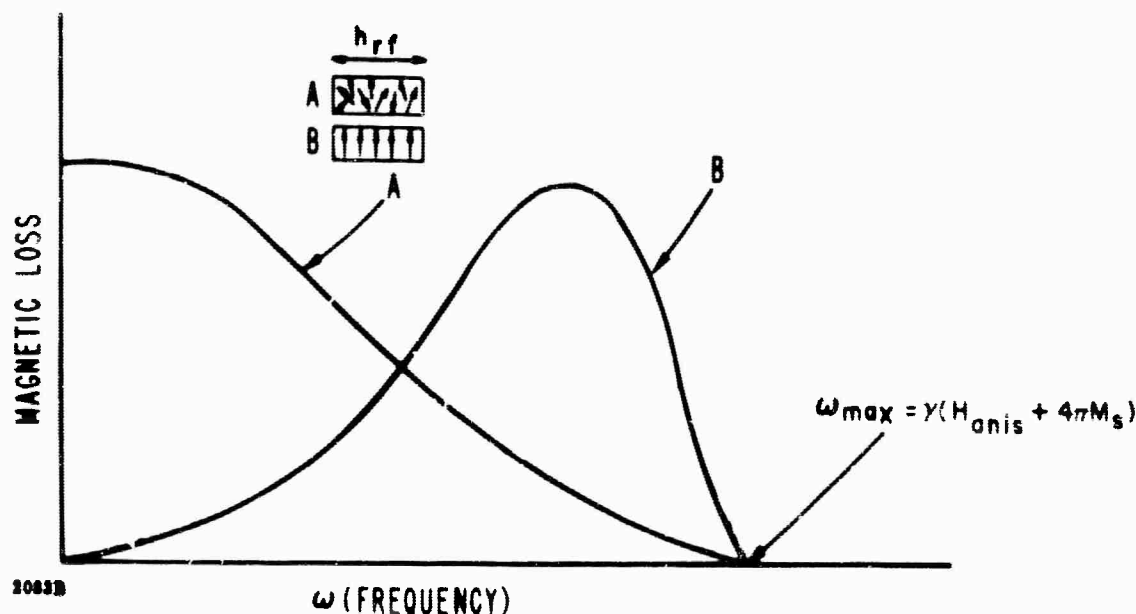
Figure 1. Low Field Losses in Ferrimagnetic Materials

---

[2] D. Polder and J. Smit, "Resonance Phenomena in Ferrites," Rev. Modern Phys., 25, 89 (1953).

[3] B. Lax and K. J. Button, Microwave Ferrites and Ferrimagnetics, McGraw-Hill Book Company, New York, 1962, pp. 444-450.

* The resonance aspects will be discussed in greater detail in Section 3.3.3.

resonance of the various domains and should obey established permeability relationships for ferrimagnetic materials at microwave frequencies. These relations should be entirely similar to those of the usual saturated ferrite body, since this usual case corresponds to the action of a single domain.

Experimental results indicate[4] that the following equation can be used to approximate the resonance frequency observed for toroidal geometries normally employed in ferrite digital phase shifters:

$$\omega \approx \gamma 4\pi M_R \tag{2}$$

This relationship is important to the design of phase shifters. The phase shift is proportional to the magnetization but, as indicated here, so are the magnetic losses. Therefore, the magnetization chosen for a given frequency must produce ample phase shift per unit length and also place the point of operation out of the magnetic loss region as predicted by equations (1) and (2). For a given frequency of operation, ω, the value of $4\pi M_s$ utilized in FDPS is generally such that $1/3 < \dfrac{\gamma 4\pi M_s}{\omega} < 3/4$. This minimizes the magnetic losses present at the operating frequency. The value of the magnetization of the material determines the point of operation in these devices in a fashion similar to the dc applied magnetic field for normal ferrite devices.

The values of the remanent and saturated magnetization are therefore very important to the choice of a material for FDPS.

The value of the remanence ratio $\left(R_R = \dfrac{4\pi M_R}{4\pi M_s}\right)$ indicates the degree of unfavorably oriented domains and to this extent affects the shape and width of the resonance absorption curve. High remanence ratio will better confine the absorption peak such as curve B in Figure 1; low remanence ratio will produce more reciprocal absorption, and shift the resonance peak (see Section 3.3.3).

This brings up the question of the importance of ferromagnetic resonance linewidth to the operation of digital phase shifters. The linewidth is normally measured on spherical samples with an applied field in accordance with the equation

$$\omega = \gamma H_{app} \tag{3}$$

where H_{app} is the applied dc magnetic field in oersteds.

---

[4] B. N. Enander, "A New Ferrite Isolator", Proceedings of the IRE 4.4, 1421 (October, 1956).

3-4

The resonance loss characteristics of a remanent toroid are without doubt much broader than those measured on a uniformly magnetized sphere. The normally measured linewidths on spheres will influence the selection of materials for application in digital phase shifters. Experimental evidence indicates that the width of the resonance absorption of a material in the remanent state (toroidal geometry) is dependent on the remanence ratio of the material and thus the sample shape.[*] The criterion for linewidth selection should therefore be "a minimum measured linewidth (as per equation (3))consistent with a maximum remanence ratio for the $4\pi M_s$ desired." Linewidth values are of primary concern for low frequency applications where line broadening can contribute to magnetic losses at the operating frequency. Linewidths generally increase with decreasing temperature; therefore, at low temperatures linewidth broadening could contribute magnetic losses at the operating point. Additional analyses and experimental verifications must be performed to specify optimized materials as far as linewidth is concerned.

Other material parameters which must be discussed in regard to FDPS are dielectric constant, dielectric loss tangent, coercive fields, density, grain size and peak power thresholds.

Dielectric loss tangents of acceptable materials should be as low as possible. Values in the range of 0.0001 or less as measured at X band are desirable.

Dielectric constants of most any value are acceptable but should be reproducible to ± 0.1 of the measured values. The dielectric constant of the material will affect the structural configuration and the match of the phase shifter. In most configurations the higher the dielectric constant, the greater will be the differential phase shift per unit length. Any variation in dielectric constant will affect the length of material required to achieve a given phase shift, and this variation should be kept to a minimum.

Each of these material parameters will be discussed in later sections.

3.3.1 Remanent Magnetization

The most important parameter related to the hysteresis loop is the remanent magnetization. As mentioned previously, the magnetic losses and phase shift per unit length are related directly to this parameter.

---

[*] Discussed in more detail in Section 3.3.3 .

Most microwave materials cannot be driven into saturation using the nominal drive fields (approximately 25 oersteds maximum) available on square loop testers using nominal size probes or turns of wire.

The hysteresis loop normally observed is therefore not the saturated loop but is, in general, very representative of the hysteresis loop utilized in digital phase shifter operation. To classify and optimize materials, it is necessary to measure the absolute value of the remanent magnetization at the drive fields normally used in digital phase shifters. It is desirable that the above drive field be as low as possible consistent with near maximum values of the remanent magnetization.

To classify and evaluate materials the following procedure appears adequate:
1. The $4\pi M_s$ of the material should be measured, in general, independent of the hysteresis loop at applied fields greatly exceeding that required for saturation. $4\pi M_s$ values measured on this program were obtained from a vibrating sample magnetometer using spherical samples (approximately 50 mils in diameter) and applied fields greater than 5 Koe. Other equipment can be used where magnetometers are not available.
2. The hysteresis loop should be observed at the drive fields available. The drive fields should be, where possible, ten times the coercive field of the material. For most toroidal geometries, the remanent magnetization has been observed to change very little between drive fields of 8 to 10 times the coercive field of the material. From the hysteresis loop, the "squareness" and coercive field can be measured. The "squareness" is defined as

$$S_D = \frac{4\pi M_{RD}}{4\pi M_D} \tag{4}$$

where S_D is the "squareness", $4\pi M_{RD}$ is the remanent magnetization for the drive field used, and $4\pi M_D$ is the magnetization at the peak of the drive field. The $4\pi M_D$ can be measured as follows:

If the core reverses an amount of flux $\Delta\phi$ in a time Δt, the average voltage V produced during switching is

$$\langle V \rangle = N \frac{\Delta\phi}{\Delta t} \tag{5}$$

where N is the number of turns threading the core. If A is the cross-sectional area of the core and B_D is the change in flux intensity at the drive field used,

$$\Delta\phi = A \, \Delta B_D, \tag{6}$$

and

$$\Delta B_D \doteq \Delta(4\pi M_D) \tag{7}$$

3-6

for the low drive fields used for toroidal geometries. Therefore

$$\Delta\phi = A \, \Delta(4\pi M_D), \tag{8}$$

and

$$(4\pi M_D) = \frac{<V>\Delta t}{A\,N} . \tag{9}$$

Using proper integrating circuits and known values of A and N, $\Delta(4\pi M_D)$ can be measured (see Figure 2 for interpretation of $\Delta(4\pi M_D)$. It is recommended that cali- bration sample (s) be used for ease in the measurement and use of $<V>\Delta t$.

3. With the measured value of "squareness" and $4\pi M_D$, the $4\pi M_{RD}$ can be computed. For drive fields of eight to ten times the coercive field of the material,

$$4\pi M_{RD} \doteq 4\pi M_R \tag{10}$$

for most materials. If desired, the remanence ratio of material may then be computed as

$$R_R = \frac{4\pi M_R}{4\pi M_S} \tag{11}$$

It has been experimentally noted that values of "squareness" as defined, cannot be used to properly classify materials. Since the shape of the saturated hysteresis loop changes with toroid shape and is affected by strains and stresses in the material, the "squareness" of materials, with identical composition and $4\pi M_S$ values, may be equal but the values of $4\pi M_D$ and $4\pi M_{RD}$ for these materials at known drive fields could be quite different. In some instances, materials have been noted to possess higher values of "squareness" but comparative lower values of remanent magnetization.[5]

Typical values of "squareness" for the better materials are in the 0.85 to 0.95 region and typical values of remanence ratio for these same materials are in the 0.6 to 0.80 region.

For optimized digital phase shifter materials, it is desired that the remanence ratio be as high as possible and that the $4\pi M_R$ of the material be temperature stable where possible The remanent magnetization of materials has been observed, in general, to exhibit temperature characteristics similar to that of the $4\pi M_S$ of the material.[5]

5 Third Quarterly Report on Microwave Phase Shifters for Inertialess Scanning (Non Reciprocal).
   Westinghouse report on Contract DA-28-043-AMC-00228(E), sponsored by USAECOM,
   Fort. Monmouth, New Jersey. p. 4-15 (April, 1965).
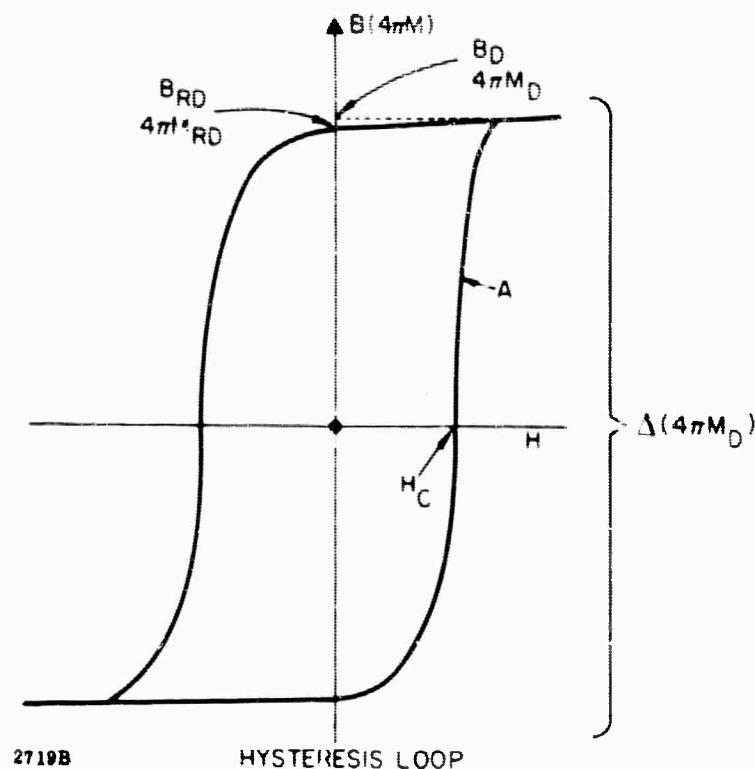
Figure 2. Hysteresis Loop of Ferrimagnetic Materials

In a polycrystalline ferrite or garnet, the intrinsic magnetization in the indi-
vidual crystals (cubic) prefers to be in the so called easy direction. The easy directions
are determined by the magnetocrystalline anistropy, the stress anisotropy (magneto-
striction), and the shape anisotropy. If such a material has only magnetocrystalline
anisotropy, the remanence ratio can be calculated to be 0.87. This result assumes that
in the saturated state the magnetization in all crystals is parallel to the applied field
and relaxes to the nearest easy direction (this direction is along the body diagonal, a
$<111>$ axis in cubic materials with negative anistropy) when the field is removed. This
ideal value sometimes is difficult to obtain because of the unfavorable contributions of
the other anisotropies.

A unidirectional anisotropy can sometimes be built into the material by con-
trolling the stress and shape of the material, thus producing higher values of the re-
manence ratio. Quenching, lattice deformations, applied pressure, etc., are tech-
niques sometimes used.[6]

6 J. B. Birks and J. Hart, Progress in Dielectrics, Vol. 5, Academic Press Inc., Publishers,
   New York, 1963. (H. P. Peloschek, "Square Loop Ferrites and Their Applications", pp 37-93).

3-8

High remanence ratios can be obtained if the magnetocrystalline anisotropy is large in comparison to the other anisotropies. This implies low magnetostriction, low unfavorable internal stresses, and a dense homogeneous material (high density).

In microwave applications the resonance linewidth and shape which are dependent on the remanence ratio will be most favorable and applicable for those materials possessing high remanence ratios.

The remanence ratio depends primarily on the composition, method of preparation, grain size, and homogeneity of the material[6].

3.3.2 Coercive Force

The coercive force (H_c) of the material is another very important parameter of the hysteresis loop (see Figure 2). Acceptable materials for most applications demand low coercive fields to minimize power consumption. For low coercive force, a dense, chemically and structurally homogeneous material is required with anisotropy fields as low as possible. The coercive force seems most greatly affected by composition, grain size and porosity.

3.3.3 Magnetic Loss in Toroidal Ferrites

More complete analysis and interpretation of magnetic loss in ferrite toroids have been pursued to establish possible operating regions for ferrite digital phase shifters. Involved in this effort is the study of the ultimate limits which magnetic losses place on the saturation magnetization of ferrite materials used in FDPS in various frequency bands, as well as the possible influence of toroid geometry.

The magnetic loss referred to here is believed to be the result of resonance in the various magnetic domains of the toroid. Magnetic loss can be associated with domain wall motion or rotation of the magnetization within domains. Since domain wall motion relaxes well below the microwave frequency range[7], the overall magnetic loss of the sample is a result of losses associated with rotation of the magnetization in each domain. This rotational resonance corresponds to gyromagnetic resonance of the magnetization in the effective field of each specific domain. Remanent ferrite toroids are never completely saturated and always possess a number of magnetic domains. Each domain may have different demagnetizing factors, and in each domain the magnetization will exhibit resonant precession at a characteristic frequency determined by the anisotropy field of the material and these demagnetizing fields. When the applied frequency is equal to this frequency, resonance losses will be observed.

---

[7] Rado, Wright, and Emerson. Phys Rev. 80, 273 (1950).

Thus, depending on the geometry of a given domain, its resonant frequency should vary between rather large limits. It is well known that in the case of adjacent antiparallel domains there is a doubling effect of the demagnetizing factors or depolarizing fields as first discussed by Polder and Smit.[?] In the case of complete antiparallel alignment of magnetizations of adjacent domains, the resonant frequency approaches $\gamma 4\pi M_s$ (See Equation 1). Since there is no applied field in ferrite materials operating in the remanent state, the effective field (or the resonant frequency) of the individual domains will be determined by the demagnetizing factors for the particular domain in question and by the anisotropy field of the material. Some limits on the possible frequencies where resonance loss can occur can be postulated. The highest resonance frequency that one could justify in the present model would be a frequency of

$$\omega_{max} = \gamma\left(\frac{4}{3}\ \frac{K_1}{M_s} + 4\pi M_s\right) \tag{12}$$

where K_1 is the first order magnetocrystalline anisotropy constant, and it is assumed in this situation that in each domain the magnetization lies along an easy direction. In any practical case, the peak loss will occur at frequencies below ω_{max}, since this is a limiting value requiring completely antiparallel domains, and a remanent magnetization of zero. Some resonance loss would in all probability extend up to this frequency since some domains may have the proper configuration to experience this relatively high frequency resonance.

Based on this domain model, the major resonance peak will be determined by the effective field of the largest domains, and the major domains should be related to the overall sample dimensions. That is, a long toroid should have a different resonance frequency from a short toroid because of the different demagnetizing factors of the two samples. Some detailed analytical work has been carried out in this area by Davis[*] who predicts that the resonant frequency should vary from approximately $\frac{\gamma 4\pi M_s}{4}$ for a long, thin toroid to approximately $\frac{\gamma 4\pi M_s}{2}$ for a short toroid. Davis' analysis neglects the contribution of anisotropy fields and the effects of neighboring antiparallel domains. Both of these factors will, in any practical case, increase the resonant frequency, and thus his theory can be expected to predict lower resonant frequencies than are found experimentally. The trend predicted by Davis, however, should hold true, and some correlation should be found between toroid dimensions and the frequency at which peak loss occurs.

[*] L. E. Davis, "Permability of Toroids in Latching Ferrite Devices", to be published.

In a much simplified form (neglecting damping) the peak loss should occur at a frequency given by Kittel's equation with appropriate demagnetizing factors inserted for the legs of the toroid. Since no applied field is present this equation becomes:

$$\omega_{res} = \gamma \left\{ \left[(N_x + N_x^a - N_z) \, 4\pi M_s \right] \left[(N_y + N_y^a - N_z) \, 4\pi M_s \right] \right\}^{\frac{1}{2}} , \qquad (13)$$

where N_x^a, N_y^a are the effective demagnetizing factors arising from anisotropy effects and are given by:

$$N_x^a = \frac{K_1}{4\pi M_s^2} \left[2 - \sin^2\theta - 3\sin^2 2\theta \right] \qquad (14)$$

$$N_y^a = \frac{2K_1}{4\pi M_s^2} \left[1 - 2\sin^2\theta - \frac{3}{8}\sin^2 2\theta \right]. \qquad (15)$$

Here θ is the angle the magnetization makes with a <100> direction of the crystallites, as measured in a {110} plane. If the magnetization is assumed to lie along the easy direction of a negative anisotropy material, the resonance equation reduces to:

$$\omega_{res} = \gamma \left\{ \left(-\frac{4}{3} \frac{K_1}{M} + N_x \, 4\pi M_s \right) \left(\frac{4}{3} \frac{K_1}{M} + N_y \, 4\pi M_s \right) \right\}^{\frac{1}{2}} , \qquad (16)$$

where N_z has been set equal to zero in accordance with the toroidal geometry.

For a typical garnet toroid with $\frac{K_1}{M_s} \doteq 40$ oe, $4\pi M_s = 1780$ gauss, and a length to width ratio of 10 to 1 for the toroid legs, the resonance frequency becomes:

$$\omega_{res} = \gamma \sqrt{(53 + 176)(53 + 1600)}$$

$$\omega_{res} = 1730 \text{ Mc}.$$

For a short toroid with $N_x = N_y \doteq 0.5$,

$$\omega_{res} = \gamma(53 + 890) = 2640 \text{ Mc}.$$

Both calculations above assume the material to be completely saturated in the remanent state. In any practical case the remanent state does not correspond to complete saturation, but rather the toroid will contain appreciable volumes of unfavorably oriented domains. The effect of these unfavorably oriented domains is to increase the effective demagnetizing fields in accordance with the Polder-Smit[2] arguments. Thus the peak

resonance loss will be shifted to higher frequencies because of the increased depolar-
i   σ fields at the domain walls.

This upward shift is not calculable because of the complexities of the domain
pattern. However, the general trends or effects can be interpreted. The more highly
saturated the material, the less important will be these multi-domain effects and the
lower will be the resonant frequency. The peak loss frequency should approach that
predicted by Davis or equation (16) above as complete saturation is reached. Con-
versely, as the domain pattern approaches complete antiparallelism, or the remanent
magnetization approaches zero, the peak loss frequency should approach $\gamma 4\pi M_s$ since
the Polder-Smit mechanism is then of over-riding importance.

The practical implications of this argument might perhaps be clarified with
the aid of the sketch of Figure 3. Here is depicted the overall loss of the toroid as
the summation of losses of different magnetic domains. The major domains (denoted
 A in Figure 3) have demagnetizing factors reflecting the overall toroidal geometry.
The loss in the region labeled B arises from minor domains in unsaturated regions of
the toroid (corners, etc.). The resonant frequencies of these domains extend up to a
maximum of $\omega_{max} = \gamma\left(\dfrac{4}{3}\ \dfrac{K_1}{M_s} + 4\pi M_s\right)$ since they are principally influenced by
neighboring anti-parallel domains and not the overall toroidal geometry. The resonant
frequencies of the major domains does, however, depend on sample geometry, and
this peak should shift toward higher frequencies as the toroid is made shorter. Thus
Figure 3a is a sketch of the loss curve for a long thin toroid, while 3b sketches the
loss curve expected for a shorter, nearly square toroid.

Some experimental results undertaken to better understand the loss mechanisms
are reported in the experimental data section of this report and tend to support the do-
main model discussed here. Other aspects or predictions of this model are as yet un-
tested and require further experimental work.
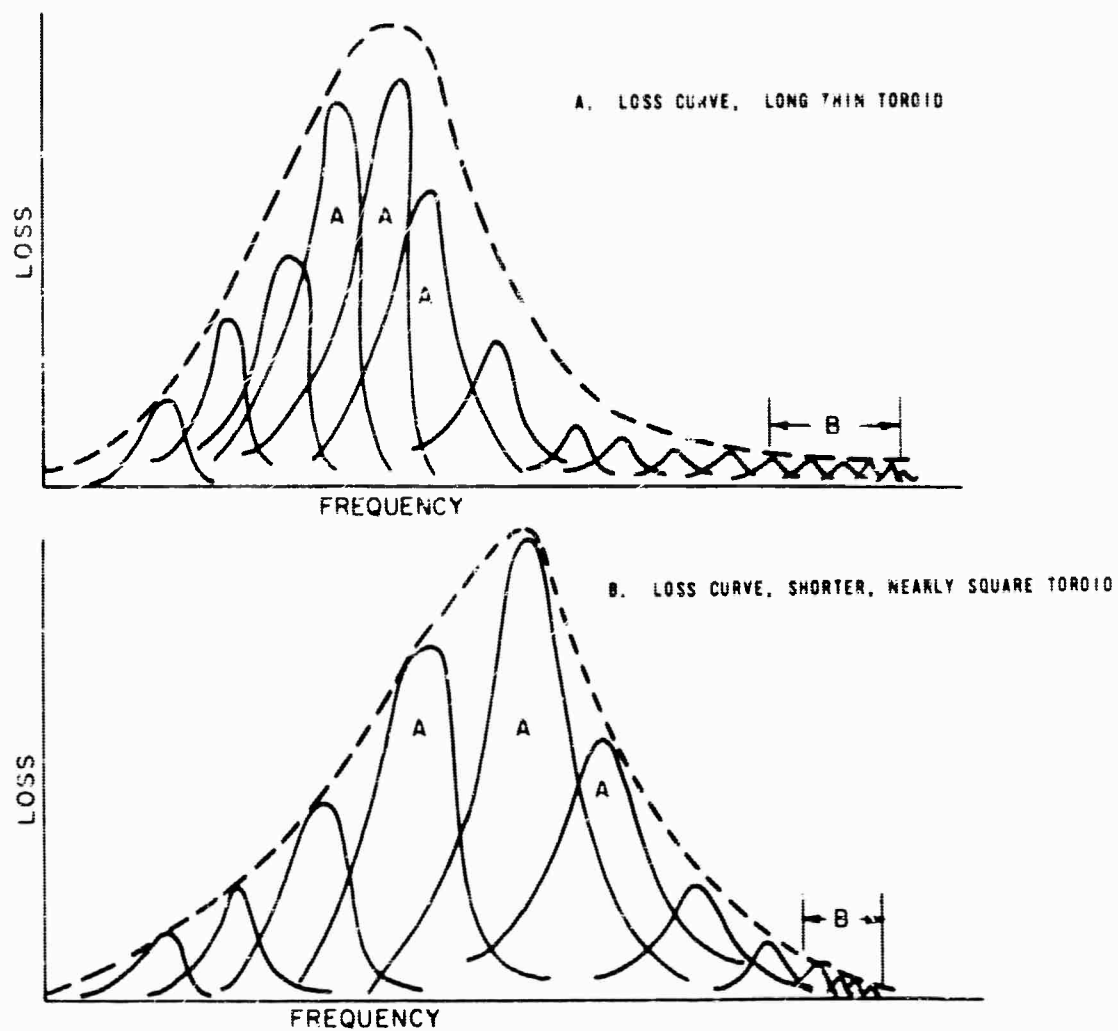
Figure 3. Overall Loss of Toroidal Geometry Depicted as Composed of discrete Loss Peak from Different Magnetic Domains

2721B

To be sure, the peak loss is of little interest in the operation of FDPS since one must operate quite far from this region. However, by more fully understanding the loss mechanisms, better control of these losses can be anticipated. Some observations that can be drawn from this model are discussed below.

1. The highest resonant frequency for a domain in a remanent toroid is, according to this domain model, given by

$$\omega_{max} = \gamma\left(\frac{4}{3}\ \frac{K_1}{M_s} + 4\pi M_s\right).$$ (17)

   This is not necessarily the highest frequency at which losses can occur since the linewidth of the material may be broad enough to extend these losses to somewhat higher frequencies. Figure 4 illustrates quite simply how a material with a broader linewidth may have magnetic losses extending to higher frequencies than a material with narrow linewidth even though both have the same upper limit on resonant frequency. The extent to which line-width influences the upper limit of magnetic loss is yet to be determined. The importance of these linewidth effects will depend on the volume of the high frequency domains and hence on the ratio, $4\pi M_r/4\pi M_s$.

2. If the material were completely saturated, then the entire sample would resonate at a frequency given by Equation (16). There would be no multidomain pattern and resonant frequencies would not extend up to ω_{max}. The width of the resonance loss curve would depend only on linewidth as in the more conventional devices. Thus, in order to confine resonance loss and therefore to use a larger magnetization in any given frequency band without incurring loss, one must strive for higher remanent magnetizations, approaching the saturation magnetization. This is particularly important in low frequency work where the avoidance of magnetic loss now dictates that values of magnetization well below that given by ω/γ must be used. The use of such low magnetizations then leads to very little differential phase shift per unit length. If the resonance losses were all confined to a narrow region of frequencies given by Equation 16, then appreciably larger magnetization could be used and operation nearer the resonance of the major domain could be employed, thus providing much larger phase shift per unit length.

3. If short toroids of material are used, Davis' calculations indicate that the resonant frequency should occur at a frequency near

$$\omega = \gamma\left(\frac{4}{3}\ \frac{K_1}{M} + 2\pi M_s\right).$$

Moreover, if the linewidth of the material is narrow and the remanence high, it may be possible to operate at low microwave frequencies with the material effectively biased above resonance, and thereby use toroids with large values of $4\pi M_S$, and thus larger values of phase shift per unit length. Above resonance operation would, however, carry with it the usual problems of greater frequency dependence, etc.

4. Loss mechanisms depend on the saturation magnetization of the material, since loss in each domain is additive. Phase shift is, however, proportional to the remanent magnetization. The phase shift produced by the various domains may cancel one another, and thus only the net remanent magnetization is important in determining the differential phase shift. To obtain maximum differential phase shift per unit loss then it is very important to maximize the ratio of remanent to saturation magnetization.

5. These observations all point out the importance of maximizing the ratio of $4\pi M_R / 4\pi M_S$. In addition to ceramic techniques two possible means of achieving increased ratios of $4\pi M_R / 4\pi M_S$ can be suggested. One possibility involves the use of grain oriented ferrites[9] with easy directions of magnetization circumferential about the toroid. A second possible improvement would be the use of toroid geometries that eliminate the unmagnetized regions at corners, etc. Ince and Stern[10] have employed a "corner correction factor" in their calculations that is empirically derived to account for the fact that some regions of the toroid contribute nothing to differential phase shift. Since these regions do contribute to loss (and are probably a severe limitation on low frequency operation), they should be eliminated.

Finally, it may be pointed out that high power or nonlinear effects also occur on a domain by domain basis and thus the domain model outlined above can be introduced into the spin wave model presented in the First Semi-Annual Report to obtain a more meaningful interpretation of the effective field than the $4\pi M_S$ assumed in that discussion. This treatment modified by the above domain considerations will be discussed in a later section of this report. The general conclusions are unaffected, and the acceptable limits on the allowable magnetization are relaxed slightly. Ultimately, of course, these limits are set in any particular case by the allowable loss in the specific device.

---

[9]Sperry Microwave Electronics Company final reports on Rome Air Development Center Contract No. AF30(602)-2757 and U. S. Army Electronics Laboratory Contract No. DA-36-039-SC89214.

[10]W. Ince and E. Stern, "Waveguide Non-Reciprocal Remanence Phase Shifters," paper to be presented at London Conference on Magnetism, (Sept. 1965).
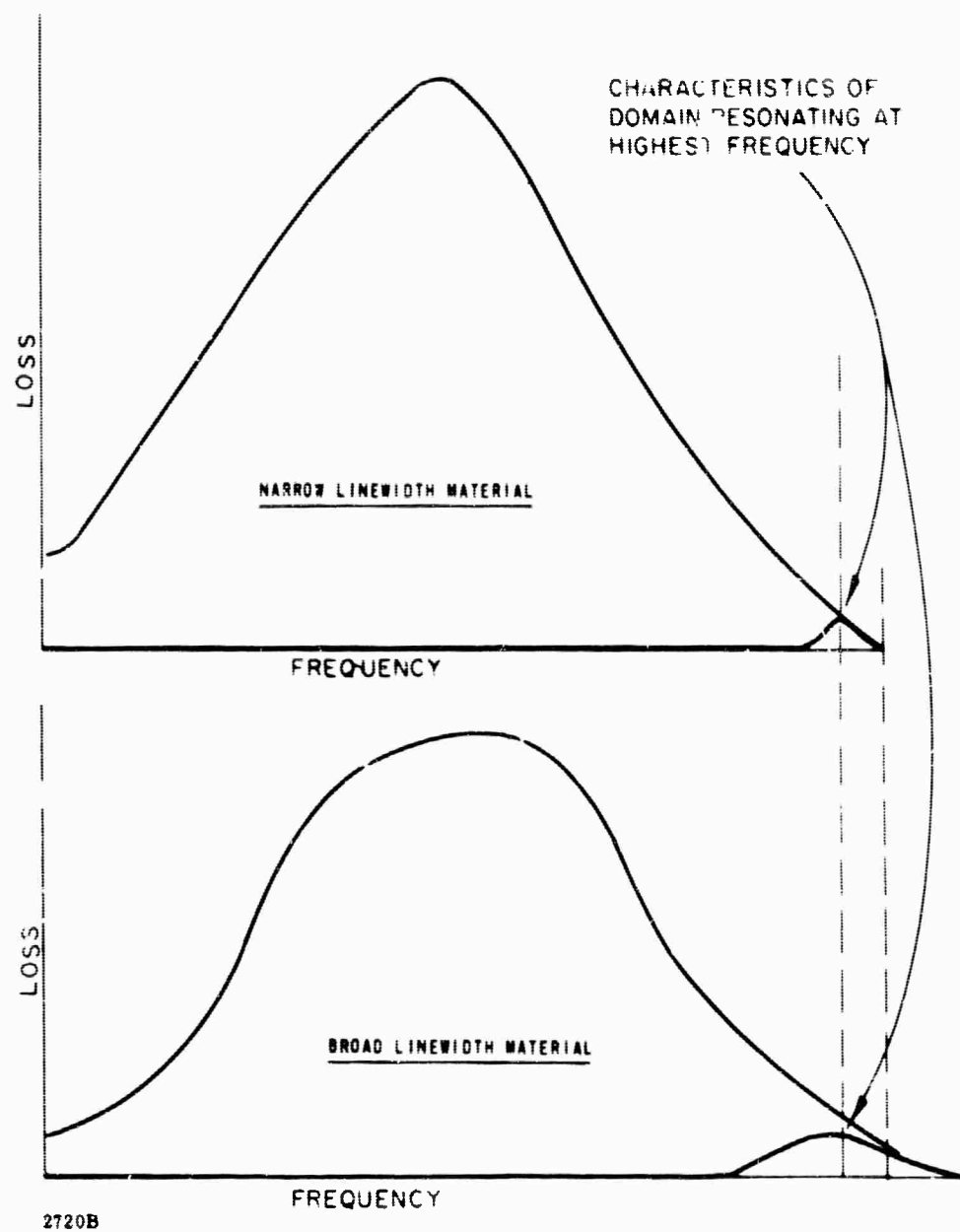
Figure 4. An Illustration of the Extension of Magnetic Loss to
Higher Frequencies by Linewidth Contributions

3.3.4 Switching Mechanisms

The switching and dynamic behavior of ferrimagnetic oxides have been treated in detail in two summary articles on this subject. These articles are as follows:

1. J. B. Birks and J. Hart, Progress in Dielectrics, Volume 5, Academic Press, Inc., Publishers, New York, 1963, (H. P. Peloschek; "Square Loop Ferrites and their Applications", pp 37 93).

2. Harvey Rubinstein, "Switching Properties of Ferrites and Garnets", Scientific Report No. 6 (Series 2), Gordon McKay Laboratory of Applied Science, Harvard University, Cambridge, Mass. (Nov. 30, 1962) Cont. No. AF19(604)5487, AFCRL.

These articles deal with all of the possible switching mechanisms as well as the analytical expressions which describe the behavior of flux reversal in ferrimagnetic oxides. The highlights of these articles as they pertain particularly to switching aspects of materials used in FDPS are discussed here.

To define a ferrimagnetic model for discussion, assume that a ferrite toroid has a magnetization resting in one of the two remanent states. The time necessary to reverse this magnetization and put it in the other remanent state is called the switching time, t_s. This switching time depends on the type of ferrite and the pulse shape used to reverse the magnetization and the amplitude of the drive field. Much information exists in the literature which shows that the inverse switching time $1/t_s$ is a linear function of the applied switching field. The analytical expression which relates this relationship is

$$t_s(H-H_o) = S, \qquad (18)$$

where S is a constant for a material at a given temperature and is called the switching coefficient, and $(H-H_o)$ is the actual drive field. In this case, H is the applied drive field and H_o is generally a function of the material; in general, H_o is approximately equal to the coercive field of the material. The switching coefficient of ferrimagnetic materials is expressed in oersteds-microseconds. A typical $1/t_s$ vs applied field curve for low switching fields is shown in Figure 5. This data indicates primarily domain wall motion. More complete data on the switching coefficient is shown in Figure 6. It is apparent in this data that there are three sections of essentially straight portions of the curve. Each of these sections is related to certain switching mechanisms taking place in the material. Switching mechanisms taking place for low applied fields

are of the domain wall displacement type. This is called the wall displacement mode of switching and generally occurs for low switching fields. The second section of the curve is given by nonuniform or incoherent rotation of domains and this occurs for medium switching fields. For high switching fields, the switching mechanisms are detailed by coherent rotation of domains. Incoherent rotation means that both domain rotation and wall motion are present at the same time. Coherent rotation means that the entire material reverses its magnetization by rotation of all domains.[6]
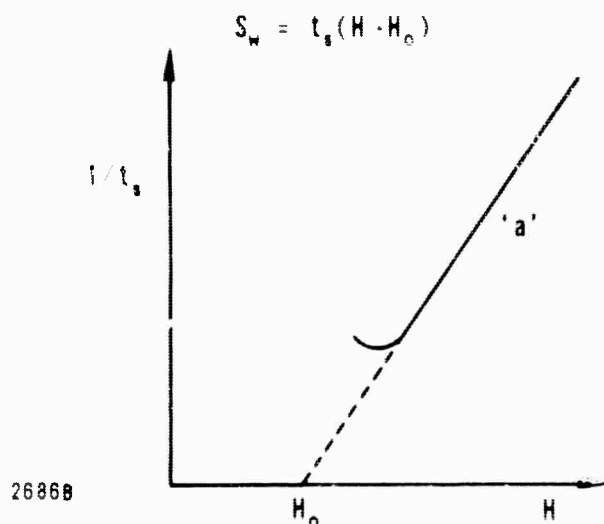
$$S_w = t_s(H - H_o)$$

Figure 5. In a 1 t_s versus H diagram, a straight line 'a' represents the switching properties depending on the field. The slope of this line $S_w = t_s(H-H_0)$ is an important quantity called the switching coefficient. The field H_0 at which the extrapolated line 'a' intersects the H-axis can be identified as the threshold field.[6]

S_w, S_i, and S_c designate the switching coefficients for pure wall displacements, incoherent rotations and coherent (domain rotation), repectively. It has been found that the switching coefficients for these three modes of flux reversal in ferrites may differ by a factor of 20. That is, the switching coefficient for pure wall displacement may be a factor of 20 higher than the switching coefficient for coherent rotations. Typical switching constant S versus applied field characteristics are shown in Figure 7.

26908
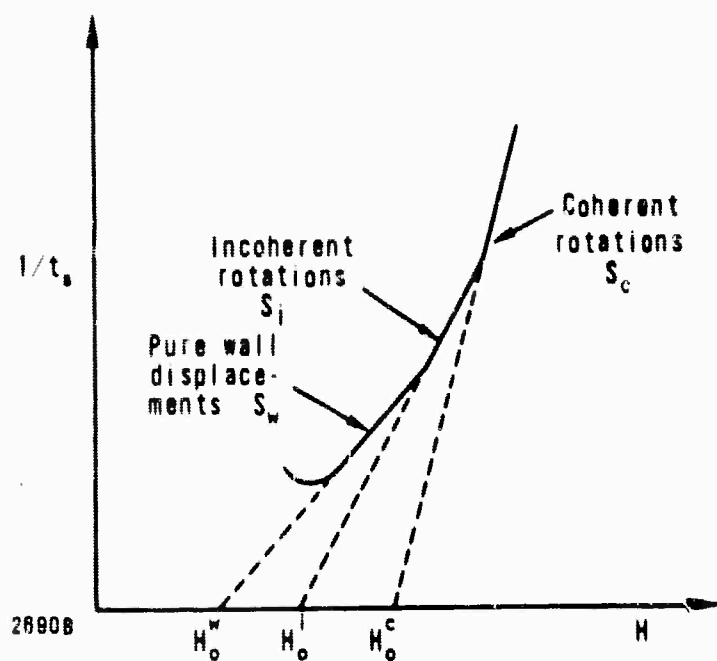
Figure 6. An investigation of the switching time t_s for low, medium and high fields. H shows that the slope of the $1/t_s$ versus H line has several straight portions. For low fields the mode of flux reversal is due to pure wall displacements and the switching coefficient is S_w with a threshold field H_o^w. For medium fields the flux reversal is due to incoherent rotation and S_i and H_o^i are representative. For high fields the flux reversal occurs due to coherent rotation and S_c and H_o^c are representative. The transition from one mode of switching to another is in reality not so sharp as shown in the figure[6].

Figure 7. The switching coefficients S_w, S_i and S_c appear in a general S versus H diagram as three straight lines parallel to the H-axis[6].

2408B

The switching coefficient, S_w, is a constant only at a fixed temperature. Figure 8 illustrates the temperature dependence where the switching coefficient and the threshold field decrease with increasing temperature. This behavior has only been preliminary-investigated for wall switching. The origin of the temperature dependence of S_w is not known precisely but it can be assumed to originate from a variation of the damping characteristics of the wall motion, and the variation of the wall density due to changes in the magnetization and the anisotropy field of the material.

Figure 8. The switching coefficient S_w depends on the temperature. In this Figure this behaviour is illustrated for three temperatures [6]

The observation of the output waveform of different square loop cores indicates that in the normal low field flux reversal, two different processes are involved in this switching (wall motion and incoherent rotations). (See Figure 9.) The relative amounts present of these two mechanisms seem to depend on the material. The high initial peak in the voltage output curve is evident of the first process -- which apparently is a fast process which lasts for only a short time and seems already completed before the field pulsing current has reached its full amplitude. The second process is slower and reverses the bulk of the material. The area under the curve represents the amount of flux reversal. For practical applications, output waveforms of the type shown are encountered. It is assumed that the first peak is caused by rotational processes while the bulk of the material reverses by wall displacement.

3-20

Another explanation of this phenomenon favors the nucleation of reverse domains which produces the first peak of the output curve while the rest reverses by wall displacements due to the expanding domains nucleated. This second explanation is the generally accepted theory of low field flux reversal.[6] At a certain nucleation field the domains of reverse magnetization are formed and produce a sharp peak in the output voltage. If the threshold field H_o is surpassed, the nucleated domains begin to expand but these wall displacements progress much slower than the formation of domains. Since wall displacements seem to switch the bulk of the material, a good square loop material which has to reverse its magnetization in a short time must have many walls nucleated with a narrow distribution of the fields required to switch these walls. This means a homogeneous distribution of the magnetic pole density on the grain boundaries and a narrow angular distribution of easy directions of grains. In ceramic terms this means a homogeneous crystal size of regular oriented crystals.
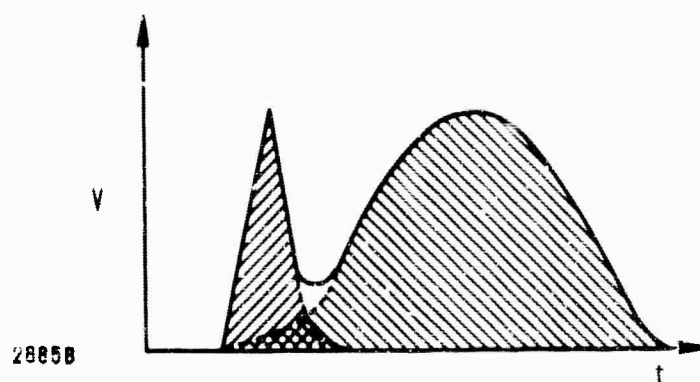
Figure 9. The output voltage in a sense wire during flux reversal consists of two peaks, each representing a particular process, which add up to the final output curve[6]

The theory for flux reversal by wall displacements (the switching mechanism normally encountered in FDPS) indicates that the walls move with a fixed velocity for a given drive field. A mathematical treatment of this motion, after approximations, reduces to a velocity equation as follows:

$$v = 2 (H_m - H_0) M_s / \beta \quad \text{for } 4\pi M_s \gg H_m \quad (19)$$

where v is the domain wall velocity, H_m the drive field, H_0 the threshold field, M_s the saturation magnetization, and β the viscous damping factor of the wall motion. The major contribution from β is due to the relaxation of wall damping. β is given approximately as follows:

$$\beta = \frac{\pi^2 \lambda}{\delta \gamma^2} \quad (20)$$

where λ is the damping parameter in seconds^{-1}, δ is the domain wall thickness in centimeters and is given approximately by

$$\delta = \sqrt{\frac{k T_c}{K_1 a}} = \sqrt{\frac{A}{K_1}} , A \approx \frac{k T_c}{a} \quad (21)$$

where k is Boltzmann's constant, T_c the Curie temperature of the material in degrees K, K_1 the first order anisotropy constant in erg/cm^3, and "a" the lattice constant of the material in centimeters. γ is equal to 1.4 times the g-factor, and for equation (20) is in cycles per oersted-seconds. λ, the damping parameter, is given approximately by

$$\lambda \approx \frac{\gamma M_s \Delta H}{2 H_r} \quad (22)$$

where ΔH is the linewidth of the material in oersteds and H_r is the field in oersteds required for ferrimagnetic resonance. Equation 19 reduces to the following expression

$$v = \frac{15.7 \delta g^2 M_s}{\lambda} (H_m - H_0). \quad (23)$$

Since the switching time t is equal to d/v where d is the distance moved by the wall, the switching time can be obtained for the case where d is the mean distance from one wall to the other:

$$t = \frac{d}{v} \quad (24)$$

$$t \approx \frac{6.4 \, d \, \lambda \, X10^{-2}}{\delta \, g^2 \, M_s \, (H_m - H_0)} \quad (25)$$

From this equation the switching coefficient S_w is deduced to be:[6]

$$S_w = t (H_m - H_c) = \frac{6.4 \, c \, \lambda \times 10^{-2}}{\delta g^2 M_s} = \frac{\beta d}{2 M_s} \quad (26)$$

$$\beta^6 = \frac{12.8 \, \lambda \times 10^{-2}}{\delta g^2}$$

Typical values for S_w calculated from this equation are in the range of 0.1 to 1.0 oersteds-microsecond, for many of the typical microwave ferrimagnetic materials. This is in good agreement with the measured values obtained on many of these same materials from plotting the inverse switching time versus applied field.

To summarize the discussion, it has been indicated that the switching constant S is smaller for rotation of domains than for domain wall displacements and that typical switching constants S_w for wall motion are the order of 0.1 to 1.0 oersted-microsecond. Since it is noted that the switching constant for domain rotation is possibly smaller than the switching constant for wall motion, one might expect a slightly lower value than those quoted above for a mixture of the two mechanisms. It is noted from equation (18) that for these values of switching coefficients, very fast switching times can be achieved only at the expense of fairly large driving fields. From equation (26) it is noted that the switching constant is directly proportional to the domain thickness (the size of the domains), the damping constant of the material, and inversely proportional to the magnetization of the material. This gives direct information on the material parameters which control the switching constant.

Discussion has been given to the switching constant for low switching fields. This mainly involves the process of domain wall motion and can be treated fairly well analytically. It has also been indicated that the fastest switching mechanism is that of domain rotation, but in this process the switching fields must be much higher. With larger switching fields, many processes may be involved, particularly that of both mechanisms together (that of domain rotation and domain wall motion). The proper mixture of these two processes to get minimum switching time is difficult to treat analytically; however, both situations can be treated individually.

Some attention can be given to the analytical expression for the coercive field for domain wall motion and that of domain rotation. The coercive field for domain wall motion is given in the following equation:[1]

$$H_c = \frac{2 K_1 (\Delta \nu)}{\pi M_s} \left[0.386 + \log \sqrt{\frac{2 \pi M_s^2}{K_1}} \right] \tag{27}$$

This equation has been derived empirically and agrees quite well with the experimental data. In this equation, $(\Delta \nu)$ is the fractional volume of nonmagnetic inclusions, and H_c is the coercive field in oersteds. The agreement of this expression with coercive fields measured on many of the microwave garnet materials at Sperry is quite good.

In the domain rotation process, the magnetization changes its orientation against the anisotropy energy of the material. That is, normally the magnetic moments lie along the direction of the anisotropy field. These magnetic moments must be reversed against the anisotropy field in a rotation process where the entire magnetization is in motion simultaneously. The applied field must be of sufficient strength to at least pull the magnetization over the anisotropy energy barrier. It is noted that the rotational coercive force required to rotate the magnetic moments from the anisotropy field will be dependent on the angle which the applied field is incident. The minimum field for obtaining the lowest field is at an angle of 135° to the initial easy direction of the crystallites.[1] In this case the anisotropy field for cubic materials for the rotational process is of the order of $H_c \approx \frac{K_1}{M_s}$, where K_1 is the anisotropy constant of the material and M_s is the magnetization. For yttrium iron garnet this number is calculated to be approximately 40 oersteds compared to something like 0.5 oersted for the coercive field by domain wall motion. Therefore, there is at least an order of magnitude difference between the coercive fields of these flux reversal processes. Since the

[1] Harvey Rubinstein, "Switching Properties of Ferrites and Garnets", Scientific Report No. 6 (Series 2) Gordon McKay Laboratory of Applied Science, Harvard University, Cambridge, Mass. (Nov. 30, 1962, Cont. No. AF19(604)5487, AFCRL.

switching field at all times must be at least greater than the coercive field, this implies that for flux reversal the applied switching field must be much greater for rotational processes than for domain wall motion processes, and thus the switching power required is expected to be much greater for domain rotation. However, a proper mixture of these two processes could allow for fast switching time for nominal switching fields. Presently no analytical expressions are available to predict the proper mixture for fast switching with minimum fields.

Rubinstein[11] has shown that the switching coefficient for domain wall motion is given by the following expression

$$S_w = \frac{\lambda M_s d}{C(\gamma^2 M_s^2 + \lambda^2)} \sqrt{\frac{K_1}{A}} \qquad (28)$$

where c is a constant. This equation is noted to be in agreement with equation 26 with the use of equation 21 for the expression of A. This expression, coupled with equation 18, indicates that the two parameters S_w and H_o measure the performance of a toroidal material in a switching experiment. The devices generally then would require a material in which both S_w and H_o are small in order to keep the power dissipated as low as possible and to simultaneously have rapid switching. It also indicates that the switching coefficient for wall motion is dependent on the distance that domain wall must move for the reversal process. This could be very well dependent not only on grain size in structural effects but also on the rise time of the switching field. In the event where new walls are nucleated during the initial part of the pulse, the difference in the parameters S_w and H_o between single crystals and polycrystals is not particularly pronounced.[11] In polycrystalline materials there are generally many domain walls to use to switch the materials, while in single crystal the domain walls are less predominant, no great improvement is noted in the switching constant between single and polycrystalline materials.

The study of high field behavior of switching in toroids indicates that the inverse switching time is found to be proportional to the square of the switching field. This has been verified in some experimental work. It is noted that in Figure 6, the three flux reversal processes can be approximated by a parabolic function rather than

three linear functions. This basically indicates that the inverse switching time is proportional to the square of the switching field for high field switching (Seems to hold for $H_m > 2$ oersteds for YIG). The switching constants are modified in accordance with this expression, and the analytical treatment has been discussed by Rubenstein.

Some discussion can be offered regarding the use of toroidal cores in microwave devices. For this purpose it is assumed that the magnetic material possesses a square hysteresis loop, is toroidal in shape, and wound with a single switching coil of N turns. In many applications of importance the coil may consist of only a single turn.

It has been noted that during the switching of such a core its impedance is almost entirely resistive[1]. Hence, it must be concluded that the core acts as a dissipative element during switching. An average value for this resistance can be computed as follows[1]: If the core reverses an amount of flux $\Delta\phi$ in a time t, the average voltage V produced during switching is

$$< V > = \frac{N\Delta\phi}{t} \tag{29}$$

where N is the number of turns, $\Delta\phi$ the amount of flux switched, and t the time in which the flux is switched. Since $\Delta\phi = A\Delta B$, where A is the cross-section area of the core and ΔB is the change in flux intensity, this equation can be rewritten as

$$< V > = \frac{NA\,\Delta B}{t} \times 10^{-8} \tag{30}$$

where V now is the voltage in volts, A is the cross-section area in square centimeters, ΔB is the amount of flux change in gauss, and t is the switching time in seconds. Since this voltage is the response to an applied current of amplitude I, the average resistance R seen during switching is

$$< R > = N \frac{\Delta\phi}{I\,t} \tag{31}$$

Since equation 18 relates the switching coefficient, the switching time, and the switching field, this expression can be used to calculate the current and thus the resistance. It is noted in a toroidal material the switching field is given by

$$H = \frac{0.2\,N\,I}{D} \tag{32}$$

where H is the switching field in oersteds, N is the number of turns threading the core, I is the switching current in amps, and D is the average diameter of the core. Using this equation together with equation (12), the following expression is obtained:

$$I = (\frac{S_w}{t} + H_0) \quad \frac{5\,D}{N}$$

$$I \approx -\frac{5\,S_w\,D}{Nt} \quad \text{for } S_w \gg H_0 t$$

$$(33)$$

Using equations 30 and 33, the average resistance of the core can be written as

$$<R> = \frac{0.2\,N^2 A \Delta B \times 10^{-8}}{D(S_w + H_0 t)} \approx \frac{0.2\,N^2 A \Delta B \times 10^{-8}}{D S_w} \quad \text{for } S_w \gg H_0 t \quad (34)$$

From these equations it is seen that the resistance of the core is determined by its shape, the particular material composition and the number of turns in the winding. When the core dimensions and number of turns are fixed, the resistance is determined only by the material through the parameters ΔB and S_w. With all other characteristics the same, the faster switching material (that is, the material with smaller S_w) will have the higher resistance. The average power dissipated by the core is given approximately by[11]

$$<P> = <V>\,I \tag{35}$$

$$<P> = \frac{DA\,\Delta B\,r}{t}(S_w + H_0 t)\,10^{-7} \tag{36}$$

$$<P> = \frac{DA\Delta B\,r}{t}\,S_w \times 10^{-7} \quad \text{for } S_w \gg H_0 t \tag{37}$$

where P is in watts and r is the switching rate of the material in cycles/sec. It is noted that this is the expression for one complete trip around the hysteresis loop rather than just one switching action, so it really involves two switching processes. It is noted that ΔB really is the change in the flux in going from one remanent state to the other, and is approximately equal to the change in the magnetization; this could also be written as ΔM_R. Since A x D is proportional to the volume of the material in the toroid, the power dissipated by the switching is proportional to its volume and increases as the inverse of the reversal time and directly as the switching rate of the core.

Equation 37 is comparable to the expression,

$$P \text{ (watts)} = 4 H_c (M_R) V R \times 10^{-7} \tag{38}$$

derived from the area under the hysteresis curve, where

H_c = coercive field in oersteds

M_R = remanence magnetization in gauss

V = volume of the sample in cm^3

R = switching rate in cycles/sec

P = power dissipated (watts) in the ferrimagnetic material for one complete trip around the hysteresis curve.

For a given core size and switching time a material with low S_w, low threshole field and small flux density is required in order to reduce the driving power. For large toroidal cores, fast switching times or high repetition rate, the energy dissipated in the core can become quite high. It appears as heating of the toroid and thus changes the properties of the material. This can be particularly bad for materials with low Curie temperatures which possess magnetizations which change with temperature. When rapid switching is desired, expensive circuitry is required and the cost of this circuitry increases rapidly with increasing power. So this expression for power indicates that improved magnetic materials can lead to substantial economies in the circuitry.

To illustrate the usefulness of these equations, assume a material with the switching constant S_w of 0.5 oersted-microseconds, H_0 of 0.5 oersteds; D, the average diameter of the core, is approximately 1 centimeter, ar ' the cross-sectional area of the core is 1 square centimeter   Assume that the $4\pi M_s$ of the material is approximately 600 gauss -- which would be approximately that required for an S band device. This produces a ΔB or ΔM of approximately 100 gauss, in a switching time t, of 1 microsecond. Using the above expressions, this produces an average voltage required of 1 N volts. where N is the number of turns around the toroid. The average current required is 5/N amps and the average resistance of the core is $0.2N^2$ ohms. Using a switching rate of 20 Kc, the average power dissipated in the core for any number of turns around that core is 0.2 watts. The tradeoffs that are possible can be noted with regard to the number of turns around the core of the material. If N = 1. the voltage is 1 volt, the current is 5 amps, and the resistance is 0.2 ohms

Considerable attention must be given to the material parameters which control S_w and H_0 in order to minimize the switching coefficient and remain compatible with minimizing the switching power required for the toroids. However, as the switching coefficient goes down, the average resistance of the core goes up, and this in turn means more switching voltage and less current to arrive at appropriate switching times.

In summary, it is noted that - - -

- The switching constant of material is directly dependent upon the average distance the domain walls must travel and the damping constant of the material, and inversely proportional to the domain wall thickness and the magnetization of the material.

- λ, the damping parameter, is directly dependent on the magnetization and linewidth of the material.

- The switching constant is also dependent on the type process used; that is, it is generally larger for domain wall motion than for domain rotation. However, this must be coupled with the point that for domain rotation, H_0 (or the coercive field) is much larger than that for domain wall motion by generally an order of magnitude.

- To achieve fast switching with minimum drive field and thus minimum power, it would be desirable to have a small switching coefficient and a small H_0. However, from the design equations for the resistance and power consumed in the core, it can be seen that for the minimum switching coefficient, the resistance of the core is higher and thus requires larger voltages to produce the required switching current.

- From equation (37), the average power dissipated in the core is proportional to the volume of the core, the change in magnetization going from one remanent state to the other, the switching rate, and the switching coefficient; the average power is inversely proportional to the switching time.

- Therefore, the power consumed indicates that one should work with minimum volume material, the smallest possible magnetization, and the minimum switching constant for a given switching time.

The switching time normally required in FDPS of approximately 1 microsecond seems easily achievable with presently available materials using nominal drive fields and the switching mechanism of domain wall motion. The yttrium gadolinium aluminum iron garnets have been switched in a time of 0.1 μsec at a rate of 2 Mc[']. Measured values by Sperry of S_w on these materials are in the region of 0.3 to 0.5 oe-μsec[13].

3.3.5 Peak Power

The high power handling capability of digital phase shifters depends on both waveguide structure designs and intrinsic material properties. Structural considerations are discussed in Section 3.4.4, and the following paragraphs consider only the intrinsic material properties affect on the high power threshold or h_{crit}.

Possible material factors influencing the degradation in performance of FDPS at high power levels were discussed in the First Semi-Annual Report. Modifications in these ideas introduced by the domain model discussed in Section 3.3.3 are reviewed here.

The onset of these nonlinear or high power effects is observed experimentally as an abrupt increase in insertion loss when the rf power, or magnetic field, exceeds a certain critical level. This increase in insertion loss may also be accompanied by a decrease in differential phase shift. The decrease in phase shift is believed to be caused by heating of local regions of the toroid which may decrease the saturation magnetization, if the material has a temperature dependent magnetization. This sequence of events then sets up local demagnetizing fields which cause the entire toroid to assume a lower remanent magnetization and thus a lower differential phase shift. The initial high power absorption is the triggering mechanism, and by increasing the material's threshold power level for the onset of high power absorption, the degradation in phase shift and increased insertion loss can be avoided.

It is well known that high power effects in ferrites arise from the buildup of oscillations of pairs of spin waves whose frequencies are degenerate with the applied microwave frequency or equal to one half the operating frequency. The half-frequency spin waves are more closely coupled to the uniform precession of the magnetization than are the degenerate spin waves. Thus, the diversion of energy from the uniform precession to the half frequency spin waves is called a first order process, while the

[12]W. L. Shevel and H. Chang, "New Approach to High Speed Storage - Low Flux Density Materials", J. Appl. Physics supp to vol. 31, 125s (May 1960).

[13]D. R. Taft and L. R. Hodges, 'Square Loop Garnet Materials for Digital Phase Shifter Applications" J. Appl. Physics 36 (part 2), 1263 (March 1965).

coupling to degenerate spin waves is termed second order.

The second order process has a lowest threshold field, h_{crit}, when the material is biased to resonance and results in a saturation of the main resonance absorption line at high power levels. Since digital phase shifters are always operated far from resonance, this second order process is of little importance here.

The first order process (energy scattering to half frequency spin waves) may occur when the material is biased to resonance, or it may be observed as an anomalous absorption below the field required for resonance. Since phase shifters are normally operated in this below resonance region, the first order process involving the coupling of energy to half frequency spin waves is the limiting process in the high power operation of digital phase shifters.

The critical rf field strength at which first order high power effects set in is conventionally expressed as

$$ h_{crit} = \frac{\omega_H \, \gamma^2 \, \Delta H \Delta H_k}{\gamma \omega_m \, \sin\theta_k \cos\theta_k \, (\omega_k + \omega_H - \omega_m N_Z + \omega_{ex} \ell^2 k^2)} \tag{39} $$

where

ω_k = spin wave freq. ,

k = $2\pi/\lambda_k$ = spin wave number

λ_k = distance between spins that are in phase with one another

ω_H = γH where H is the applied field

ω_m = $\gamma 4\pi M_s$

N_Z = demagnetizing factor parallel to the dc field

ω_{ex} ≈ γH_{ex}

H_{ex} = internal exchange field ($H_{ex} \sim 10^6$ gauss)

θ_k = angle between dc applied field and direction of $\vec{k}$

ℓ = lattice constant of material

ΔH = conventional uniform precessional linewidth

ΔH_k = "spin wave linewidth"

The power handling capability can be improved by increasing the resonance linewidth, ΔH, or the spin wave linewidth, ΔH_k. The power handling capability can also be increased by controlling the position of the operating frequency with respect to the spin wave manifold. This control can be exercised by the dc applied field in conventional devices.

Figure 10 shows the usual spin wave manifold with the operating frequency ω and the first order spin wave frequency $\omega_k = \omega/2$ shown on the ordinate. When sufficiently high rf power is applied $\left(h_{rf} > h_{crit} \right)$, energy at the signal frequency ω will be absorbed through conversion to the spin wave frequency $\omega_k = \omega/2$. If, however, the external field is raised so that the bottom of the spin wave manifold ω_b is greater than $\omega/2$, then no spin waves will exist at $\omega_k = \omega/2$ and the first order process will be forbidden. This situation is depicted in Figure 11, and the threshold power level for subsidiary absorption will be extremely high.
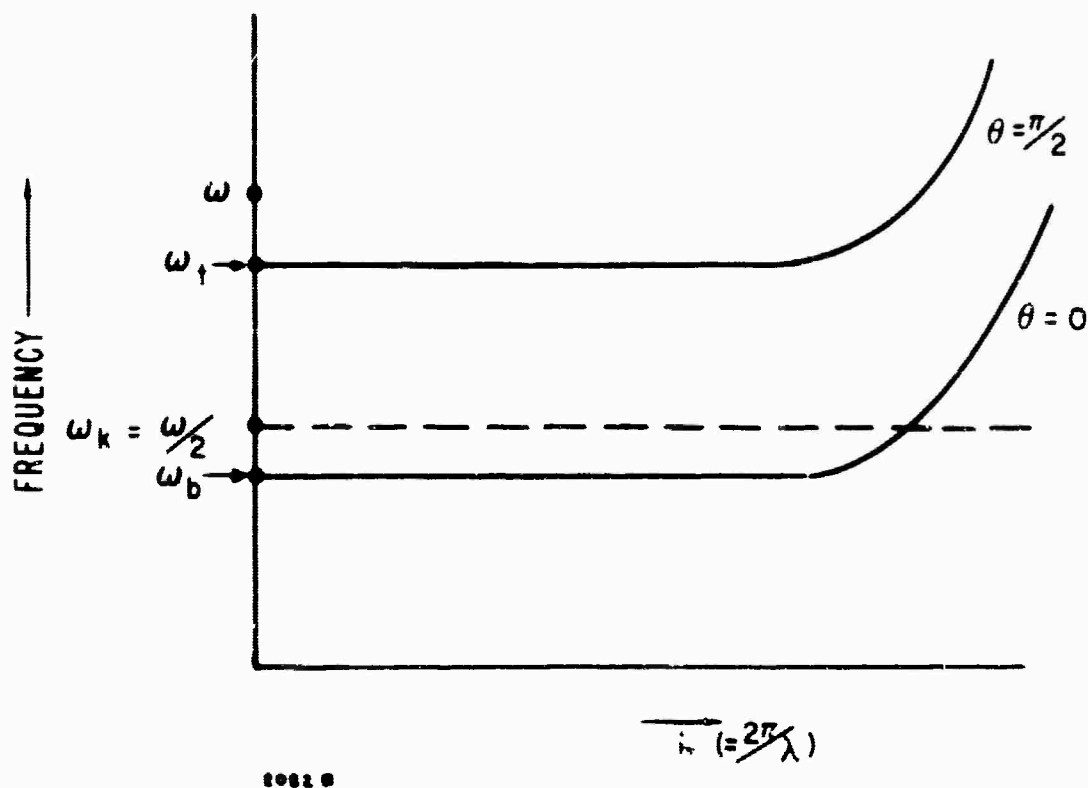
Figure 10. Operating Conditions for $\omega/2$ Spin Waves Within the Spin Wave Manifold
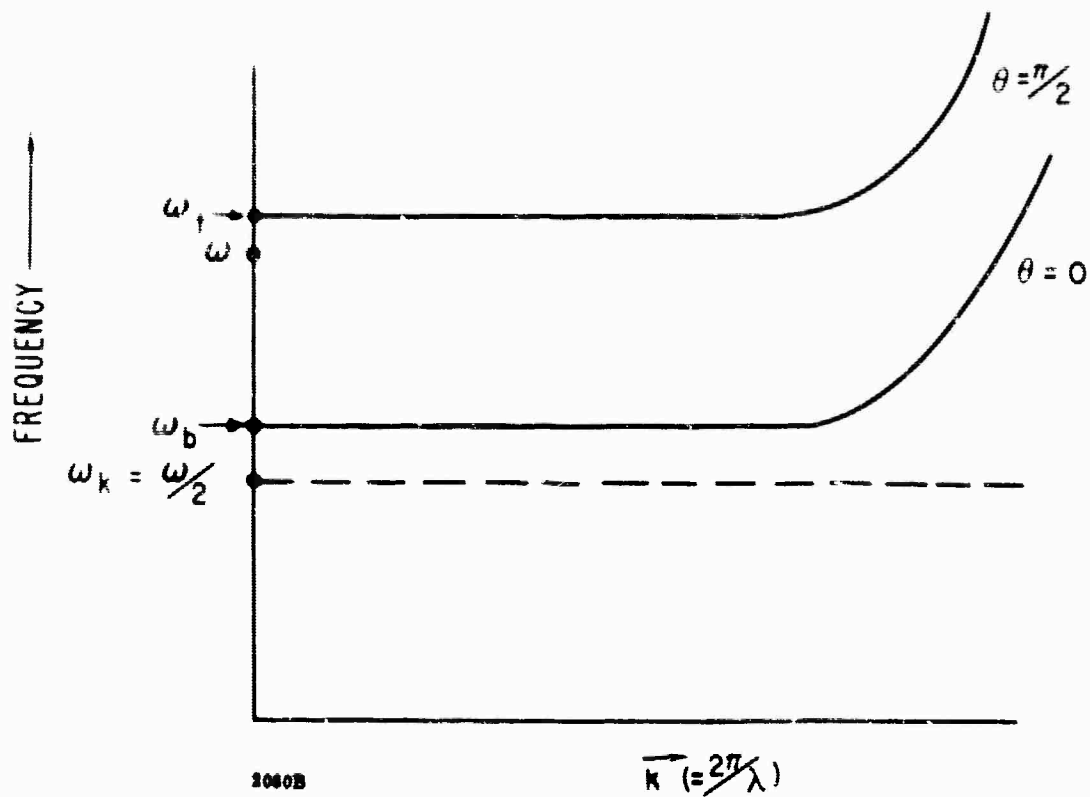
Figure 11. Operating Conditions for ω/s Spin Waves Below the Spin Wave Manifold

Consider now the case shown in Figure 12, the normal set of conditions for very low applied fields. Here once again the spin wave frequencies $\omega_k = \omega/2$ are outside the spin wave manifold for low k, but at high k numbers, spin waves are degenerate with this frequency. This situation is not as favorable as that of Figure 11 when the first order process is forbidden, but does possess a higher threshold power level than the conditions of Figure 10.
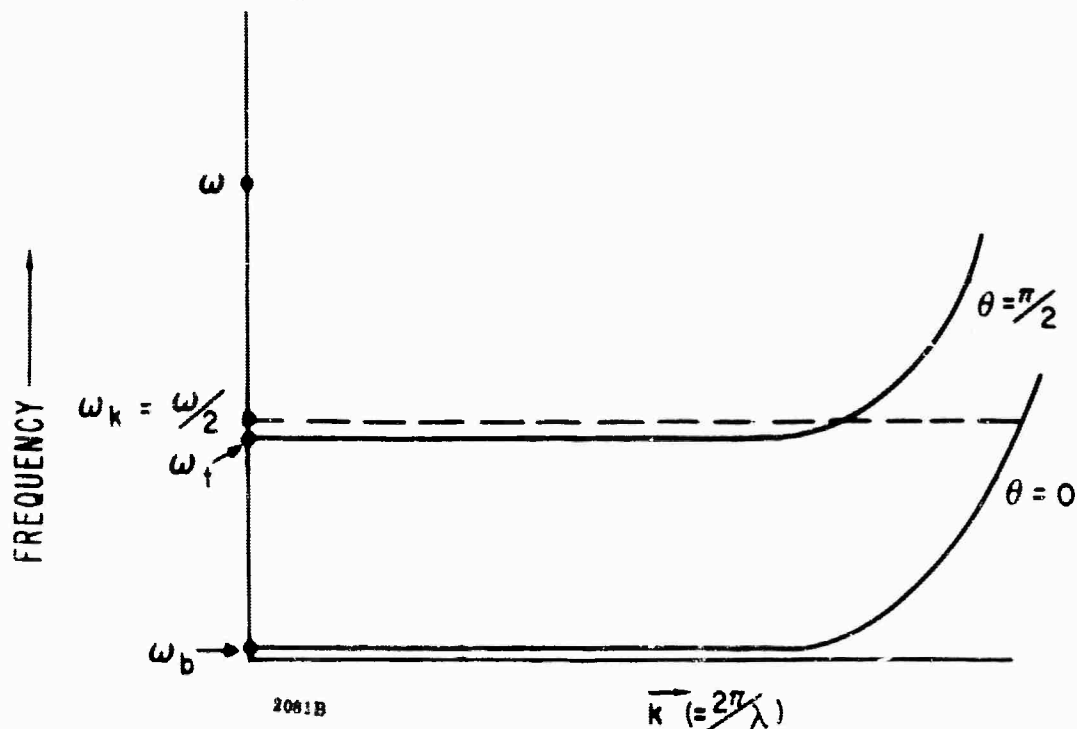
Figure 12. Operating Conditions for $\omega/2$ Spin Waves Above the Spin Wave Manifold

3-33

The higher threshold of Figure 12 arises from the fact that the spin wave line-width varies with k as[14]

$$\Delta H_k = A + Bk^2, \tag{40}$$

and by removing the degeneracy of the low k spin waves, scattering is forced to high k ($k \geq 10^5$) spin waves with larger spin wave linewidths and hence larger threshold power levels.

Since there is no field applied in latching phase shifters, the spin wave manifold cannot be positioned with respect to the frequency axis by the action of an external applied dc magnetic field. Instead, the positioning is controlled through selection of the saturation magnetization with respect to the operating frequency.

The onset of high power effects will occur on a domain by domain basis, and thus some domains will exhibit high power losses well before others. In speaking of the high power threshold for a remanent toroid one might distinguish between the threshold for the major domain and that of the most susceptible domains. Since increased loss will be apparent wherever it occurs, the initial increase in high power insertion loss is probably caused by those domains most susceptible to high power effects. For operation under the conditions of Figure 12, those domains with the greatest effective field should have the lowest threshold, and thus the antiparallel domains with effective fields approaching $\left(\frac{4}{3}\frac{K_1}{M_s} + 4\pi M_s\right)$ will be the first to exhibit high power loss. The major domains with smaller effective fields (effective fields that can be deduced from Equation (16) will have lower thresholds. However, the insertion loss will be observed to increase as soon as the rf power reaches the threshold of the antiparallel, or Polder-Smit domains. This high power loss would presumably further increase as the rf power reaches the threshold of other domains.

To operate in the region shown by Figure 12 it is required that

$$\frac{\omega}{2} > \omega_t = \gamma \left| \left| H - N_z 4\pi M \right| \; \left| H + (1 - N_z) \, 4\pi M \right| \right|^{1/2} \tag{41}$$

For a remanent toroid, $N_z = 0$, and the effective applied field may differ from one domain to the next. Then for the Polder-Smit domains with an effective field of $H_{eff} = \frac{4}{3}\frac{K_1}{M_s} + 4\pi M$, we obtain

$$\frac{\omega}{2} > \gamma \left| \left(\frac{4}{3}\frac{K_1}{M_s} + 4\pi M_s \right) \left(\frac{4}{3}\frac{K_1}{M_s} + 8\pi M_s \right) \right|^{1/2} . \tag{42}$$

---

[14] Recent data by Comstock (J. Appl. Phys., January 1965) indicates that this k dependence may be more nearly $\Delta H_k = A + Fk$, but in either event the arguments presented would hold

If we neglect the $\dfrac{K_1}{M_s}$ term with respect to $4\pi M_s$, we find as a stability criterion

$$\frac{\omega}{2} > \gamma \; 1.4 \; 4\pi M_s$$

$$\text{or } \frac{\omega_m}{\omega} < 0.36. \tag{43}$$

This is the requirement for the most susceptible domain to be effectively biased as sketched in Figure 12, and relatively safe from high power effects. For the major domains, the effective field varies with toroidal geometry. It would in any case be considerably lower than $4\pi M_s$, and for illustrative purposes we can take it as $2\pi M_s$ (see Equation 17). This leads to a stability criterion for the major domains of

$$\frac{\omega_m}{\omega} < 0.72. \tag{44}$$

Thus the threshold field for a ferrite toroid will depend on its domain pattern. A demagnetized toroid should have a lower critical rf field value than one whose remanent magnetization approaches the saturation magnetization.

For a given frequency, ω, a value of saturation magnetization can be chosen such that the low k spin waves with small spin wave linewidths are all below the critical frequency $\omega/2$, and only those spin waves of high k and high spin wave linewidths, ΔH_k, will be coupled by first order effects to the uniform precession.

If the value of $\dfrac{M_R}{M_S}$ can be made to approach unity, then we could employ much larger values of saturation magnetization while still maintaining the conditions of Figure 12 by doing away with the Polder-Smit domains in the completely saturated material. In the saturated material Equation (44) rather than Equation (43) would be applicable.

The use of completely saturated toroids thus offers the advantages of larger differential phase shift per unit loss and length, and additionally, should exhibit better high power characteristics. Two techniques of increasing the remanent magnetization were discussed in Section 3.3.3 and should be further explored.

Finally, it might be mentioned that the discussion of Section 3.3.3 indicated the possibility of operating FDPS effectively biased above resonance. If such operation could be realized, it should have very good high power handling capability since it would respond to the operating conditions of Figure 11 where spin waves with $\omega_k = \omega/2$ do not exist.

3.3.6 Desired Material Characteristics

1. **Magnetization** ($4\pi M_S$). Materials should possess magnetizations suitable to application in phase shifters operating in the frequency region from L band through X band. Values from 100 gauss to approximately 2000 gauss are required. Temperature stability of the magnetization is desired where possible.

2. **Remanent Magnetization** ($4\pi M_R$). The remanent magnetization should be the maximum obtainable for the material geometry dictated by the structural aspects of the phase shifter.

3. **Remanence Ratio** ($4\pi M_R/4\pi M_S$). The remanence ratios should be the maximum obtainable. Values greater than 0.60 on all compositions are desired.

4. **Ferromagnetic Linewidth** (ΔH). Materials possessing low linewidths (less than 150 oersteds) are desired. The full importance of linewidth to the operation of FDPS is presently not established.

5. **Dielectric Loss Tangent.** Values less than 0.0001 (as measured at X band and room temperature) are desired.

6. **Curie Temperature.** Curie temperature values greater than 200°C are desired for all materials.

7. **Dielectric Constant.** Any value normally obtained in ferrimagnetic materials is acceptable provided reasonably good temperature stability and reproducibility is demonstrated. Reproducibility should be ±0.1 of the established value.

8. **Coercive Field** (H_c). A value as low as possible consistent with the above properties is desirable. Values less than 1 oersted for all compositions are desired.

9. **Anisotropy Field** (H_{anis}). A value as low as possible for each material is desired.

10. **Peak Power Threshold.** For high power applications, the spin wave linewidth (ΔH_k) should be as large as possible consistent with the above desirable properties. The relationship

$$\frac{\gamma 4\pi M_S}{\omega} < 0.5 \text{ should be maintained where possible.}$$

11. **Grain Size.** Large average grain size is desired. The optimum value will depend on the composition. Values in the 10 to 30 micron area seem acceptable for most materials.

12. **Density.** Porosity and inclusions should be minimized; therefore maximum density should be maintained. Values of 97% or greater of theoretical density seem acceptable.

13. **Stress and Strain.** Unfavorable stresses and strains should be reduced to a minimum. Magnetostrictive energy should be minimum. At present, materials possessing magnetostrictive constants of zero or near zero appear to be most desirable.

14. **Other Properties.** All other properties (g-factor, zero field permeability, etc.) can be those which are compatible with the above properties.

15. **Temperature Stability.** As many properties as possible should exhibit temperature stability. The $4\pi M_S$, $4\pi M_R$ and ΔH values appear to be the most critical.

3.4 STRUCTURAL ASPECTS OF NONRECIPROCAL FERRITE DIGITAL PHASE SHIFTERS

3.4.1 Introduction

The propagation constant of a microwave structure (Γ) describes the effect of the interaction between the structure and the wave traveling through it, and is equal to

$$\Gamma = \alpha + j\beta \tag{45}$$

where
α = the attenuation constant
β = the phase constant.

In a nonreciprocal phase shifter of length ℓ, β is not equal for both directions of propagation ($\beta_+ \neq \beta_-$) and $\Delta\beta\ell = (\beta_+ - \beta_-)\ell$ is the difference in the phase shift (or electrical length) of the structure for the two directions of propagation. In general, $\alpha_+ \neq \alpha_-$, but in the case of FDPS they are very small and very nearly equal.

3.4.2 Differential Phase Shift

A single magnetized slab of ferrite appropriately placed in the waveguide (see Figure 13A) causes nonreciprocal (or differential) phase shift between the two directions of propagation for a given direction of the magnetizing field; conversely, differential phase shift can also be obtained for a given direction of propagation between two different orientations or magnitudes of the magnetizing field. Two ferrite slabs properly located in the waveguide and magnetized in opposite directions (Figure 13B) could be made to yield twice as much phase shift. The next logical extension is shown in Figure 13C where a ferrite toroid is shown as being formed by filling the gap between these slabs at the top and bottom so as to essentially eliminate the demagnetizing fields of the slabs in the direction of the magnetization.

While these basic ideas have been known for some time, it is only recently that the toroid geometry has been exploited to any extent. The twin slab configuration is useful primarily only as a model for analyzing the toroid geometry; in practice, it is found that two ferrite slabs placed close enough together to yield the desired additional phase shift, over the single slab configuration. are difficult to magnetize in opposite directions. It is the tendency of the external magnets to complete their circuits by mutual coupling of the flux to the exclusion of the ferrite.
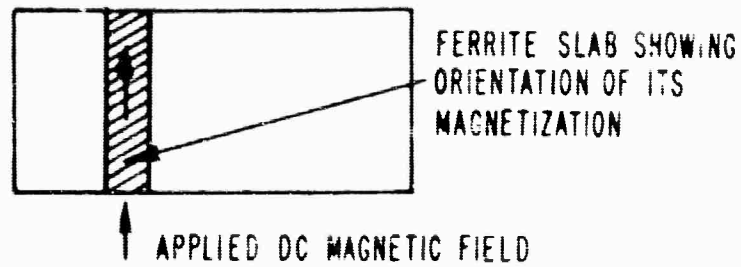
(A) SINGLE SLAB FERRITE PHASE SHIFTER
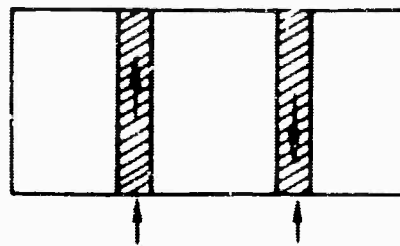
(B) TWIN SLAB FERRITE PHASE SHIFTER SHOWING THE SLAB
ON THE LEFT MAGNETIZED UP AND THAT ON THE RIGHT
MAGNETIZED DOWN
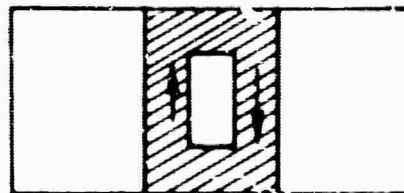
2701B

(C) TOROIDAL FERRITE PHASE SHIFTER

Figure 13. Three typical ferrite phase shifter configurations showing the
orientation of the magnetization of the ferrite

An outline of the procedure for solving for $\beta \pm$ is presented below for the loss-less case. A twin slab model with dielectric loading between the slabs is shown in Figure 14A. This is the same model used by Ince and Stern[10]. Because of the symmetry of the structure, the origin of the coordinate axes can be placed at the center of the waveguide and only those regions designated 1, 2, and 3 must be considered. A pure TE_{10} mode is assumed (so that $E_x = E_y = \partial E_z / \partial Z = 0$) with propagation according to $e^{j(\omega t - \beta y)}$. Maxwell's equations give $K^2 = \omega^2 u\epsilon - \beta^2$ for the wave number, and for the three regions

(A) MODEL USED BY INCE AND STERN   (B) MODEL USED BY SCHLOEMANN
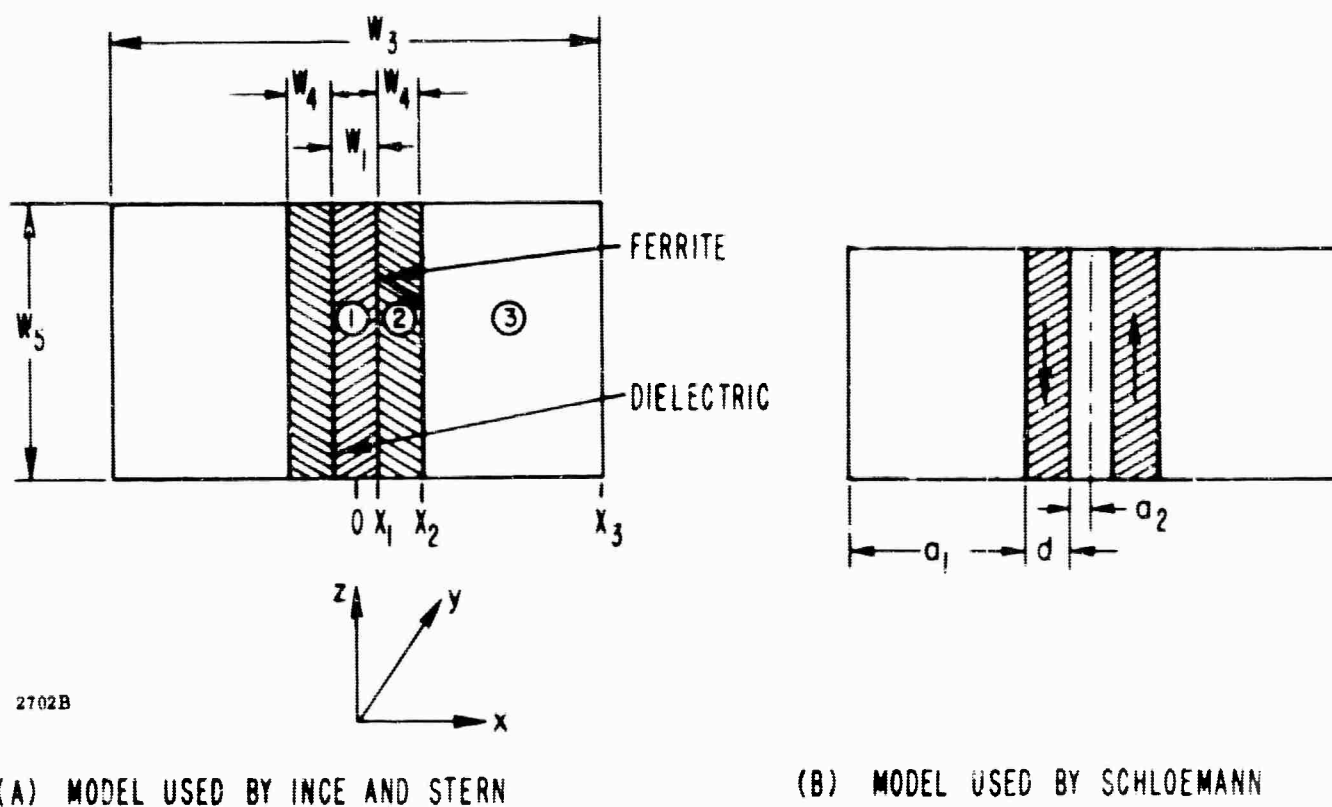
Figure 14. Twin Slab Phase Shifter Models Used in the Theoretical Analyses by Ince and Stern and by Schloemann

$$E_{z1} = A_1 \cos K_1 X \qquad\qquad 0 < X < 1/2W_1 \qquad\qquad \left.\vphantom{\begin{array}{c}1\\1\\1\end{array}}\right\} \text{Region 1}$$

$$E_{z2} = A_2 \cos K_2 X + jA_2' \sin K_2 X \qquad 1/2W_1 < X < 1/2W_1 + W_4 \qquad \text{Region 2} \qquad (46)$$

$$E_{z3} = A_3 \cos K_3 X \qquad\qquad 1/2W_1 + W_4 < X < 1/2W_3 \qquad \text{Region 3}$$

and

$$h_{ym} = \frac{1}{j\omega\mu} \frac{\partial E_{zm}}{\partial x}$$

$$h_{xm} = Z_w E_{zm}$$

where

ω = the operating frequency,

$\mu = \mu_0$ — Region 1

$\mu_\pm = \mu_0 \left[1 \mp (\gamma 4\pi M_r/\omega)^2 \right]$ — Region 2

$\mu = \mu_0$ — Region 3

$\epsilon = \epsilon_m$ = permittivity of Region m,

E_{zm} = rf electric field in Region m,

Z_m = wave impedance

h_{ym} = component of rf magnetic field in region m tangential to the boundary of the region,

h_{xm} = transverse component of rf magnetic field in region m

$$K_1 = (\omega^2 \mu_0 \epsilon_1 - \beta^2)^{1/2}$$

$$K_2 = (\omega^2 \mu_\pm \epsilon_2 - \beta^2)^{1/2}$$

$$K_3 = (\omega^2 \mu_0 \epsilon_0 - \beta^2)^{1/2}.$$

If the quantities $K_m X_m$ are now defined as angles θ_m at the boundaries of these regions, there are the following:

$$\theta_1 = K_1 X_1 \qquad\qquad\qquad \text{Region 1}$$

$$\theta_2 = K_2 X_1 \qquad\qquad\qquad \text{Region 2}$$

$$\theta_3 = K_3 X_2 \qquad\qquad\qquad \text{Region 3}$$

$$\theta_4 = K_2 X_2 \qquad\qquad\qquad \text{Region 2}$$

The boundary conditions require that the tangential field components be continuous at the boundaries. Thus, for example, $E_{z1} = E_{z2}$, and

$$A_1 \cos \theta_1 = A_2 \cos \theta_2 + jA_2' \sin \theta_2.$$

3-40

When this is done at each of the two boundaries for the E_{zm} and h_{ym} fields, there results a set of four equations containing the quantities A_m. Cramer's rule states that the determinant of the coefficients of A_m must equal zero if there is to be a non-trivial solution. The expansion of this determinant then yields the characteristic equation:

$$\frac{\tan(\theta_4 - \theta_2)}{K_2} = \frac{K_3 \cot \theta_3 - K_1 \tan \theta_1}{K_2^2 + (1-m^2) K_1 K_3 \tan \theta_1 \cot \theta_3 \pm m\beta(K_3 \cot \theta_3 + K_1 \tan \theta_1)} \quad (47)$$

where

$$m = \frac{4\pi \gamma_1 M_r}{\omega}.$$

This is substantially the same equation derived by Ince a..u Stern[10] in their analysis and, for the case where $\epsilon_1 = \epsilon_0$, should be equivalent to the form used by Schloemann[15] before simplification.

The model used by Schloemann is shown in Figure 14 B. Schoemann uses a normalized angle α_1 defined as

$$\alpha_1 = \frac{2\pi a_1}{\lambda_0} (1 - \Gamma^{-2})^{1/2}$$

where a_1 is shown in Figure 14B and Γ is a normalized propagation constant.

Schloemann argues that for practical values of differential phase shift, α_1 is imaginary so that $\cot \alpha_1 = -j \coth |\alpha_1|$ and hence $\cot \alpha_1$ is independent of a_1 for $|\alpha_1| \gg 1$. This inequality implies that the rf fields are strongly concentrated in the ferrite and essentially independent of the location of the waveguide walls. Under these conditions the characteristic equation can be simplified, and the results applied wherever the strong field approximation holds. However, in those geometries for which $|\alpha_1| \gg 1$, the differential phase shift is found to be either very frequency dependent or subject to moding problems. In practice, this is normally overcome by reducing the width of the waveguide and/or the ferrite which results in smaller values of a_1 and makes this strong field concentration approximation technically invalid. Typically, if

$$\frac{2\pi}{\lambda_0} = 4 \qquad \text{(radians/inch)}$$

$$\Gamma^2 = 9 \qquad \text{(radians/inch)}^2$$

$$a_1 = .13 \qquad \text{(inches)}$$

then

$$\alpha_1 = (.13)4(1-9)^{1/2}$$

$$= j 1.47 \qquad \text{(radians)}$$

Thus, in most practical cases we are limited to small values for $|\alpha_1|$ and hence a_1 is a determining factor.

3-41

Some of the conclusions that can be made from the analytical study of Ince and Stern are:

- A displacement of the fields takes place between the two magnetic states, $+M_r$ and $-M_r$. The amount of this displacement increases with increasing m ($m = 4\pi\gamma M_r/\omega$). The effect is most pronounced in the case of the transverse magnetic field component h_x. At the center of the waveguide $h_{x+}/h_{x-} \approx 1.4$ when $m = 0.4$, and $h_{x+}/h_{x-} \approx 2.8$ when $m = 0.8$.

- In the cases where the dielectric constant, ϵ'_1, of the material in the toroid slot is greater than that of the toroid, ϵ'_2, then for maximum phase shift there is an optimum slot width W_1 ($W_1 > 0$); when $\epsilon'_1 < \epsilon'_2$; however, the optimum slot width is zero ($W_1 = 0$).

- Phase shift increases and phase slope decreases with increasing frequency and slab width W_4.

- The conditions under which the phase slope is least give maximum phase shift.

- These conditions can be realized by reducing the width of the waveguide.

The following example is based on Figure 8 of reference 10. Under the conditions

$$\epsilon'_1 = 13$$
$$\epsilon'_2 = 12$$
$$m = 4\pi\gamma M_r/\omega_o \approx 0.8$$
$$\lambda_o = 3.331 \text{ cm}$$
$$\omega_o = 9 \text{ Ghz}$$
$$w_1 = .04\lambda_o$$
$$w_3 = 0.3\lambda_o$$
$$w_4 = .05\lambda_o$$

the differential phase shift is calculated to be 16.5 (8.1) $\approx$ 131 degrees per cm and 15.25(9.9) = 151 degrees per cm at 8.1 Ghz and 9.9 Ghz, respectively. However, when $W_3 = 0.5\lambda_o$, the differential phase shift is 12.6(8.1) = 102 and 13.4(9.9) = 133 degrees at 8.1 Ghz and 9.9 Ghz. Thus when $W_3 = 0.3\lambda_o$, the phase slope is 20/141 (14.2 percent) but when $W_3 = 0.5\lambda_o$ the phase slope is 31/118 or 25 percent.

Similar conclusions can be reached from Schloemann's analysis, where the use of a dielectric constant of 16 and various values of $\gamma 4\pi M_r/\omega$ for the ferrite are close to several experimental models. The assumptions of no dielectric loading, $\epsilon_1 = \epsilon_0$, and widely spaced waveguide walls, however, depart from most geometries investigated on this program. Referring to Figure 5 of reference 15 and using

$$\epsilon'_1 = 1$$
$$\epsilon_2 = 16$$
$$K' = \pm \gamma 4\pi M_r/\omega_0 = \pm .25$$
$$\omega_0 = 9 \text{ Ghz}$$
$$\lambda_0 = 3.331 \text{ cm}$$
$$D = 2\pi d/\lambda, \qquad D_0 = 2\pi d/\lambda_0 = 0.7$$
$$A_2 = 2\pi a_2/\lambda = 0.05,$$

the phase shift is shown to be 28 degrees per cm and 31 degrees per cm at 8.1 and 9.9 Ghz, respectively. The phase slope is 10 percent. This phase shift seems to be about what one might expect based on Ince and Stern's calculations using m = 0.8 and noting that here $K' = .25$. The phase slopes appear to be in approximate agreement.

3.4.3 Losses in Waveguide Structures

The losses in digital phase shifters include dielectric loss, wall loss and magnetic loss. In FDPS the latter is frequently the largest contributor, and unlike the other losses, the severity of magnetic loss increases with decreasing frequency. Intrinsic material loss considerations were discussed in Section 3.3.3. For a given intrinsic material loss (μ'), waveguide geometry will further influence overall loss.

The effect of magnetic losses in waveguide configurations are calculated by including the component μ'' in the rf permeability in the characteristic equation. Solutions to this equation will then contain a real part and an imaginary part which represent the phase shift $\beta\pm$ and the attenuation $\alpha\pm$, respectively. A more meaningful quantity is the figure of merit F equal to the differential phase shift per unit (db) of loss. Thus $F = \beta_+ - \beta_- /\alpha$ where $\alpha = \alpha_+ = \alpha_-$. The theoretical analyses provide some design criteria in terms of this figure of merit.

In his treatment of losses Schloemann[15] shows that, with waveguide walls at infinity ($a_1 = \infty$), zero separation of the ferrite slabs ($a_2 = 0$), and a ferrite dielectric constant of 11, the figure of merit peaks up at a slab thickness of $\frac{1}{25}\lambda$.

[15] E. Schloemann, "Theoretical Analysis of Twin-Slab Phase Shifters in Rectangular Waveguide.", Raytheon Technical Memorandum T-637, March 23, 1965.

The treatment by Ince and Stern[10] shows that for a waveguide width of $.761\lambda$, $4\pi\gamma M_r/\omega = .8$, $\mu''/\mu' = .01$, ferrite dielectric constant $\epsilon' = 12$, and a dielectric load between the slabs with ϵ of 13 then, for a slab thickness of $\frac{1}{25}\lambda$, the width of the dielectric load giving maximum figure of merit is $.10\lambda$.

3.4.4 Peak Power Considerations

Ferrite phase shifters become lossy at high power levels. The power level at which the loss versus peak power curve turns upward is usually called the threshold power level. (See Figure 15A.) This power level (P_T) is partly determined by the critical field strength of the ferrite, h_{crit}, as discussed in Section 3.3.5. The threshold power level is also strongly influenced by waveguide geometry since, at any power level, the actual field strength in the ferrite is a function of the geometry and electrical properties of the components of the structure, the input power level, and frequency. The critical field is that field which causes a noticeable disruption of the normal precession of the magnetization. When the pertinent component of rf magnetic field exceeds h_{crit}, the ferrite begins to absorb energy.

For a ferrite with a given value of h_{crit}, there are several ways in which the threshold power level can be increased through careful design of the FDPS. The geometry of the ferrite and/or associated structures can be adjusted to reduce the magnitude of the rf magnetic field components at the ferrite while still maintaining sufficient phase shift interaction.

The threshold power level varies across the width of the ferrite because the rf magnetic field components do and, other things equal, minimum P_T will be associated with those regions containing maximum rf field. Ince and Stern[10] and Schloemann[15] have shown that the critical field component is the transverse component (h_x) which reaches a peak at the center of the toroid. The geometry of the structure may be adjusted to reduce h_x at the center of the waveguide. This is done by increasing the size of the waveguide, decreasing the size of the toroid, increasing the size of the slot or reducing the dielectric constant ϵ_1' of the material in the slot. Since P goes as h^2, if h_x is reduced by a factor of 2, then P_T will be increased by a factor of 4.

Ince and Stern show that, using $\epsilon_1' = 1$ and $4\pi \gamma M_r / \omega = 0.8$, if the slot width is increased from 0 to $.16\lambda_o$, h_x goes from .036 to .023 so that P_T would be increased by a factor of $(.036/.023)^2 = 2.4$. In this case the differential phase shift per unit length also decreases. The required phase shift can be regained by using a longer toroid without affecting the unit's high power performance. Through a better selection of dielectric constant and width, more favorable results can be obtained. A dielectric with $\epsilon = 13$ and a slot width of $.05\lambda_0$ would decrease h_x by .77, and thus increase P_T by a factor of 1.65. At the same time the phase shift per unit length would increase by almost 33%.
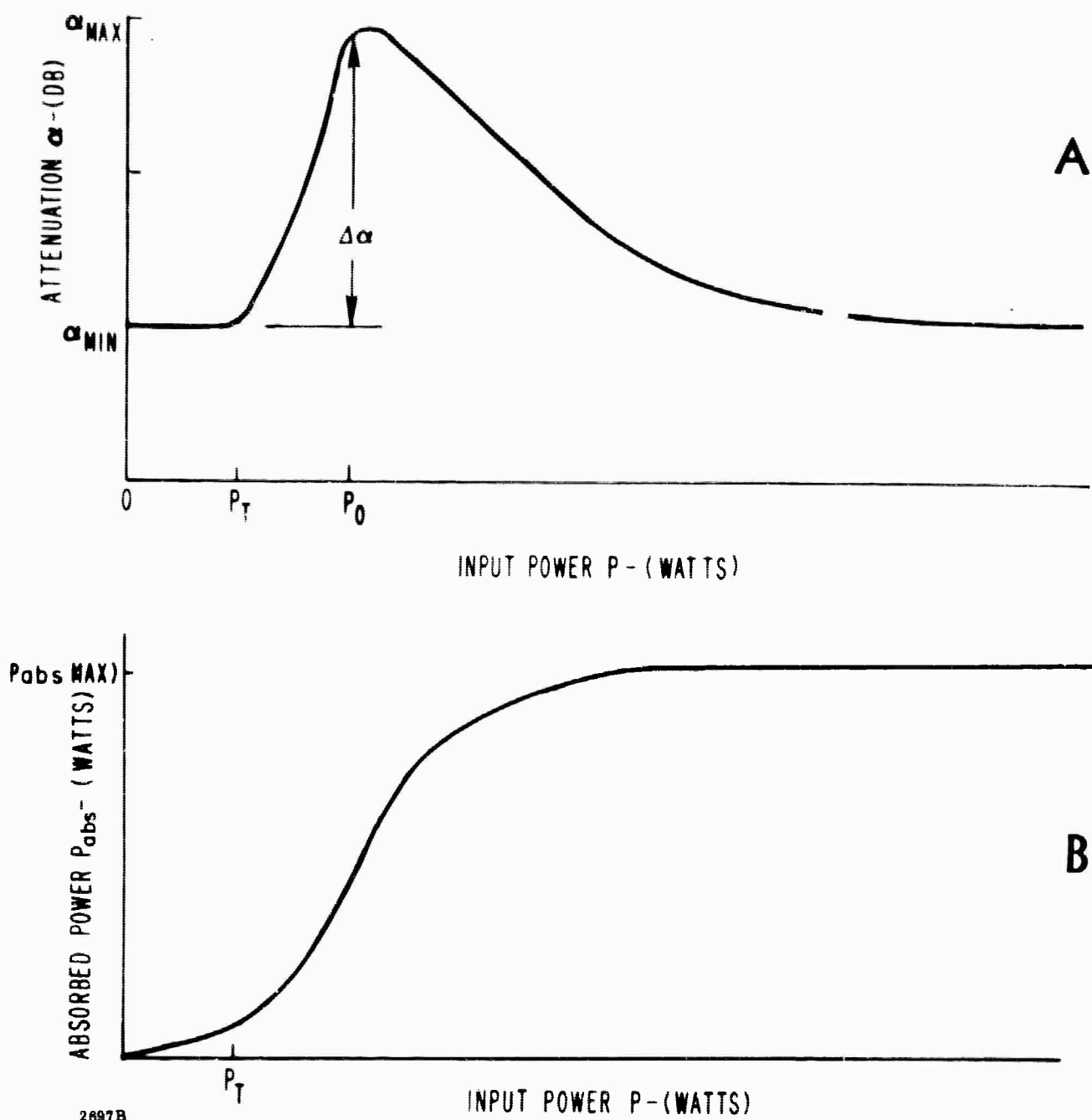
Figure 15.   Attenuation and Absorbed Power Versus Input Power Showing the Threshold Power Level

The following factors are found to influence theoretically the threshold power level:

1. h_{crit}: P_T increases as h^2_{crit}. h_{crit} is almost entirely a function of the ferrite material and operating frequency, as discussed in Section 3.3.5.

2. Waveguide height b: P_T varies directly with b.

3. Waveguide width a: P_T may or may not be a function of a. For large ratios of toroid width to waveguide width, P_T will depend only weakly on a. For small ratios, its functional dependence increases so that in the infinitely thin ferrite case P_T varies directly with a.

4. Slot width: Increasing the slot width decreases h_x and thus increases P_T.

5. Dielectric constant of ferrite or dielectric load: Reducing the dielectric constant of the ferrite reduces h_x and hence increases P_T. Filling the slot of the toroid with dielectric reduces h_x. The greater the dielectric constant of this material, the greater the reduction in h_x and subsequent increase in P_T.

6. Remanent magnetization: Reducing the remanent magnetization of the ferrite toroid also reduces h_x.

Thus many different factors influence the threshold power level of the device. Some adjustments adversely affect other phase shifter characteristics. A case in point is the reduced phase shift per unit length resulting from increased slot width. As in most devices then, the device designer must select the best compromise for the particular application at hand.

Figure 15 shows the attenuation α and absorbed power P_{abs} versus input power P. As P increases from P = 0, the attenuation is constant ($\alpha = \alpha_{min}$) corresponding to a linearly increasing P_{abs}. At $P = P_T$ the attenuation increases rather rapidly to α_{max} corresponding to $P = P_0$. Beyond this power level, the spin system begins to saturate as more and more pairs of spin waves go unstable. Ultimately, the point is reached where no further energy can be transferred to the lattice via the spin waves[16]. Beyond this point, P_{abs} decreases, and there will be a power level $P \gg P_T$ at which the attenuation has returned essentially to α_{min}. It can be shown that

16 R. E. Willoughby, "High Power, SPDT, Fast Ferrite Switch," Journal of Applied Physics, March 1965 Part 2, p 1247.

the power level at which the attenuation has returned to within $\Delta \alpha$ of α_{min} is given by

$$P = \frac{P_{abs \ (max)}}{1 - \dfrac{1}{10^{\Delta \alpha / 10}}} \quad .$$

Whether the ferrite is still capable of yielding practical values of phase shift at $P >> P_T$ is not known at this time. It would certainly be expected to yield less phase shift than at $P < P_T$. There is a possibility that this approach may be feasible in the event of very high power operation.

4. EXPERIMENTAL RESULTS

4.1 GENERAL

The program goals for this reporting period were as follows:

- Study of the effects of magnetostriction or coercive field and squareness.

- Evaluate and tabulate the hysteresis properties of representative microwave ferrite materials.

- Evaluate and tabulate the hysteresis properties of additional garnet materials.

- Continue the study and interpretation of grain size effects on hysteresis properties.

- Study of strain relief in machined toroids by heat treatment to improve remanence ratios and coercive fields.

- Study the reproducibility of microwave ferrimagnetic materials for FDPS application.

- Determine what parameters affect losses, phase shift, phase slope, switching energy and threshold power level in a FDPD.

- Continue the evaluation of materials in the X band waveguide test structure.

- Begin similar evaluations in low frequency coaxial structure.

- Obtain a better understanding and interpretation of the ferrimagnetic material properties and how these properties influence the characteristics of FDPS operating in the frequency range from L through X band.

These goals have been achieved in part (some are continuing goals) during this reporting period and the following sections detail the experimental data and results obtained.

This section is presented as a continuation and/or addition to the experimental investigations reported in the First Semiannual Report. Repetition and overlap will be presented only as required for completeness.

4.2 ADDITIONAL MEASUREMENT EQUIPMENT

Equipment is in operation for measuring the following properties of ferrimagnetic oxides: density, saturation magnetization ($4\pi M_s$), g-factor, linewidth (ΔH), anisotropy field, Curie temperature, dielectric constant, dielectric loss tangent, grain size, extraneous phases in materials, squareness, and coercive field. The equipment used to measure these properties was described in the First Semiannual Report.

During this reporting period, it became apparent that the measurement of $4\pi M_S$ and "squareness" (referred to erroneously as remanence ratio in First Semiannual Report) are not sufficient to evaluate properly and classify the materials for FDPS applications. The additional measurement required (and of major importance) is that of the absolute value of the remanent magnetization ($4\pi M_R$). For a given geometrical configuration the phase shift per unit length is directly proportional to the $4\pi M_R$: in addition, the $4\pi M_R$ for a given material should be maximized through design of toroidal geometries. This aspect directly influences the design considerations for optimized rf structures. The square loop tester was therefore modified for the measurement of the remanent magnetization for drive fields normally utilized in FDPS.

The schematic diagram of the circuit used is shown in Figure 16. The technique and analytical expressions utilized were discussed in Section 3.3. The "squareness" $\left(S_D = \dfrac{4\pi M_{RD}}{4\pi M_D} \right)$ is measured from the hysteresis loop. The peak reading voltmeter is calibrated using a toroidal material of known remanent magnetization supplied by Don Temme of M.I.T. Lincoln Labs. The $4\pi M_D$ is then obtained using the "squareness" measurement. For regular shaped samples of moderate size (0.5" diameter x 1" long), the relative accuracy is approximately $\pm 3\%$. The drive field used is normally 5 to 10 times the coercive field of the material.

4.3 MATERIAL INVESTIGATIONS

The First Semiannual Report contained a listing and description of many garnet materials which were prepared and evaluated. Special attention was devoted to those compositions exhibiting temperature stability of the magnetization. These compositions included principally the gadolinium and aluminum substituted yttrium iron garnets. Other rare earth (dysprosium, holmium, ytterbium, erbium and samarium) substituted yttrium iron garnets were prepared and evaluated for possible high peak power applications.

The remanent magnetization (which was not previously measured on these samples) has been measured during this reporting period for many of these compositions and this information is included in Table I.

The preparation procedure used in fabricating these materials was described in the First Semiannual Report. The same basic preparation procedure has been used to prepare all materials. Modified procedures will be described where utilized.

Table I. REPRESENTATIVE DATA OF GARNET

EVALUATED AT ROOM TEMPERATUI
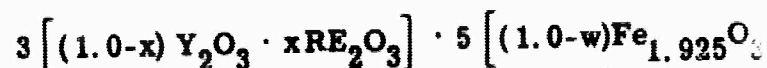
$$3\left[(1.0-x)\,Y_2O_3 \cdot x\,RE_2O_3\right] \cdot 5\left[(1.0-w)Fe_{1.925}O_3\right.$$

SMEC NO.	COMPOSITION x	w	BATCH SIZE (gms)	WAXING TIME (HRS)	FIRING SCHEDULE °C/hr	SAMPLE SHAPE	DENSITY gms/cm³	PARTICLE SIZE (MICRONS)	DIELECTRIC LOSS TAN. (X BAND)	DIELECTRIC CONSTANT (X BAND)	g FACTOR	LINE WIDTH AN (X BAN)
G-289-4G	0	0	750	16	1475/5	F	5.11	16	<0.0001	15.7	2.01	3
G-289 S	0	0	750	16	1475/5	D	5.09	15	<0.0001	15.7	2.02	4
PG-232-58C	0	0	1450	24	1475/5	F	5.10	NM	<0.0001	16.0	2.02	4
PG-232-71-3	0	0	1450	24	1475/5	G	5.06	NM	<0.0001	16.0	2.02	4
PG-232-61F	0	0	1450	24	1475/5	E	5.11	16	<0.0001	16.0	2.02	3
D30A1-37C	0	0	3700	24	1475/5	F	5.07	NM	<0.0001	16.0	2.02	4
G-290M	0	0.03	750	16	1475/5	D	5.07	16	<0.0001	15.5	2.01	3
G-404-2C	0	0.05	750	16	1475/5	E	5.08	NM	<0.0001	15.8	2.01	3
G-404-2C	0	0.05	750	16	1475/5	D	5.07	9	<0.0001	15.7	2.01	3
G-291Q	0	0.08	750	16	1475/5	D	5.05	15	<0.0001	15.4	2.01	3
G-243-2C	0	0.10	750	16	1475/5	D	5.02	10	<0.0001	15.2	2.01	36
PG-243-5y	0	0.10	710	16	1475/5	E	5.02	NM	<0.0001	15.2	2.01	3
G-292-R	0	0.12	750	16	1475/5	D	5.04	10	<0.0001	15.3	2.01	30
G-293-P	0	0.15	750	16	1475/5	F	5.04	NM	<0.0001	15.1	2.01	3
G-293-2B	0	0.15	750	16	1475/5	F	5.02	NM	NM	NM	2.01	3
G-293-U	0	0.15	750	16	1475/5	D	5.04	8	<0.0001	15.0	2.01	3
G-293-R	0	0.15	750	16	1500/5	D	5.04	14	<0.0001	15.0	2.01	30
G-238-5C	0	0.20	750	16	1500/5	D	4.99	10	<0.0001	14.9	2.02	3
G-250-2B	0	0.25	750	4	1475/5	F	4.86	NM	<0.0001	14.4	NM	N
G-250-4B	0	0.25	750	16	1500/5	F	4.97	NM	<0.0001	14.6	2.03	50
G-250-4C	0	0.25	750	16	1500/5	D	4.98	9	<0.0001	14.6	2.03	50
G-345-K	0.01 Dy	0	750	16	1475/5	D	5.09	NM	<0.0001	15.6	NM	N
G-129-2C	0.02 Dy	0	750	16	1475/5	D	5.13	NM	<0.0001	15.7	1.99	8
G-351-2D	0.05 Dy	0	750	16	1475/5	D	5.17	NM	<0.0001	15.6	1.94	16
G-321-G	0.08 Dy	0	750	24	1475/5	F	5.23	12	0.0002	15.7	1.90	23
G-131-2C	0.10 Dy	0	750	16	1475/5	D	5.26	NM	<0.0001	15.9	1.88	280

A

$$)Fe_{1.925}O_3 \cdot wA\ell_{1.925}O_3\big]$$

FACTOR	LINE WIDTH ΔH (oe) X BAND	4πMs (GAUSS)	DRIVE CURRENT Ib (AMPS RMS)	COERCIVE FIELD Hc(oe)(60~)	COERCIVE FIELD (HD/Hc)	SQUARENESS SD	4πMR0 (GAUSS)	REMANENCE RATIO R0	
2.01	30	1800	4.7	0.54	6	0.90	1240	0.69	
2.02	40	1780	3.3	0.28	10	0.84	1173	0.66	
2.02	40	1780	5.2	0.36	10	0.90	1358	0.76	
2.02	45	1780	10.0	0.36	10	0.87	1250	0.70	
2.02	35	1780	4.4	0.50	10	0.90	1037	0.58	
2.02	45	1780	6.20	0.42	10	0.90	1304	0.73	
2.01	33	1650	4.65	0.39	10	0.86	1280	0.78	
2.01	30	1375	4.80	0.55	10	0.83	780	0.57	
2.01	31	1375	5.75	0.49	10	0.84	995	0.72	
2.01	33	1200	4.90	0.42	10	0.83	793	0.66	
2.01	38	960	7.20	0.61	10	0.81	720	0.75	
2.01	35	960	6.10	0.70	10	0.87	581	0.61	
2.01	30	900	7.05	0.60	10	0.84	660	0.73	
2.01	36	700	8.7	0.60	10	0.86	505	0.72	
2.01	34	675	10	0.68	10	0.87	485	0.72	
2.01	33	675	7.75	0.66	10	0.80	490	0.73	
2.01	30	675	4.60	0.39	10	0.78	470	0.70	
2.02	36	380	4.30	0.37	10	0.87	305	0.80	
NM	NM	220	10	0.92	7.2	0.66	125	0.57	
2.03	50	220	8	0.55	10	0.71	130	0.59	
2.03	50	180	6.25	0.51	10	0.77	135	0.75	
NM	NM	1780	4.30	0.37	10	0.86	1200	0.67	
1.99	80	1780	4.20	0.36	10	0.87	1320	0.74	
1.94	165	1770	5.45	0.46	10	0.72	1005	0.57	
1.90	230	1765	7.4	0.50	10	0.87	1225	0.69	
1.88	280	1700	5.10	0.43	10	0.83	1155	0.68	

*SAMPLE SHAPE

B

27740

$$3\left[(1.0-x)Y_2O_3 \cdot xRE_2O_3\right]\cdot 5\ (1.0-w)Fe_{1.92\bar{b}}$$

SMEC NO.	COMPOSITION x	w	BATCH SIZE (gms)	WAXING TIME (HRS)	FIRING SCHEDULE °C/hr	SAMPLE SHAPE	DENSITY gms/cm³	PARTICLE SIZE (MICRONS)	DIELECTRIC LOSS TAN. (X BAND)	DIELECTRIC CONSTANT (X BAND)	g FACTOR	LINE WIDTH ΔH (oe) X BAND
G-295-J	0.15 Gd	0	750	16	1475/5	F	5.32	NM	<0.0001	16.0	2.02	37
G-295-E	0.15 Gd	0	750	16	1475/5	B	5.30	NM	<0.0001	16.0	2.02	40
G-295-F	0.15 Gd	0	750	16	1475/5	A	5.30	NM	<0.0001	16.0	NM	NM
G-295-G	0.15 Gd	0	750	16	1475/5	C	5.30	NM	<0.0001	16.0	NM	NM
G-429-C	0.25 Gd	0	750	16	1475/5	D	5.42	NM	<0.0001	16.0	2.02	70
G-296-10C	0.30 Gd	0	750	24	1475/5	F	5.49	NM	<0.0001	16.1	2.02	65
G-296-18G	0.30 Gd	0	3000	24	1475/5	A	5.45	NM	<0.0001	16.1	2.02	82
G-296-18J	0.30 Gd	0	3000	24	1475/5	C	5.45	NM	<0.0001	16.1	2.02	80
G-296-18H	0.30 Gd	0	3000	24	1475/5	B	5.44	NM	<0.0001	16.1	2.02	80
G-297-C	0.45 Gd	0	750	16	1475/5	F	5.70	18	NM	NM	2.03	107
G-298-C	0.60 Gd	0	750	16	1475/5	F	5.82	16	<0.0001	16.4	2.05	210
G-287-2C	0.04 Dy	0.08	750	24	1500/5	F	5.10	NM	NM	NM	1.94	140
G-286-2B	0.02 Dy	0.08	750	16	1475/5	F	5.09	NM	<0.0001	15.8	1.97	85
G-286-5B	0.02 Dy	0.08	750	16	1475/5	F	5.11	NM	<0.0001	15.5	1.98	86
G-430-D	0.06 Dy	0.05	750	16	1475/5	D	5.18	NM	<0.0001	15.3	1.91	195
G-300-C	0.30 Gd 0.04 Dy	0	750	16	1475/5	F	5.57	NM	NM	NM	1.94	170
G-299-2B	0.30 Gd 0.02 Dy	0	750	16	1475/5	F	5.53	NM	NM	NM	1.98	130
G-251-27C	0.15 Gd	0.05	750	24	1500/5	F	5.28	18	<0.0001	15.6	2.02	45
PG-251-2E	0.15 Gd	0.05	1500	32	1475/5	F	5.21	NM	<0.0001	15.7	2.02	50
G-305-2C	0.15 Gd	0.07	210	12	1475/5	F	5.28	NM	0.0003	15.7	NM	NM
G-302-C	0.15 Gd	0.02	750	16	1475/5	F	5.26	8	NM	NM	2.02	52
G-303-M	0.15 Gd	0.15	750	16	1500/5	F	5.21	NM	<0.0001	15.1	2.03	95
G-330-3B	0.30 Gd	0.05	220	4	1475/5	F	5.40	NM	<0.0001	15.8	2.02	80
G-284-E	0.01 Ho	0.08	750	16	75/5	F	5.09	NM	NM	NM	2.00	72
G-288-E	0.15 Gd 0.02 Dy	1.05	750	16	1475/5	F	5.32	NM	NM	NM	1.98	105

NM - Not Measured

2975-2 S/A

4-4

A

$$_3] \cdot 5 \; (1.0-w)Fe_{1.925}O_3 \cdot wA\ell_{1.925}O_3]$$

ELECTRIC CONSTANT (X BAND)	g FACTOR	LINE WIDTH ΔH (oe) X BAND	$4\pi M_s$ (GAUSS)	DRIVE CURRENT I_D (AMPS RMS)	COERCIVE FIELD H_c (oe)(60~)	COERCIVE FIELD (F_D/H_c)	SQUARENESS S_D	$4\pi M_{RD}$ (GAUSS)	REMANENCE RATIO R_R		
16.0	2.02	37	1530	8.8	0.61	10	0.84	1010	0.66		
16.0	2.02	40	1530	5.7	0.65	10	0.81	960	0.63		
16.0	NM	NM	1530	5	0.60	10	0.87	950	0.62		
16.0	NM	NM	1530	4.2	0.60	10	0.62	960	0.63		
16.0	2.02	70	1300	7.50	0.65	10	0.60	590	0.45		
16.1	2.02	65	1240	8.6	0.81	10	0.81	815	0.66		
16.1	2.02	82	1240	5.8	0.70	10	0.71	580	0.47		
16.1	2.02	80	1240	4.8	0.70	10	0.58	635	0.51		
16.1	2.02	80	1240	6.1	0.70	10	0.74	620	0.50		
NM	2.03	107	1040	10	1.29	5.5	0.62	360	0.35		
16.4	2.05	210	770	10	1.90	3.7	0.60	240	0.31		
NM	1.94	140	1120	6.7	0.47	10	0.84	730	0.65		
15.8	1.97	85	1240	7.1	0.49	10	0.88	775	0.63		
15.5	1.98	86	1240	8.5	0.57	10	0.86	840	0.68		
15.3	1.91	195	1300	5.35	0.45	10	0.85	950	0.73		
NM	1.94	170	1220	10	0.72	9.3	0.83	820	0.67		
NM	1.98	130	1240	9.3	0.63	10	0.79	890	0.72		
15.6	2.02	45	1150	6.6	0.48	10	0.88	845	0.73		
15.7	2.02	50	1150	7.4	0.99	10	0.89	880	0.77		
15.7	NM	NM	935	8.0	0.54	10	0.83	660	0.71		
NM	2.02	52	805	10	0.90	7.5	0.80	500	0.62		
15.1	2.03	95	795	10	0.91	7.6	0.97	375	0.76		
15.8	2.02	80	940	10	1.10	6.1	0.57	380	0.41		
NM	2.00	72	1165	7.6	0.50	10	0.88	840	0.72		
NM	1.98	105	1135	10	0.84	8	0.76	660	0.58		

B

4.3.1 Garnet Materials

Table I lists the microwave and magnetic properties of the following families of garnet materials:

$$3\left[(1-x)\,Y_2O_3\cdot xRE_2O_3\right]\cdot 5\left[(1-w)Fe_{1.925}O_3\cdot wA\ell_{1.925}O_3\right]$$
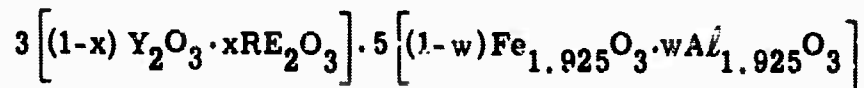
where RE represents the rare earth oxides of gadolinium, dysprosium, terbium, erbium and holmium.

The sample nomenclature being used on this program is as follows:

Example: G-251 - 15 C

Designates a particular composition

Designates the batch number of this particular composition

Designates the particular sample pressed from this composition and batch
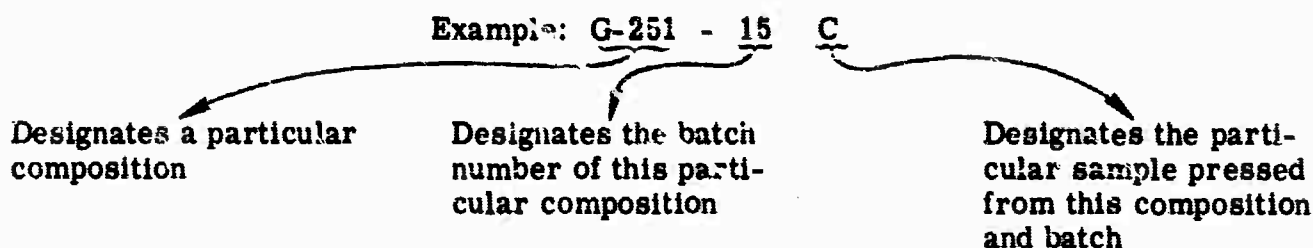
Data of particular importance to note in Table I are as follows:

1. Compare the $4\pi M_s$ values with the measured $4\pi M_{RD}$ (approximately the remanent magnetization) values and the squareness with remanence ratios.

2. It is apparent that no samples are being driven into saturation at the drive fields used.

3. Remanence ratios $\left(R_R = \dfrac{4\pi M_{RD}}{4\pi M_s}\right)$ are typically in the 0.6 to 0.8 region for squareness values of 0.8 to 0.9.

4. In general, the values of squareness obtained with typical drive fields cannot be used to classify the exact values of remanent magnetization. Typically, however, samples possessing higher values of squareness possess large remanent magnetizations. Representative examples of this trend are presented in Figures 17 and 18. Figure 17 presents magnetization versus squareness data measured on nine different batches of the same composition (G-289, YIG) and 25 different batches of G-251 (15% Gd and 5% Aℓ substituted YIG). Processing variables were altered in some batches to vary squareness. Similar data are presented in Figure 18 for 22 batches of G-296 (30% Gd substituted YIG). For a given squareness value, the spread in remanent magnetization is as much as ± 40 gauss. For a given remanent magnetization, the spread in squareness is approximately ± 0.025. The relationship and controlling factors of these two parameters are presently not clearly detailed. Processing parameters including the physical characteristics of the starting oxides are believed to influence their control heavily. Squareness and coercive fields are certainly affected by
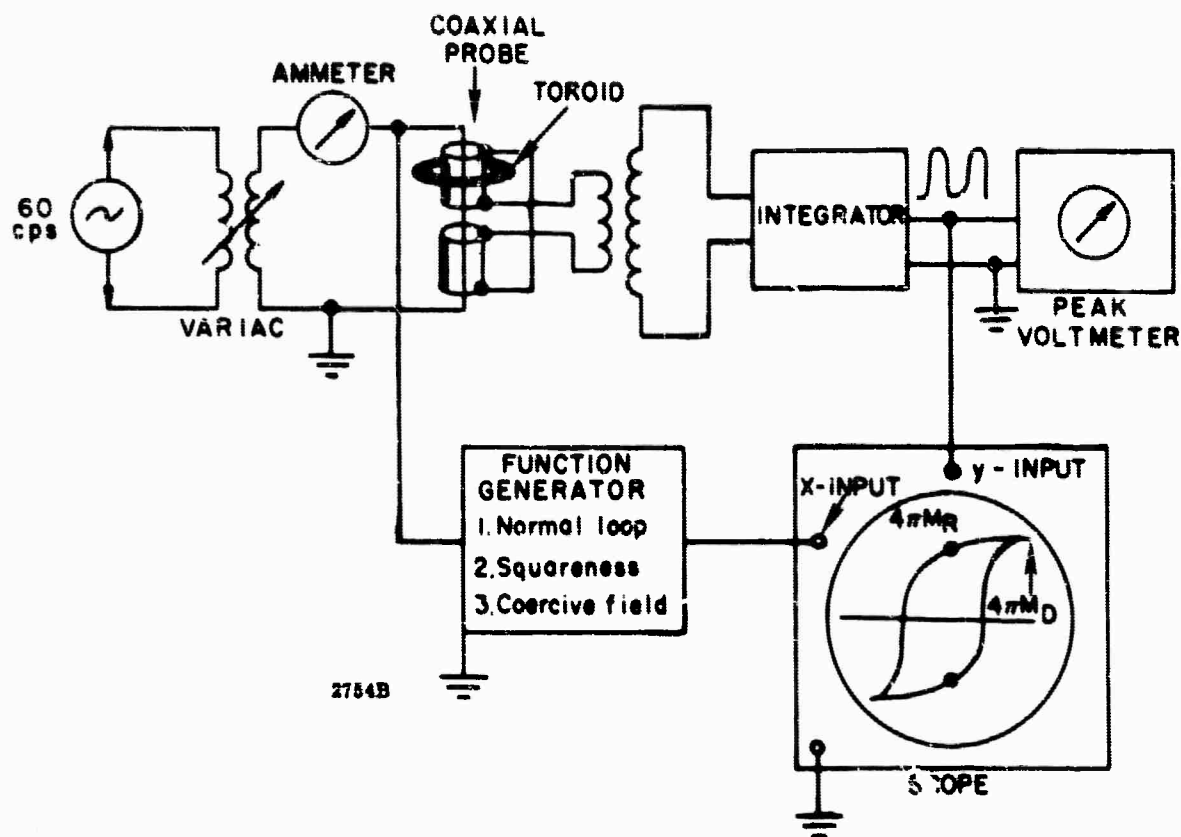
Figure 16.   Schematic of Square Loop Tester Modified for Measuring the Remanent Magnetization
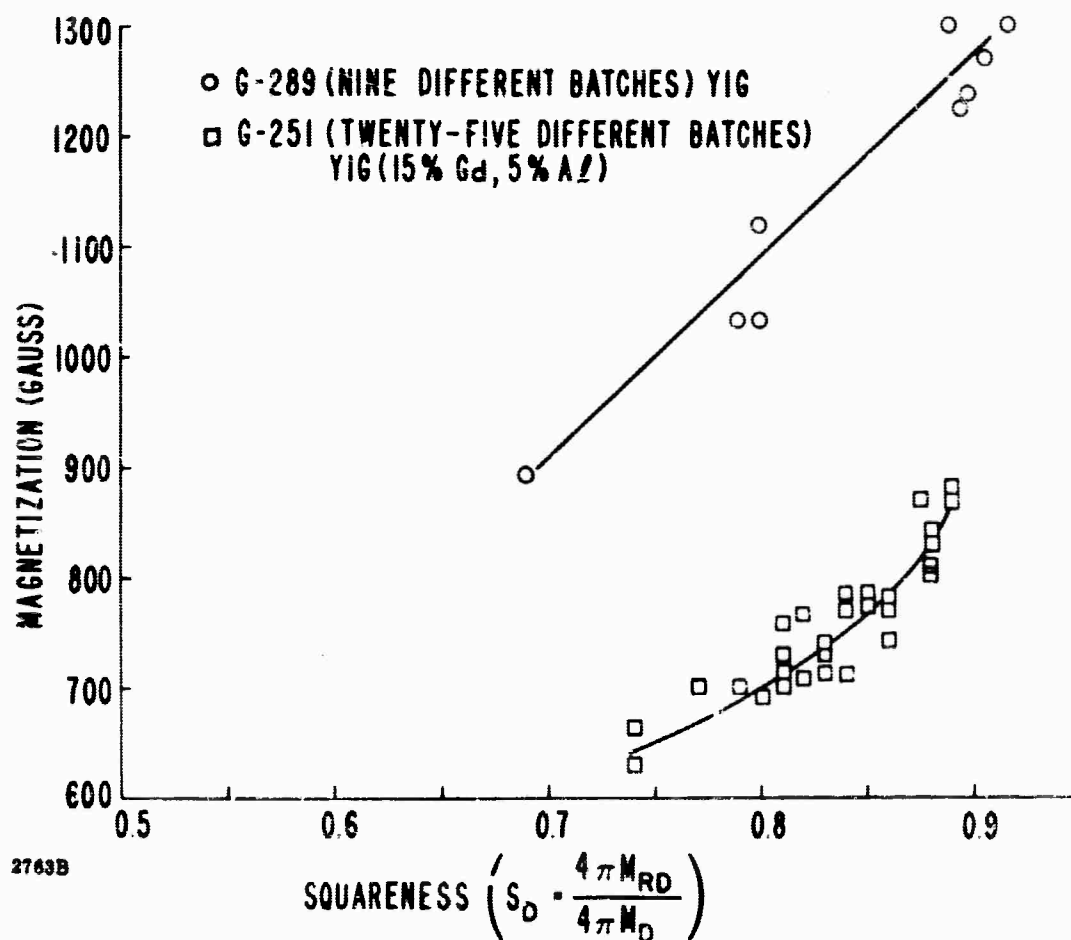
Figure 17.   Magnetization Versus Squareness for G-289 (YIG) and G-251, YIG (15% Gd, 5% Al)

particle sizes; however, when squareness is improved by optimizing particle size, it is not completely clear, at present, whether this adjustment also improves the remanent magnetization proportionately. For a given drive field, a reduction in coercive field by optimizing particle sizes would produce some increase in the remanent magnetization. In conclusion of this discussion, higher values of squareness (may imply also lower coercive field) typically produce larger values of remanent magnetization. The measurement of squareness alone, however, is not sufficient to classify the remanent magnetization (not sufficient to compute absolute or even relative values of remanent magnetization).

5. The drive fields used in Table I for the measurement of $4\pi M_{RD}$ are typical for those utilized in phase shifters. The measured values of $4\pi M_{RD}$ at these drive fields are not the saturated remanent magnetization values; however, the values tabulated should be very near those encountered in digital phase shifter applications. It is expected that the values of remanent magnetization ($4\pi M_{RD}$) would not increase greatly for larger drive fields. Typical data for a square toroid of G-296 are presented in Figure 19. These data indicate that at a drive field of 10 H_c, the remanent magnetization has reached a value of 95% maximum even though the material is only 80% saturated at this drive. This indicates that very little would be gained in phase shift by driving much harder. The gain in phase shift would certainly not compensate for the increased drive power required.

6. The coercive field and remanence ratios do not seem to be a strong function of composition. Large ranges in $4\pi M_s$ and $4\pi M_{RD}$ values can be obtained by aluminum and rare earth substitutions. Rare earth substitutions can be made to improve peak power thresholds without severely altering the hysteresis properties of the material.

7. Values of remanent magnetization seem to be influenced to a degree by the toroid shape. Particularly note the compositions G-296 and G-295 in Table I. Round or thin-walled square toroids of the same composition generally possess high values of remanent magnetization than narrow slotted, thick-walled toroids. This indicates that where possible thin-walled toroids with appropriate dielectric loading should be used in phase shifter designs for maximum utilization of the magnetization.

8. It has been observed when toroids are annealed after machining to improve squareness, that improvement is also generally obtained in the remanent magnetization and coercive field.
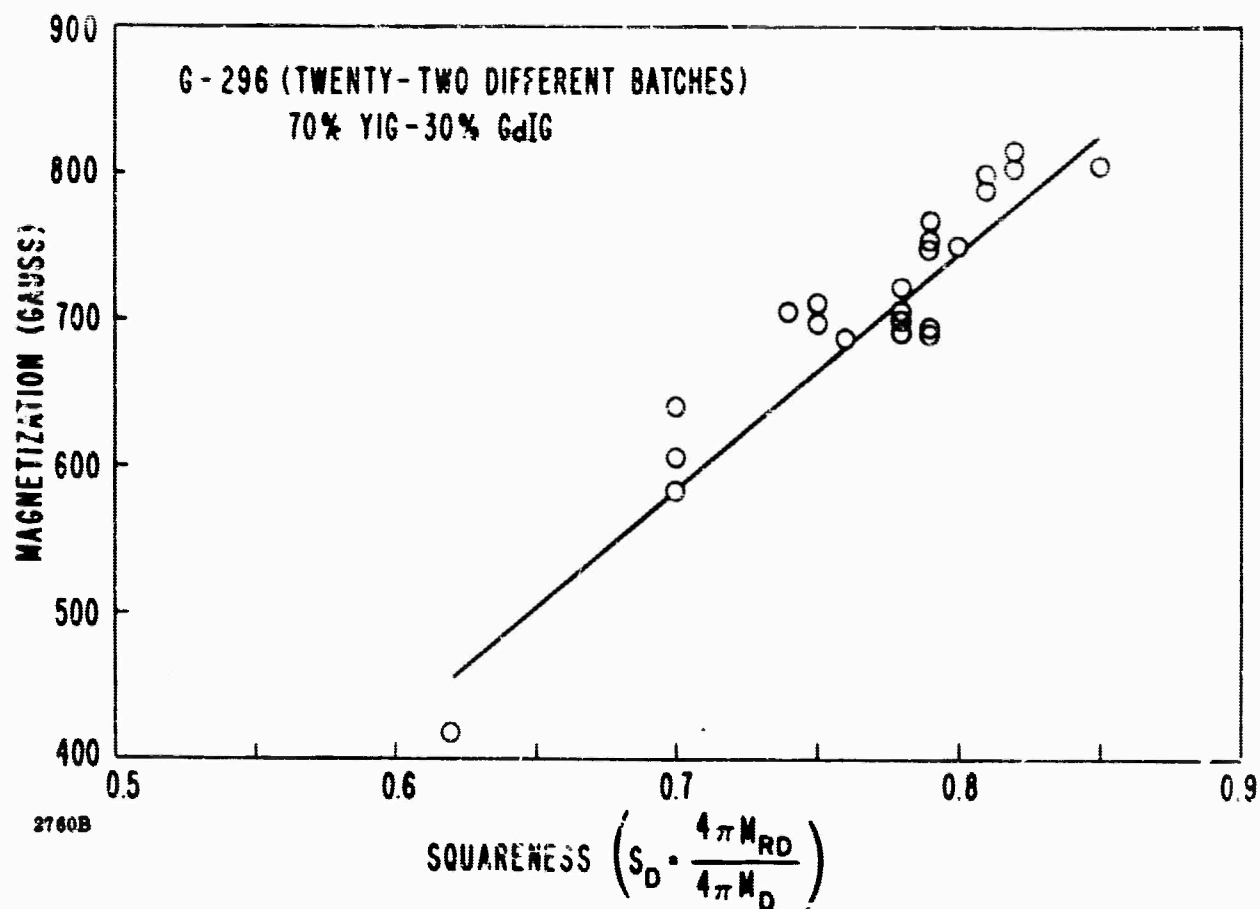
Figure 18.   Magnetization Versus Squareness for G-296, 70% YIG - 30% Gd IG
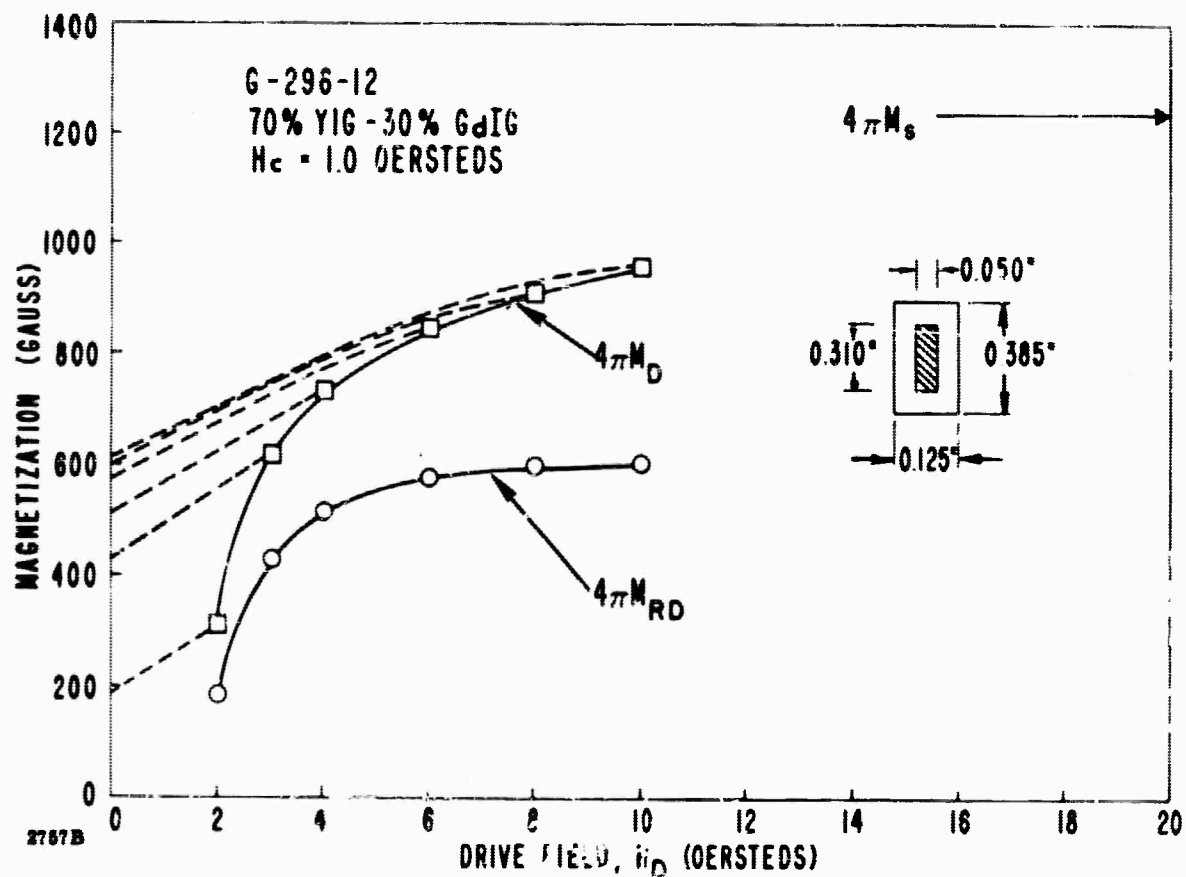
Figure 19.   Magnetization Versus Drive Field for a Rectangular Toroid

9. Many of the samples tabulated in Table I were used in the magnetic loss investigations to be discussed later in the report.

Some problems have been encountered in reproducing (batch to batch) samples of the same composition possessing comparable values of squareness and remanent magnetization. These problems have been most predominent for those compositions containing gadolinium. Some typical data were presented in Figures 18 and 19 where variations of ± 0.05 in squareness have been observed for identically processed batches. Many of these batches were experimental in that processing parameters were not closely controlled and, in some cases, purposely altered to study optimized techniques. The problems observed are believed to be associated with the particle size of the raw oxides and the subsequent processing of the oxides. Details are presently being studied to isolate the problem areas.

The characteristics of some controlled batches (same size, processed identically) have been observed with particular emphasis on the reproducibility of hysteresis properties. Tabulated in Table II are data obtained on six identical large batches of yttrium iron garnet. The coercive field, remanent magnetization, and remanence ratio were reproduced quite well for these batches. The variations observed are comparable to measurement accuracies.

Table III contains data collected on 12 different samples (same size, processed identically) from the same batch of material (yttrium iron garnet). The sample-to-sample variation in remanent magnetization noted in Table III is comparable to the batch to batch variation presented in Table II. Measurement accuracies are again comparable to the variations observed.

4.3.2 Ferrite Materials

The compositions and properties of the ferrite materials prepared and evaluated during this period are listed in Table IV.

The compositions were composed of —

- Nickel ferrite
- Nickel zinc ferrites
- Magnesium manganese aluminum ferrites
- Lithium ferrites.

The nickel zinc ferrites are characterized by reasonably large values of $4\pi M_s$ as shown in Table IV. These compositions were investigated principally to tabulate their hysteresis properties. No effort was expended in trying necessarily to optimize the hysteresis properties.

The magnesium manganese ferrite compositions were known to possess good hysteresis properties since these materials are very often used for computer applications. The studies conducted on this program were to yield hysteresis properties of materials previously found acceptable for microwave applications. Good squareness was obtained on essentially all compounds, but remanence ratios were relatively low. The coercive fields also were not as low as the values measured on garnet materials possessing comparable $4\pi M_s$ values.

The lithium ferrites exhibited very square hysteresis properties. These materials are particularly inviting from the standpoint that they possess very high Curie temperatures ($680^\circ C$) and very good hysteresis properties. However, the dielectric loss tangents of those materials are extremely high. This has been a problem in using the lithium ferrite compounds for microwave applications. No consistent techniques are presently known to reduce these loss tangents to acceptable values for use in digital phase shifters. Some interest has been expressed in these materials for temperature compensating effects in digital phase shifters using composite toroidal geometries. This interest has been expressed by the MIT Lincoln Laboratory investigators* in regard to external temperature compensation of phase shifters.

For the compounds studied, the particle size variation in the ferrites is much broader than that observed in the garnet materials. Particle sizes range from 2 to 3 microns to greater than 200 microns. This variation is attributed to the fact that these materials are much more sensitive to firing temperatures than are the garnet materials.

Experimental data collected to date indicate that the coercive field continues to decrease with increasing particle size. However, an optimum particle size range exists for maximum values of squareness. It appears that the particle size in some of the ferrite materials may need to be reduced rather than increased as concluded from the study of the garnet materials. The optimum particle size desired for maximum squareness seems to fall in the region of 10 to 30 microns, depending on the specific composition.

Measured values of remanent magnetization and remanence ratio point up the fact that while hysteresis loop squareness and remanence ratio generally vary together, there is no hard and fast correlation. Lithium ferrites with squareness ratios near 0.90 are observed to have remanence ratios between 0.68 and 0.43.

In general, these spinel ferrites have measured remanence ratios markedly lower than those of garnets, even when comparable squareness is measured on the two

*Private communication with Mr. E. Stern and Mr. D. Temme of MIT Lincoln Laboratory.

TABLE II.   REPRODUCIBILITY OF HYSTERESIS

SMEC NO		COMPOSITION	BATCH SIZE (gms)	SAMPLE SHAPE		$4\pi M_s$** (gauss)	DRIVE CURRENT i_g (AMPS)	COERCIVE FIELD (m.)(oe) 60~	DRIVE FIELD COERCIVE F. Hd/Hc
D80A1-36B		YTTRIUM IRON GARNET	3700	F		1780	5.4	0.38	10
-37B		$(3Y_2O_3 \cdot 5Fe_{1.925}O_3)$	3700	F		1780	6.2	0.42	10
-39B			3700	F		1780	6.3	0.43	10
-40B			3700	F		1780	6.0	0.41	10
-42B			3700	F		1780	6.0	0.41	10
-43B		↓	3700	F		1780	6.5	0.45	10

TABLE III.   REPRODUCIBILITY OF HYSTERESIS P

		COMPOSITION	BATCH SIZE	SAMPLE SHAPE		$4\pi M_s$	DRIVE CURRENT	COERCIVE FIELD	Hd/Hc
PG-232-71		YTTRIUM IRON GARNET							
#1		$(3Y_2O_3 \cdot 5Fe_{1.925}O_3)$	1450	G*		1780**	9.5	0.34	10
#2							10	0.41	9
#3							10	0.37	10
#4							9.9	0.36	10
#5							10	0.44	8
#6							10	0.35	10
#7							10	0.36	10
#8							10	0.36	10
#9							10	0.38	9.5
#10							10	0.23	8.5
#11							10	0.40	9
#12		↓	↓	↓		↓	10	0.37	10

2975 -2 S/A

A

F HYSTERESIS PROPERTIES (BATCH TO BATCH)

CURRENT (S)	COERCIVE FIELD (H_c)(oe) 60~	DRIVE FIELD/COERCIVE FIELD H_d/H_c		SQUARENESS S_d	$4\pi M_{rd}$ (GAUSS)	PERMANENCE RATIO (R_d)
	0.38	10		0.89	1220	0.69
	0.42	10		0.90	1270	0.71
	0.43	10		0.90	1240	0.70
	0.41	10		0.87	1260	0.71
	0.41	10		0.90	1265	0.71
	0.45	10		0.89	1245	0.70

* See Table I

** Typical value ± 20 gauss

NOTE: Average $4\pi M_{RD}$ = (1250 ± 25) gauss

HYSTERESIS PROPERTIES (SAMPLE TO SAMPLE)

	0.34	10		0.88	1245	0.70
	0.41	9		0.85	1195	0.67
	0.37	10		0.87	1250	0.70
	0.36	10		0.86	1200	0.67
	0.44	8		0.82	1130	0.63
	0.35	10		0.86	1230	0.69
	0.36	10		0.86	1230	0.69
	0.36	10		0.85	1220	0.69
	0.38	9.5		0.85	1215	0.68
	0.23	8.5		0.84	1170	0.65
	0.40	9		0.84	1180	0.66
	0.37	10		0.86	1225	0.69

* See Table I

** Typical value ± 25 gauss

NOTE: Average $4\pi M_{RD}$ = (1210 ± 25) gauss

B

TABLE IV. REPRESENTATIVE ROOM TEMPERATURE DATA ON FER...

SAMPLE NO.	COMPOSITION			BATCH SIZE (gms)	WAXING TIME (hrs)	FIRING SCHEDULE (°C/hrs)	SAMPLE SHAPE*	DENSITY (gm/cm³)	PARTICLE SIZE (MICRONS)
117Z	$Li_{1.0}Mn_{0.02}Fe_{4.875}O_8\pm$			860	4	1200-7	F	4.41	>150
114Z	$Li_{1.0}Mn_{0.02}Fe_{5.0}O_8$			880	4	1200-7	F	4.45	>200
119Z	$Li_{1.0}Mn_{0.02}Fe_{4.0}Al_{0.875}O_8\pm$			810	4	1200-7	F	4.33	25
119-2F	$Li_{1.0}Mn_{0.02}Fe_{4.0}Al_{0.875}O_8\pm$			810	4	1250-2	F	4.40	NM
119-J	$Li_{1.0}Mn_{0.02}Fe_{4.0}Al_{0.875}O_8\pm$			810	4	1250-7	F	4.33	NM
26-5	$Ni_{0.90}Zn_{0.10}Mn_{0.02}Fe_{1.9}O_4\pm$			1350	4	1250-7	F	5.16	7
73-3Z	$Ni_{0.87}Zn_{0.13}Mn_{0.02}Fe_{1.9}O_4\pm$			1500	4	1250-7	F	5.14	8
23-2Z	$Ni_{0.80}Zn_{0.20}Mn_{0.02}Fe_{1.9}O_4\pm$			1380	4	1250-7	F	5.07	7
23-3H	$Ni_{0.70}Zn_{0.30}Mn_{0.02}Fe_{1.9}O_4\pm$			1350	4	1250-7	F	5.12	8
29-3Z	$Ni_{0.70}Zn_{0.30}Mn_{0.02}Fe_{1.9}O_4\pm$			1350	4	1250-7	F	5.13	8
15-3Z	$Ni_{0.60}Zn_{0.40}Mn_{0.02}Fe_{1.9}O_4\pm$			1350	4	1250-7	F	4.91	NM
91-Z	$Ni_{0.44}Zn_{0.56}Mn_{0.02}Fe_{1.9}O_4\pm$			1300	4	1250-7	F	5.01	4
62-Z	$Ni_{0.35}Zn_{0.65}Mn_{0.02}Fe_{1.9}O_4\pm$			1370	4	1200-7	F	5.11	NM
62-S	$Ni_{0.35}Zn_{0.65}Mn_{0.02}Fe_{1.9}O_4\pm$			1370	4	1225-7	F	5.07	NM
62-R	$Ni_{0.35}Zn_{0.65}Mn_{0.02}Fe_{1.9}O_4\pm$			1370	4	1200-1	F	5.11	NM
62-Z	$Ni_{0.35}Zn_{0.65}Mn_{0.02}Fe_{1.9}O_4\pm$			1370	4	1250-7	F	5.11	>120
PF83-18C	$58\%MgO\cdot6\%ZnO\cdot36\%Fe_2O_3$			3100	4	1320-7	F	4.30	6
PF83-18B	$58\%MgO\cdot6\%ZnO\cdot36\%Fe_2O_3$			3100	4	1320-7	F	4.30	NM
PF83-16Z	$58\%MgO\cdot6\%ZnO\cdot36\%Fe_2O_3$			3100	4	1300-7	F	4.30	NM
PF83-17E	$58\%MgO\cdot6\%ZnO\cdot36\%Fe_2O_3$			3100	4	1300-7	F	4.22	NM
PF83-12B	$58\%MgO\cdot6\%ZnO\cdot36\%Fe_2O_3$			880	4	1300-7	F	4.12	NM
118-Z	$47.75\%MgO\cdot5.25\%MnO\cdot47\%Fe_2O_3$			1500	4	1300-7	F	4.33	7
116-Z	$50\%MgO\cdot1.5\%MnO\cdot2.5\%Al_2O_3\cdot46\%Fe_2O_3$			1000	4	1300-7	F	4.18	4
17-2Z	$MgO_{1.50}Mn_{0.10}Fe_2O_3$			1350	4	1300-7	F	3.90	4
121-Z	$Mg_{0.87}Mn_{0.04}Cu_{0.1}Co_{0.03}Al_{0.27}Fe_{1.48}O_4\pm$			370	4	1300-7	F	4.35	16
65-25C	$51.62\%MgO\cdot5.68\%MnO\cdot9.1\%Al_2O_3\cdot33.6\%Fe_2O_3$			4330	4	1400-7	F	3.38	NM

A

ON FERRITE COMPOSITIONS PREPARED AND EVALUATED

PARTICLE SIZE (MICRONS)	DIELECTRIC LOSS TAN X-BAND	DIELECTRIC CONSTANT X-BAND	ε_{eff} FACTOR	LINE WIDTH ΔH X-BAND	$4\pi M_S$ (GAUSS)	I_D (AMPS)	H_c (OE., 60~)	DRIVE FIELD COER FIELD	SQUARENESS S_D	$4\pi M_R$ (GAUSS)	R_R	
>150	NM	NM	2.17	375	3360	10	1.9	3.7	.96	2290	.68	
>200	NM	NM	2.10	390	3470	10	1.7	4.0	.94	2274	.65	
25	NM	NM	2.11	768	1350	10	3.4	2.1	.95	758	.56	
NM	NM	NM	NM	NM	1350	10	2.3	3.2	.90	727	.54	
NM	NM	NM	NM	NM	1350	10	3.1	2.2	.92	711	.53	
7	NM	NM	2.25	304	3770	10	3.4	2.2	.69	893	.24	
8	NM	NM	2.25	268	3900	10	3.1	2.4	.67	1082	.28	
7	NM	M	2.24	222	4240	10	2.4	3.1	.70	1459	.35	
8	NM	NM	2.2	132	4730	10	1.7	4.3	.77	2167	.46	
8	NM	NM	2.17	138	4730	10	1.5	5	.69	1898	.43	
NM	NM	NM	NM	NM	4700	10	1.1	6.5	.70	2194	.47	
4	NM	NM	2.1	105	4200	4.7	.30	10	.59	1688	.40	
NM	NM	NM	NM	NM	3080	10	.22	10	.43	877	.28	
NM	NM	NM	NM	NM	3080	2.6	.19	10	.35	664	.22	
NM	NM	NM	2.08	73	3369	6.5	.47	10	.36	756	.20	
>120	NM	NM	NM	NM	3360	2.2	.16	10	.30	557	.17	
6	<0.0001	13.3	2.1	470	2200	10	1.8	4	.85	1161	.53	
NM	<0.0001	13.3	NM	NM	2200	10	1.8	4	.85	1134	.52	
NM	NM	NM	NM	NM	2200	10	2.3	3.1	.84	1128	.51	
NM	<0.0001	13.1	NM	NM	2200	10	2.5	2.8	.85	1014	.46	
NM	NM	NM	NM	NM	2200	10	2.5	2.8	.83	967	.44	
7	NM	NM	2.04	270	2190	10	3.2	2.2	.93	1050	.48	
4	NM	NM	2.05	250	1903	10	3.4	2.0	.88	823	.43	
4	NM	NM	2.09	572	1622	10	1.9	3.5	.82	496	.44	
16	0.0005	12.3	2.04	260	1480	10	2.6	2.7	.65	421	.28	
NM	NM	NM	NM	NM	1140	10	.83	8.3	.79	641	.56	

B

TABLE IV. REPRESENTATIVE ROOM TEMPERATURE DATA ON

SAMPLE NO.	COMPOSITION				BATCH SIZE (gms)	WAXING TIME (hrs)	FIRING SCHEDULE (°C/hrs)	SAMPLE SHAPE*	DENSITY (gm/cm³)	PARTICLE SIZE (MICRONS)	DIELECTRIC LOSS X-BAND
65-26E	$51.62\%Mg0\cdot5.68\%Zn0\cdot9.1\%Al_2O_3\cdot33.6\%Fe_2O_3$				1100	4	1400-5	F	3.84	NM	NM
65-26F	$51.62\%Mg0\cdot5.68\%Zn0\cdot9.1\%Al_2O_3\cdot33.6\%Fe_2O_3$				1100	4	1400-5	F	3.84	NM	NM
135A	$Ni_{1.0}Li_{0.5}Mn_{0.04}Fe_{4.275}O_8\pm$				1320	4	1200-7	F	3.64	NM	0.00
59-X	$Ni_{0.25}Zn_{0.75}Mn_{0.02}Fe_{1.9}O_4\pm$				1400	4	1250-7	F	5.16	>120	NM
7S-2X	$Ni_{0.97}Zn_{0.03}Mn_{0.02}Fe_{1.9}O_4\pm$				1380	4	1250-7	F	5.06	4	NM
43-3X	$Ni_{0.93}Zn_{0.07}Mn_{0.02}Fe_{1.9}O_4\pm$				1370	4	1250-7	F	04	3-4	NM
16-8X	$Ni_{1.0}Mn_{0.02}Fe_{1.9}O_4\pm$				1370	4	1250-7	F	4.98	3-4	0.00
122-X	$55\%Mg0\cdot6\%Zn0\cdot3\%CoO\cdot36\%Fe_2O_3$				450	4	1300-7	F	4.20	5	NM
115-X	$56.48\%Mg0\cdot6.26\%Zn0\cdot11.18\%Al_2O_3\cdot26.08\%Fe_2O_3$				4180	4	1300-7	F	3.54	1-2	NM
120-3X	$56.5\%Mg0\cdot6\%Zn0\cdot1.5\%CoO\cdot36\%Fe_2O_3$				1780	4	1300-7	F	4.05	4-5	<0.00

*SEE TABLE I **Sam

NM - Not Measured

2975-2 S/A

4-14

DIELECTRIC LOSS TAN X-BAND	DIELECTRIC CONSTANT X-BAND	g_{eff} FACTOR	LINE WIDTH ΔH X-BAND	$4\pi M_s$ (GAUSS)	I_B (AMPS)	H_c (OE..60~)	DRIVE FIELD COER FIELD	SQUARENESS S_D	$4\pi M_R$ (GAUSS)	R_H	
N'	NM	NM	NM	1140	10	.85	8.3	.83	625	.55	
NM	NM	NM	NM	1140	10	.84	8.5	.83	613	.54	
0.004	8.5	2.37	NM	1125	11.0	4.09	2.0	.69	NM	NM	
NM	NM	2.03	130	1480	**	**	**	Poor	NM	NM	
NM	NM	2.35	420	3150	13.26	5.93	1.70	.70	NM	NM	
NM	NM	2.31	385	3450	13.20	5.08	2.0	.67	NM	NM	
0.0025	10.5	2.4	505	2900	12.80	6.51	1.50	.72	NM	NM	
NM	NM	2.13	660	2225	13.93	7.70	1.30	.57	NM	NM	
NM	NM	2.01	270	650	2.73	1.10	1.86	.59	NM	NM	
<0.0001	12.7	2.11	530	2350	13.47	7.50	1.35	.72	NM	NM	

**Sample Could Not Be Saturated

B

materials. It is felt that this difference may be largely due to the larger coercive fields of the ferrites and the consequently smaller ratios of H_D/H_C used. This difference in H_D/H_C would be reflected in practical phase shifters unless high capacity driver circuits were employed.

The reproducibility observed on the PF-83 series is less than satisfactory ($4\pi M_R = 1050 \pm 83$ gauss) but no effort was made in this series to achieve a high degree of reproducibility. The achievable reproducibility of FDPS materials can better be judged on the garnet series cited in Section 4.3.1.

4.3.3 Magnetostriction Studies

Some additional garnet compositions have been investigated during this period. These compositions have been concerned with the study of magnetostrictive constants of these materials. Magnetostrictive constants (sometimes referred to as stress anisotropy) in ferrimagnetic materials are comparable in many respects to magneto-crystalline anisotropy constants. The basic origin of both magnetostriction and magnetocrystalline anisotropy are thought to be the same. A search of the literature indicated that some garnet materials possess positive magnetostrictive constants and others possess negative values.[17,18,19] Solid solutions of these materials in the proper proportion would produce compounds possessing zero magnetostriction as seemed desirable to optimize the hysteresis properties and eliminate the pressure effects on toroids for application in digital phase shifters.

A negative value of the magnetostrictive constant indicates that when a stress is applied to the material, the magnetic moments will have a tendency to align themselves parallel to the stress. A positive value of magnetostriction indicates that the magnetic moments will align themselves perpendicular to the stress in the material. Magnetostrictive constants are measured in accordance with the crystalline axes of a grain. In the microwave ferrite and garnet materials, the 111 direction is the dominant axis of crystalline anisotropy. Values of magnetostrictive constants have been measured on many of the garnet materials in the 111 and the 100 direction. These are labelled λ_{111} and λ_{100}.

Yttrium iron garnet has a magnetostrictive constant $\lambda_{111} = -2.4 \times 10^6$ at $25^\circ C$.[17,19] Terbium iron garnet possesses a value of λ_{111} of $+12 \times 10^6$ at $25^\circ C$, and

[17]E.A. Nesbitt, S. Geller, G.P. Espinosa, and A.J. Williams, "Square Loop Polycrystalline Garnets with and without Magnetic Field Heat Treatment," J. of Appl. Phys. 35, 2904 (Oct. '64).
[18]A.B. Smith and R.V Jones, "Magnetostriction Constants from Ferrimagnetic Resonance," J. of Appl. Phys. 34, 1283 (April '63).
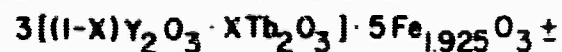[19]S. Iida, Physics Letters 6, 165 (1963).

europium iron garnet has a magnetostrictive constant (λ_{111}) of $+1.8 \times 10^6$. Solid solutions of yttrium iron garnet and terbium iron garnet or europium iron garnet should produce a composition possessing a zero value for λ_{111}. For yttrium-terbium iron garnet, the composition for zero magnetostriction is calculated to be that of approximately 83.3% yttrium iron garnet and 16.7% terbium iron garnet.

Compositions of the yttrium-terbium iron garnet family were prepared as listed in Table V. In order to investigate the effects of the magnetostrictive constant on remanence ratios and coercive fields, the compositions were prepared at different firing temperatures in attempts to vary the particle size in the material. Figure 20 is a graphical presentation of the expected variation of the magnetostrictive constant with terbium content in the yttrium terbium iron garnet family. Figure 21 shows the squareness and coercive field measured on these compositions with firing temperature as a parameter. It is noted that the squareness is maximum and the coercive field is minimum for the composition of 16.7% terbium content ($x = 0.167$). Experiments were performed to investigate the magnetostrictive effects in these compositions. A jig was designed to apply pressure to the toroids to observe the changes in the coercive field and remanence ratio as a function of applied pressure. The pressure was applied perpendicular to the diameter (unidirectional) of the round cylindrical toroid. The results observed are presented in Figure 22. It is noted that the coercive field increased and the squareness decreased for an applied load of 20 kilograms. The change in coercive field and squareness is noted to be a function of the magnetostrictive constant. For the composition possessing zero magnetostriction there was no observable change in the hysteresis properties of the material. The fact that the coercive field increased on both sides of this zero point is due to the fact that the stress on the material was not applied symmetrically. A symmetrical stress would be much better to use in studying the magnetostrictive effects. One would expect that for compositions possessing negative magnetostrictive constants, the hysteresis properties would improve for radial stress and would deteriorate for those compositions possessing a positive magnetostrictive constant. In other words, the coercive field would be expected to decrease and the remanence ratio increase for a symmetrical radial stress applied to compositions possessing negative magnetostrictive constants. The reverse would be true for compositions possessing positive values of magnetostrictive constants. These expectations are presently being pursued.

Data shown in Table V indicates that the dependence of remanence ratio on terbium content follows the same general trend as does "squareness," though the

TABLE V. YIG-TbIG COMPOSITIONS PREPARED AND EVALUATED

$$3[(1-X)Y_2O_3 \cdot XTb_2O_3] \cdot 5Fe_{1.925}O_3 \pm$$

SWEC NO	COMPOSITION X	DENSITY gm/cm³	4πMs (gauss)	ΔH(oe) (X-BAND) 25°C	g(oH) FACTOR	SQUARENESS S_d	COERCIVE FIELD H_c(oe) 60~,25°C	DRIVE FIELD (H_d oe)	PARTICLE SIZE (MICRONS)	FIRING TEM TIME °C/Hr
G-352C	0	5.08	1800	41	2.01	0.88	0.44	1.32	16	1500/5
G-352B	0	5.10	1800	27	2.01	0.87	0.68	2.04	10	1475/5
G-352D	0	5.10	1800	31	2.01	0.88	0.67	2.01	10	1450/5
G-352E	0	4.97	1750	73	2.02	0.84	1.40	4.20	4	1425/5
G-352A	0	4.74	1670	135	2.05	0.75	2.12	6.36	NM	1400/5
G-353C	0.100Tb	5.23	1756	836	1.90	0.90	0.50	1.50	18	1500/5
G-353A	0.100Tb	5.23	1745	862	1.88	0.88	0.76	2.28	12	1475/5
G-353D	0.100Tb	5.23	1730	836	1.89	0.87	0.81	2.43	11	1450/5
G-353B	0.100Tb	5.16	1715	846	1.93	0.82	1.57	4.71	3	1425/5
G-353E	0.100Tb	4.78	1600	NM	NM	0.81	1.69	5.07	NM	1400/5
G-354-2G	0.167Tb	5.32	1630	>2000	-	0.91	0.54	1.62	23	1500/5
G-354-2K	0.167Tb	5.32	1610	>2000	-	0.90	0.56	1.68	20	1475/5
G-354-2B	0.167Tb	5.34	1605	>2000	-	0.90	0.65	1.95	18	1450/5
G-354-2A	0.167Tb	5.33	1625	>2000	-	0.89	0.93	2.79	9	1425/5
G-354-2J	0.167Tb	5.04	1530	>2000	-	0.84	1.60	4.80	NM	1400/5
G-355-2H	0.250Tb	5.42	1460	Large	-	0.88	0.68	2.04	23	1500/5
G-355-2K	0.250Tb	5.40	1445	Large	-	0.87	0.63	1.89	19	1475/5
G-355-2A	0.250Tb	5.46	1470	Large	-	0.86	0.79	2.37	15	1450/5
G-355-2B	0.250Tb	5.44	1480	Large	-	0.85	1.53	4.59	7	1425/5
G-355-2G	0.250Tb	5.02	1350	Large	-	0.80	2.31	6.93	NM	1400/5
G-356A	0.350Tb	5.59	1305	Large	-	0.76	1.23	3.69	14	1500/5
G-356C	0.350Tb	5.57	1275	Large	-	0.76	1.46	4.38	10	1475/5
G-356E	0.350Tb	5.52	1300	Large	-	0.72	2.07	6.21	9	1450/5
G-356B	0.350Tb	5.23	1160	Large	-	0.72	3.12	9.36	5	1425/5
G-356D	0.350Tb	4.88	1120	Large	-	0.70	4.16	12.45	NM	1400/5

2973-2 3/4

*NM Not Measured

| DRIVE FIELD (H$_d$H$_{oe}$)	PARTICLE SIZE (MICRONS)	FIRING TEMP/ TIME °C/Hr	20 Kgm LOAD APPLIED			SAMPLE NO.	DRIVE CURRENT (AMPS)	COERCIVE FIELD (H$_c$)(oe) 60~	H$_d$/H$_c$	SQUARENESS S$_d$	4πM$_{rd}$ (GAUSS)	REMANENCE RATIO (R$_d$)
			SQUARENESS	COERCIVE FIELD (H$_c$HOe)	DRIVE FIELD (H$_d$Hoe)							
1.32	16	1500/5	0.70	0.56	1.68	-G	4.2	0.23	10	0.87	1230	0.68
2.04	10	1475/5	0.67	0.93	2.79	-H	6.6	0.45	10	0.87	1280	0.71
2.01	10	1450/5	0.68	0.92	2.76	-L	6.8	0.46	10	0.88	1240	0.69
4.20	4	1425/5	NM	NM	NM	-M	10	1.11	6	0.84	1030	0.59
6.36	NM	1400/5	0.67	2.66	7.98	-Q	10	1.89	3	0.78	605	0.36
1.50	18	1500/5	0.66	0.63	1.89	-2V	4.7	0.42	10	0.88	1170	0.67
2.28	12	1475/5	0.70	0.95	2.85	-H	7.8	0.54	10	0.87	1205	0.69
2.43	11	1450/5	0.72	0.99	2.97	-K	8.2	0.55	10	0.87	1140	0.66
4.71	3	1425/5	NM	NM	NM	-2H	10	0.76	9	0.82	1080	0.63
5.07	NM	1400/5	0.77	1.77	5.31	-2P	10	1.07	6	0.83	1075	0.67
1.62	23	1500/5	0.88	0.57	1.71	-2L	5.8	0.40	10	0.89	1125	0.69
1.68	20	1475/5	0.89	0.56	1.68	-2N	5.8	0.40	10	0.90	1070	0.66
1.95	18	1450/5	0.89	0.65	1.95	-2F	6.6	0.41	10	0.90	1070	0.67
2.79	9	1425/5	NM	NM	NM	-2C	10	0.69	10	0.87	1080	0.66
4.80	NM	1400/5	0.84	1.60	4.80	-2R	10	1.35	5	0.85	950	0.62
2.04	23	1500/5	0.66	0.86	2.58	-2W	6.4	0.46	10	0.85	935	0.64
1.89	19	1475/5	0.65	0.81	2.43	-2P	6.6	0.45	10	0.86	995	0.69
2.37	15	1450/5	0.67	1.05	3.15	-2D	8.3	0.55	10	0.84	1050	0.71
4.59	7	1425/5	NM	NM	NM	-2E	10	1.21	6	0.83	925	0.63
6.93	NM	1400/5	0.72	2.47	7.41	-2R	10	1.97	3	0.81	775	0.57
3.69	14	1500/5	0.63	1.60	4.80	-V	7.0	0.62	10	0.75	740	0.57
4.38	10	1475/5	0.63	1.80	5.40	-J	10	1.13	6	0.76	735	0.58
6.21	9	1450/5	0.65	2.52	7.56	-K	10	1.52	5	0.75	695	0.53
9.36	5	1425/5	NM	NM	NM	-L	10	2.65	3	0.71	490	0.42
2.45	NM	1400/5	-	High	-	-N	10	3.16	2	0.61	255	0.23

DATA OBTAINED USING
HIGHER DRIVE FIELDS

4-17/18

B
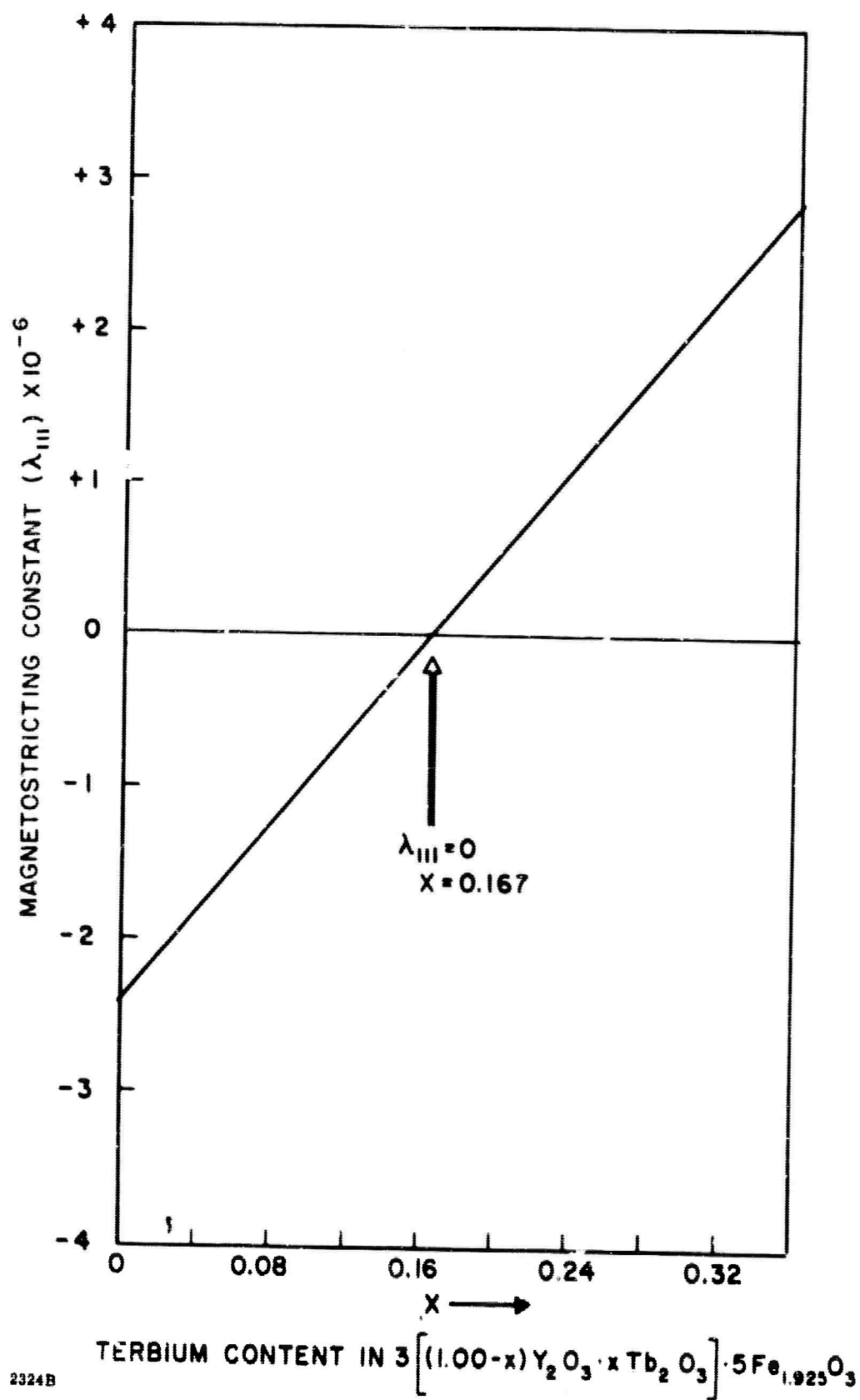
Figure 20. Magnetostrictive Constant (λ_{111}) as a function of Terbium Content in YIG-TbIG
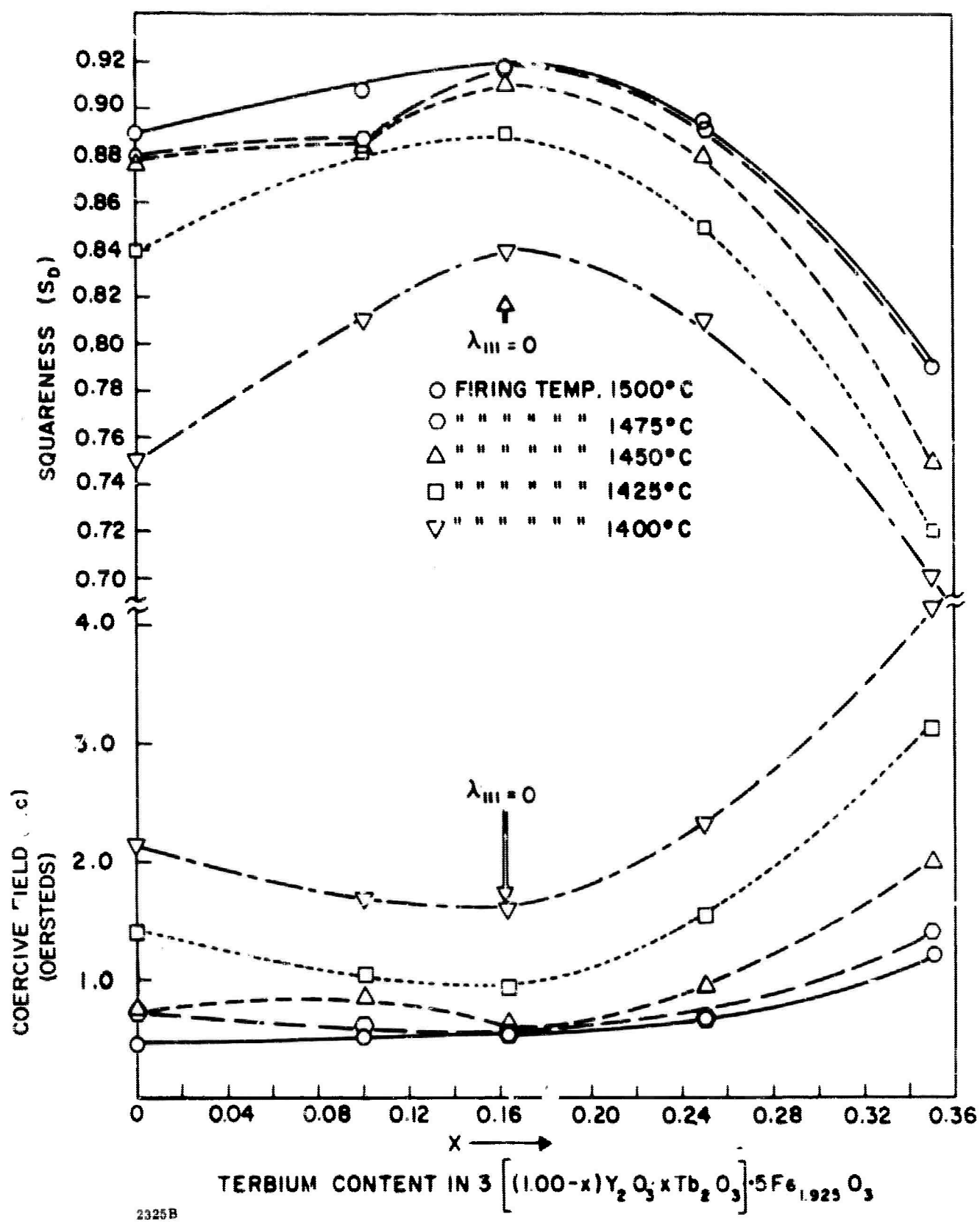
Figure 21. Squareness and Coercive Field for various firing temperatures
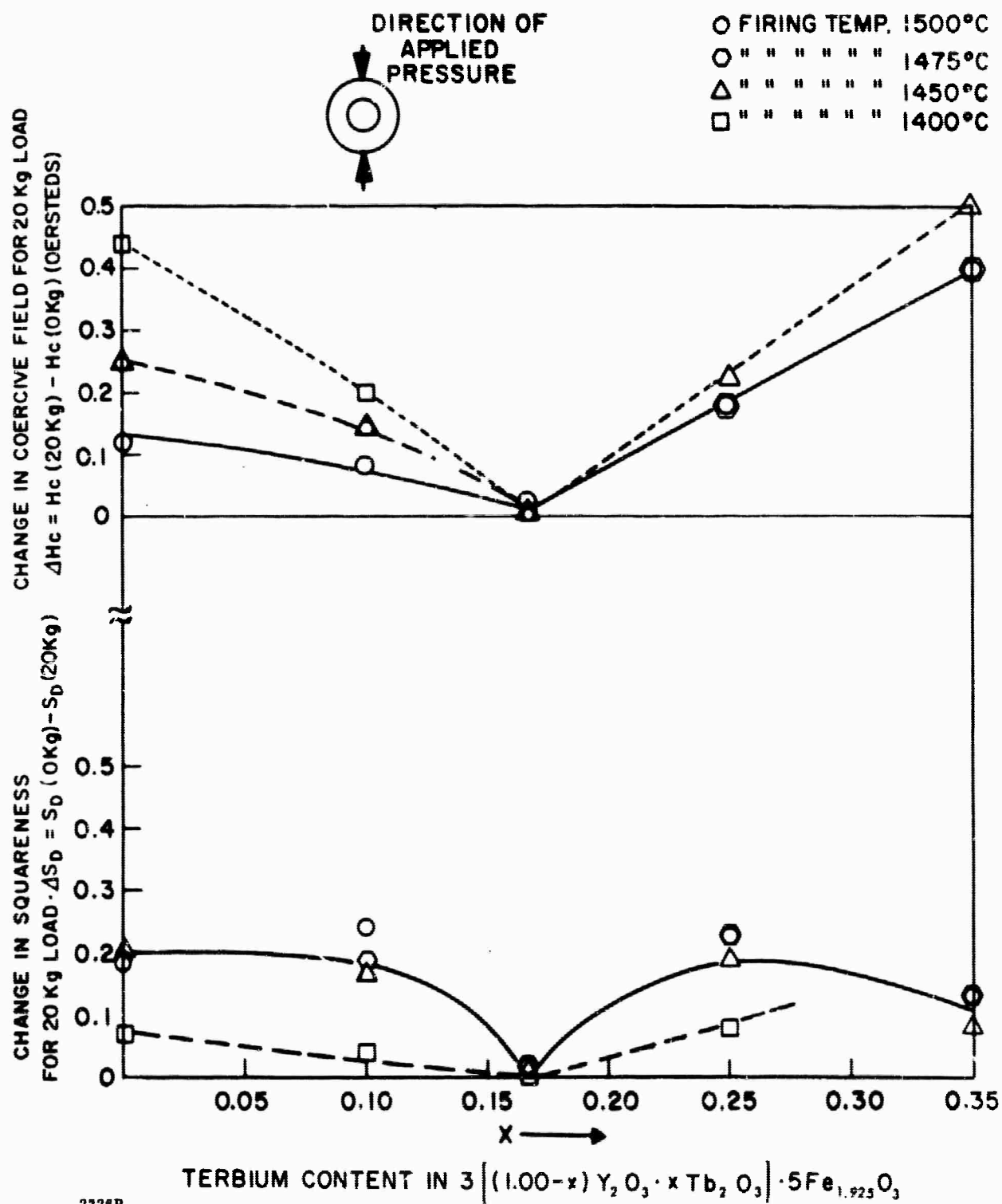versus Terbium Content in Yttrium-Terbium iron garnet

Figure 22.   Change in Squareness and Coercive field for an applied pressure of 20 Kg as a function of Terbium content in Yttrium-Terbium iron garnet

2326B

dependence is pherhaps not as marked. However, the actual value of $4\pi M_{RD}$ decreases with terbium content, since $4\pi M_s$ decreases more rapidly than remanence ratio increases.

It is also found that $4\pi M_R$ of the 16.7% terbium material is insensitive to applied stress in agreement with the squareness measurements. $4\pi M_{RD}$ of other members of the yttrium-terbium iron garnet series was found to decrease with increasing applied pressure.

The terbium compositions, as listed in Table V, demonstrate that magnetostrictive effects can be eliminated in garnet materials but still lack acceptable properties for digital phase shifter applications. The 16.7% terbium content required to reduce magnetostrictive constant to zero broadens the linewidth to such an extent that these compositions could not be used for phase shifter applications. It is not known at the present what the microwave characteristics would be of the yttrium europium iron garnets.

Other rare earth iron garnets were investigated for the purpose of finding a more suitable compound to use to compensate the magnetostrictive constants. The literature indicated that erbium iron garnet[18] possessed a magnetostrictive constant λ_{111} of $+16 \times 10^{-6}$ at $25^\circ C$. Some compositions were therefore prepared using the yttrium erbium combination as presented in Table VI. Studies of these materials showed no improvement in the hysteresis properties which indicated that the value of $+16 \times 10^{-6}$ for λ_{111} possibly was in error. In pursuit of this question, Dr. F.J. Schnettler of Bell Telephone Laboratories indicated that they (Dr. S. Iida) had measured a value of -4.9×10^{-6} for erbium iron garnet.[20] This value is in agreement with the results observed on the compounds studied. In fact, Dr. Iida has reported from his measurements that no other garnet materials with the exception of europium iron garnet and terbium garnet possessed positive magnetostrictive constants in the 111 direction (λ_{111}). The values obtained from Dr. Iida (presently unpublished data) for the magnetostrictive constants of the various garnet materials are presented in Table VII. These data were measured with an essentially dc technique, while the values quoted in reference 18 were obtained from microwave resonance measurements. Values obtained in these two ways are not in agreement, and it is apparent from our experiments that it is the dc magnetostrictive constants that influence the remanent state.

[18] Ibid, page 4-15

[20] Private communication (Measurements by S. Iida).

TABLE XI. YIG-ErIG COMPOSITIONS PREPARED AND EVALUATED

$$3[(1-X)Y_2O_3 \cdot XEr_2O_3]\cdot 5Fe_{1.925}O_3 \pm$$

S W E C NO	COMPOSITION x	DENSITY gm/cm³	4πM_s (gauss) 25°C	ΔH (oe) (X-BAND) 25°C	g (eff) FACTOR	SQUARENESS S_d	COERCIVE FIELD (H_c Koe) 60~, 25°C	DRIVE FIELD (H_d) (oe)	PARTICLE SIZE (MICRONS)	FIRING TEMP/ TIME °C/H_R	20 Kgm LOAD ±	
											SQUARENESS	COERCIVE F H_z (oe)
G-393E	0.070Er	5.16	1780	NM	NM	0.87	0.48	1.45	NM	1500/5	0.73	0.59
G-393A	0.070Er	5.18	1780	90	1.98	0.88	0.45	1.36	NM	1475/5	0.70	0.60
G-394E	0.126Er	5.23	1780	NM	NM	0.86	0.55	1.65	NM	1500/5	0.72	0.64
G-394A	0.126Er	5.28	1780	132	1.95	0.87	0.53	1.58	NM	1475/5	0.67	0.70
G-395E	0.200Er	5.37	1780	NM	NM	0.86	0.65	1.96	NM	1500/5	0.73	0.81
G-395A	0.200Er	5.38	1770	200	1.91	0.86	0.55	1.65	NM	1475/5	0.72	0.64
G-396E	0.260Er	5.43	1770	NM	NM	0.81	0.74	2.19	NM	1500/5	0.70	0.95
G-396A	0.260Er	5.37	1770	250	1.88	0.82	0.57	1.72	NM	1500/5	0.68	0.73

NM – Not measured to date.

2973-2 S/A

LD	PARTICLE SIZE (MICRONS)	FIRING TEM TIME °C/Hg	20 Kgm LOAD APPLIED			DRIVE CURRENT Io (AMPS)	COERCIVE FIELD (oe) (60~)	Hd/Hc	SQUARENESS Sd	4πMRo	REMANENCE RATIO RR
			SQUARENESS	COERCIVE FIELD Hc (oe)	DRIVE FIELD Hd (oe)						
15	NM	1500/5	0.73	0.59	1.75	4.3	0.36	10	0.84	1050	0.59
6	NM	1475/5	0.70	0.60	1.79	Sample	Destroyed			NM	NM
3	NM	1500/5	0.72	0.64	1.92	4.7	0.35	10	0.82	1140	0.64
4	NM	1475/5	0.67	0.70	2.10	5.1	0.34	10	0.86	1060	0.60
5	NM	1500/5	0.73	0.81	2.41	5.0	0.34	10	0.84	1040	0.58
9	NM	1475/5	0.72	0.64	1.92	4.5	0.34	10	0.80	990	0.56
3	NM	1500/5	0.70	0.95	2.86	5.5	0.38	10	0.80	950	0.54
2	NM	1500/5	0.68	0.73	2.18	5.1	0.46	10	0.76	880	0.50

DATA OBTAINED USING
HIGHER DRIVE FIELDS

B

Table VII. Magnetostrictive Constants For Various Rare Earth Garnets (Data obtained by Private Communication, Dr. S. Iida, University of Tokyo, Tokyo, Japan)

		$78^{\circ}K$	$196^{\circ}K$	$298^{\circ}K (25^{\circ}C)$
YIG	λ_{100}	-1.0×10^6	-1.1×10^6	-1.4×10^6
	λ_{111}	-3.6×10^6	-3.9×10^6	-2.4×10^6
SmIG	λ_{100}	$+159 \times 10^6$	$+49 \times 10^6$	$+21 \times 10^6$
	λ_{111}	-183×10^6	-28.1×10^6	-8.5×10^6
EuIG	λ_{100}	$+86 \times 10^6$	$+51 \times 10^6$	$+21 \times 10^6$
	λ_{111}	$+9.7 \times 10^6$	$+5.3 \times 10^6$	$+1.8 \times 10^6$
GdIG	λ_{100}	$+4.0 \times 10^6$	$+1.7 \times 10^6$	0×10^6
	λ_{111}	-5.1×10^6	-4.5×10^6	-3.1×10^6
TbIG	λ_{100}	$+67 \times 10^6$	-10.3×10^6	-3.3×10^6
	λ_{111}	$+560 \times 10^6$	$+65 \times 10^6$	$+12 \times 10^6$
DyIG	λ_{100}	-254×10^6	-46.6×10^6	-12.5×10^6
	λ_{111}	-145×10^6	-21.6×10^6	-5.9×10^6
HoIG	λ_{100}	-82.2×10^6	-10.6×10^6	-3.4×10^6
	λ_{111}	-56.3×10^6	-7.4×10^6	-4.0×10^6
ErIG	λ_{100}	$+10.7 \times 10^6$	$+4.1 \times 10^6$	$+2.0 \times 10^6$
	λ_{111}	-19.4×10^6	-8.8×10^6	-4.9×10^6
PmIG	λ_{100}	$+25.0 \times 10^6$	$+4.9 \times 10^6$	$+1.4 \times 10^6$
	λ_{111}	-31.2×10^6	-11.3×10^6	-5.2×10^6
YbIG	λ_{100}	$+18.3 \times 10^6$	$+5.0 \times 10^6$	$+1.1 \times 10^6$
		-14.4×10^6	-7.1×10^6	-4.5×10^6

In conclusion, the magnetostrictive effects in the garnet materials can be eliminated by terbium substitutions as indicated in Figure 22. At the present time it seems that good microwave square loop garnet materials will necessarily have to possess a nonzero value of magnetostriction. This does not look particularly deteriorating in considering these materials for digital phase shifter applications. Some techniques may be devised to actually use the magnetostrictive constants to advantage in digital phase shifter structures. These structures would be such that the various bit sizes could be tuned externally by use of pressure applied to the toroidal cores. It is believed also that the change in hysteresis properties as a function of applied pressure will reach a value beyond which any additional increase in pressure will not alter the hysteresis properties. In other words, a stress could be applied to the material such that any increase in this stress would not affect the hysteresis properties.

It should be mentioned that the magnetostrictive constants, as discussed above, are temperature sensitive. (See Table VII). The value of yttrium iron garnet does not vary rapidly with temperature. However, some of the rare earth garnet materials exhibit characteristics where the magnetostrictive constants actually change sign as a function of temperature.

Some discussions among various investigators have been directed toward the measurement of hysteresis properties. In this regard, some investigations have been made to define the changes in coercive field and remanence ratio as a function of drive field. The data indicate that a drive field approximately 10 times the coercive field is sufficient to properly characterize the coercive field, remanent magnetization and the remanence ratio. In nearly all cases the material is certainly not saturated for this drive field. However increasing the drive field by the amount necessary to saturate the material would not be advantageous since the squareness, remanent magnetization or coercive fields would not be altered in proportion. A value of drive 10 times the coercive field in all cases explored by Sperry seems sufficient to characterize the hysteresis properties for digital phase shifter applications. The squareness, remanent magnetization, and coercive field should be measured a. the same drive field.

The previously observed decrease in squareness when toroids are machined and the temperature treatment required to improve the hysteresis properties seem to be completely related to the magnetostrictive constants of the material.

Mr. Don Temme at MIT Lincoln Laboratories[21,22] reported that his investigations of machine toroids and the necessary treatment to improve squareness indicated the problem to be a surface effect. (Etching samples seems to improve them in the same fashion as heat treatment.) Sperry has since repeated some of his measurements with the same conclusion. It is interesting to note that the squareness of the materials possessing zero magnetostrictive constants is not appreciably effected by machining operations.

Techniques have been developed during this reporting period for the fabrication of toroids by pressing the center hole in the raw bar. The technique is one of pressing a metal shim in the middle of the bar and then removing the shim after the bar is pressed. Center slots of rectangular samples have been prepared down to 10 mils using this technique. This greatly reduces the machining time required for the preparation of toroids.

[21] Private communications.

[22] E. Stern and D. Temme, "Magnetostriction Effects in Remanence Phase Shifters," (to be published).

4.4 DEVICE MEASUREMENTS

In order to become more familiar with the role of the material parameters affecting device operation, an intensive program of device measurements was necessary. The following is a discussion of the results of these measurements.

4.4.1 Methods of Measurements

The methods and equipment used in the measurements were standard ones involving no basic changes. The salient features of each are presented.

Measurement of Attenuation and VSWR. Measurement of attenuation and VSWR was done in the so-called ratio-detector setup depicted in Figure 2'.A. This method, described by Hunton et al[23], yields a continuous display of the loss and VSWR across the frequency band, and assuming 30 db directivity, is accurate to 7 percent. At high power levels the attenuation was measured, essentially, by the familiar rf substitution method.

Measurement of Differential Phase Shift. Differential phase shift was measured in the phase bridge setup shown in Figure 23B. At the power splitter the rf energy divides, half the energy going into each arm. The losses of the test piece (digital phase shifter) in the lower arm are balanced and monitored by the calibrated attenuator in the upper arm. The ferrite is magnetized to the state corresponding to $\beta+$ and the calibrated phase shifter is adjusted to provide a null readout at the detector. The reading on the calibrated phase shifter is noted. The ferrite is then magnetized to $\beta-$ and the calibrated phase shifter is again adjusted for a null. The second reading can now be subtracted from the first, the remainder representing the differential phase shift. This method has an accuracy at least as good as 5 percent.

This method of measuring phase shift is easily adapted to measurements at high power levels. The calibrated phase shifter is then used in the upper arm which is strongly decoupled from the main (high power) line containing the DPS through the use of a multihole or crossguide coupler instead of the first magic-tee. A similar coupler is placed in the main line just after the test piece. The down-arm energy of this this second coupler is combined by a magic-tee with the energy flowing through the calibrated phase shifter. Providing the main-line arm of this second coupler is well terminated, the accuracy should be 5 percent or better.

---

[23] J. K. Hunton and E. Lorence, "Improved Sweep Frequency Techniques for Broadband Microwave Test," Hewlett-Packard Journal, Vol. 12, No. 4, December 1960.
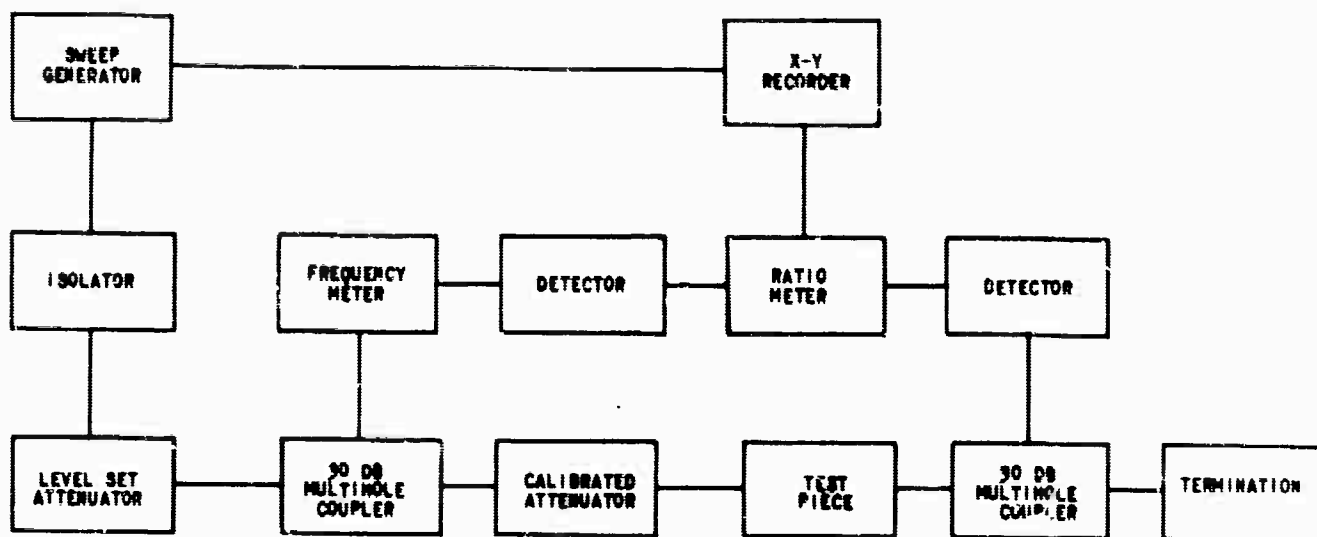
A. RATIO DETECTOR SETUP FOR MEASURING ATTENUATION AND VSWR
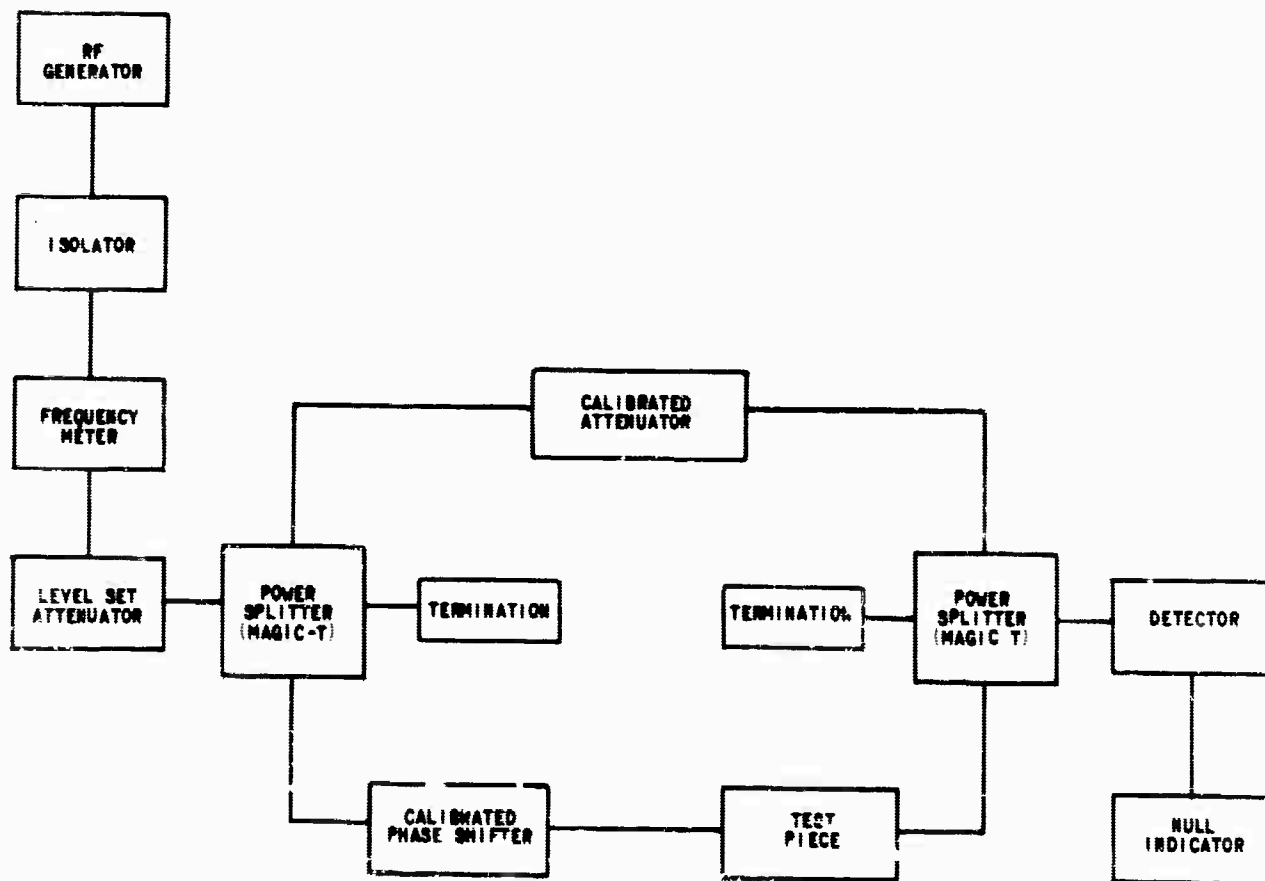
B PHASE BRIDGE SETUP FOR MEASURING PHASE SHIFT

Figure 23. Laboratory Setups for Measurement of Attenuation and Phase Shift at Low Power Levels

Measurement of Switching Energy and Switching Time. The switching energy cannot be measured directly. There are several methods by which it can be measured indirectly and two are described below.

The solid traces in the graphs of Figure 24 show the voltage pulse across and the current pulse through the charging wire of the toroid. These traces are typical of the oscillograms obtained using fast-responding current and voltage probes. The dashed lines are intended to enclose a geometrical area roughly equivalent to the irregular area actually obtained. The switching energy is then

$$U_s = V_o I_o (\Delta t) \quad \text{(Joules)} \tag{49}$$

Typically

$$V_o = 35 \text{ volts}$$

$$I_o = 10 \text{ amps}$$

$$\Delta t = 1 \text{ microsecond}$$

so $U_s = 35 \times 10 \times 10^{-6} = 350 \text{ microjoules.}$
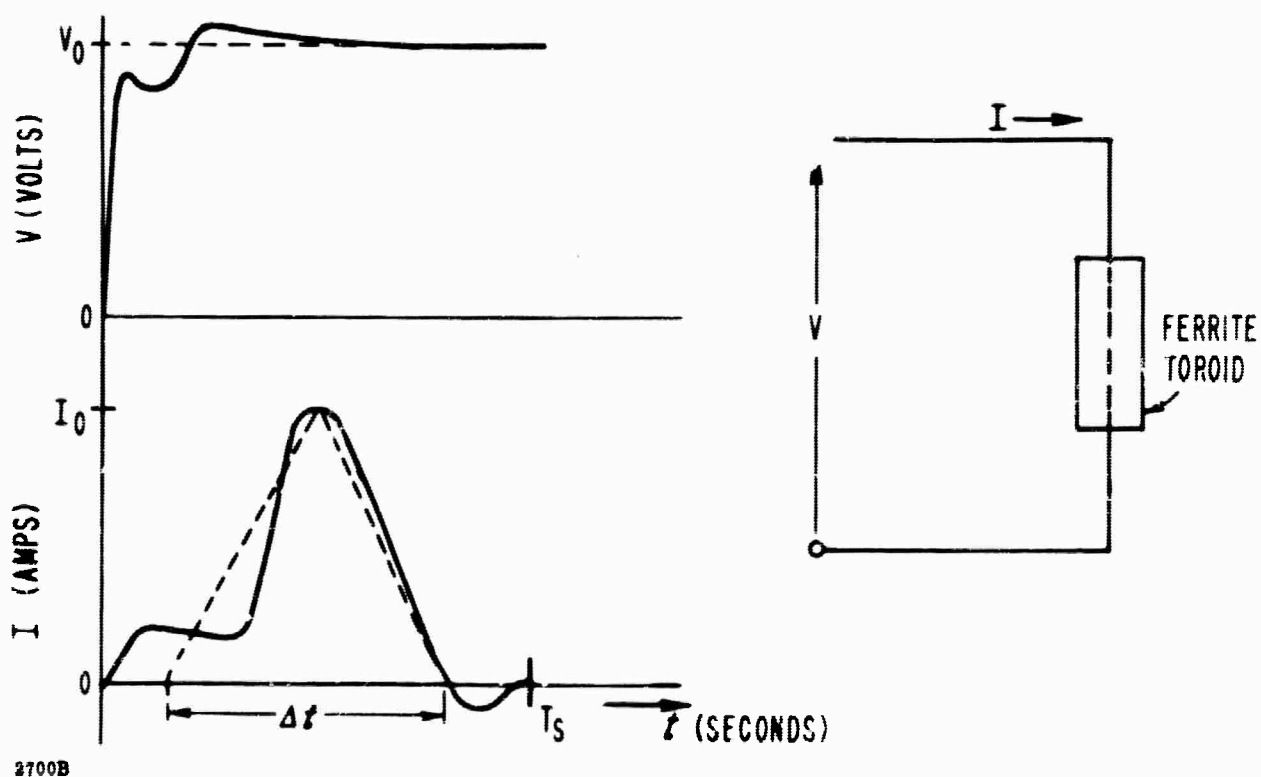
Figure 24. Typical Voltage and Current Waveforms Observed During Fast Switching of the Ferrite Toroids. The Switching Time T_s is also Shown.

4-30

The second method is that of measuring the rms voltage and current required for continuous switching at a rate R. Using this method

$$U_s = \frac{I_{rms} \times V_{rms}}{2R} \text{ joules} \qquad (50)$$

where the factor 2 is used because R is given in cycles/second and therefore represents switching from a given state to another and back again.

The two methods give nearly identical results, but only if it is possible to place the rms voltage and current meters at the same point in the line as the probes. This second method is easier, of course, in application and involves much less sophisticated equipment.

The switching time T_s, shown in Figure 24, is the time required for the ferrite magnetization to be reversed and for the ferrite to fall back to the new remanence state. The fall back to remanence is accompanied by a negative current pulse and T_s is measured from t = 0 until the time when this (negative) current pulse goes to zero.

4.4.2 Device Configuration - General Considerations

Although the information presented in the theoretical section (Section 3) may serve as a guide, the final choices of ferrite material and geometry, waveguide size and other structural parameters must be made on the basis of experiment. First thoughts were concerned with the size of the waveguide in the vicinity of the ferrite toroids. In making a choice, due account must be made for the size and dielectric constant of the toroid as well as the operating frequency.

The quantity ka = $2\pi a/\lambda$ describes the relationship of the width of the waveguide "a" to the free space wavelength λ. It is therefore proportional to frequency. In empty rectangular waveguide of width "a", the TE_{10} mode cuts off at $k_c a(TE_{20}) = \pi$; the TE_{20} mode cuts off at $k_c a(TE_{20}) = 2\pi$. As dielectric is introduced along the center line of the waveguide, $k_c a(TE_{10})$ initially decreases more rapidly than $k_c a(TE_{20})$. This occurs because the electric field of the TE_{10} mode peaks up at the waveguide center (a/2) while the electric field of the TE_{20} mode has a minimum there. The interaction between the dielectric and the field is therefore greater in the TE_{10} mode than it is for the TE_{20} mode. The expressions for the cutoff frequencies of dielectric-loaded (or, particularly, ferrite-loaded) waveguide can be calculated by setting $\beta = 0$ in the characteristic equation of section 3.4.2.

Figure 25 shows $k_c a(TE_{10})$ and $k_c a(TE_{20})$ versus c/a (c = dielectric width) for a lossless dielectric with relative dielectric constant $\epsilon' = 16$.[24]   The waveguide and ferrite sizes should be chosen so that the operating frequency range falls between these lines. Ideally, the device should operate as far above $k_c a(TE_{10})$ as possible and $ka \gtrsim 1.2\, k_c a(TE_{10})$ is usually recommended. It is seen that a value of $c/a \approx .10$ gives the maximum spread between $k_c a(TE_{10})$ and $k_c a(TE_{20})$.   Thus, Figure 25 shows the allowed ranges of ka and c/a. For example, if a value of $c/a = .33$ is chosen for a device to be operated at 9 Ghz, any ka value in the range $1.2 \le ka \le 2.6$ can be used. Thus, since $ka = 2\pi a/\lambda$ and $\lambda = 1.31$ inches, the appropriate range for the waveguide width is $.250'' \le a \le .550''$. Ideally, one would then choose a width in this range which gives a large figure of merit, minimum phase slope, and so on, and which can be matched to the empty sections of the waveguide structure. The numbered data points represent c/a and ka values of eight empirically derived configurations which exhibited essentially zero phase slope. Of these configurations number (8) was expected, and did in fact, exhibit a severe moding problem.

Of the various impedance matching schemes tried, that of using two or three section dielectric transformers, as shown in Figure 26 worked best. As an example of their design, we choose a value of $c = .125$, and $a = 1.122''$. Thus, for the ferrite loaded section, for purposes of calculating impedance only, $c/a = .125/1.122 = .111$. Referring to Figure 27 it is seen that at a center frequency of $ka = 5.4$, $\beta_3 a(c/a = .111) = 16$ and $\beta_0 a(c/a = o) = 4.5$. Thus, the ratio of the wave impedance of the loaded to the unloaded section is $Z_{w3}/Z_{wo} = \beta_0 a/\beta_3 a = .28$.

This follows from the fact that $Z_w \propto \lambda_g$. The bandwidth as defined by Young[25] is expressed as

$$w = 2\,\frac{\lambda_{g1} - \lambda_{g2}}{\lambda_{g1} + \lambda_{g2}} \tag{51}$$

and inserting λ_{g1} and λ_{g2} at 8.5 Ghz and 9.5 Ghz, respectively, for empty WR112, then $w = .17$. Referring to his tables for the impedance ratios, we find that

$Z_{w1}/Z_{wo} = 1/1.42. = .704$

$Z_{w2}/Z_{wo} = 1.42./4 = .355$

[24] P.H. Vartanian et al, "Propagation in Dielectric Slab Loaded Rectangular Waveguide," IRE Transactions of the PGMTT, April 1958.

[25] Leo Young, "Tables for Cascaded Homogeneous Quarter-Wave Transformers," Transactions of the PGMTT, April 1959, p 233.
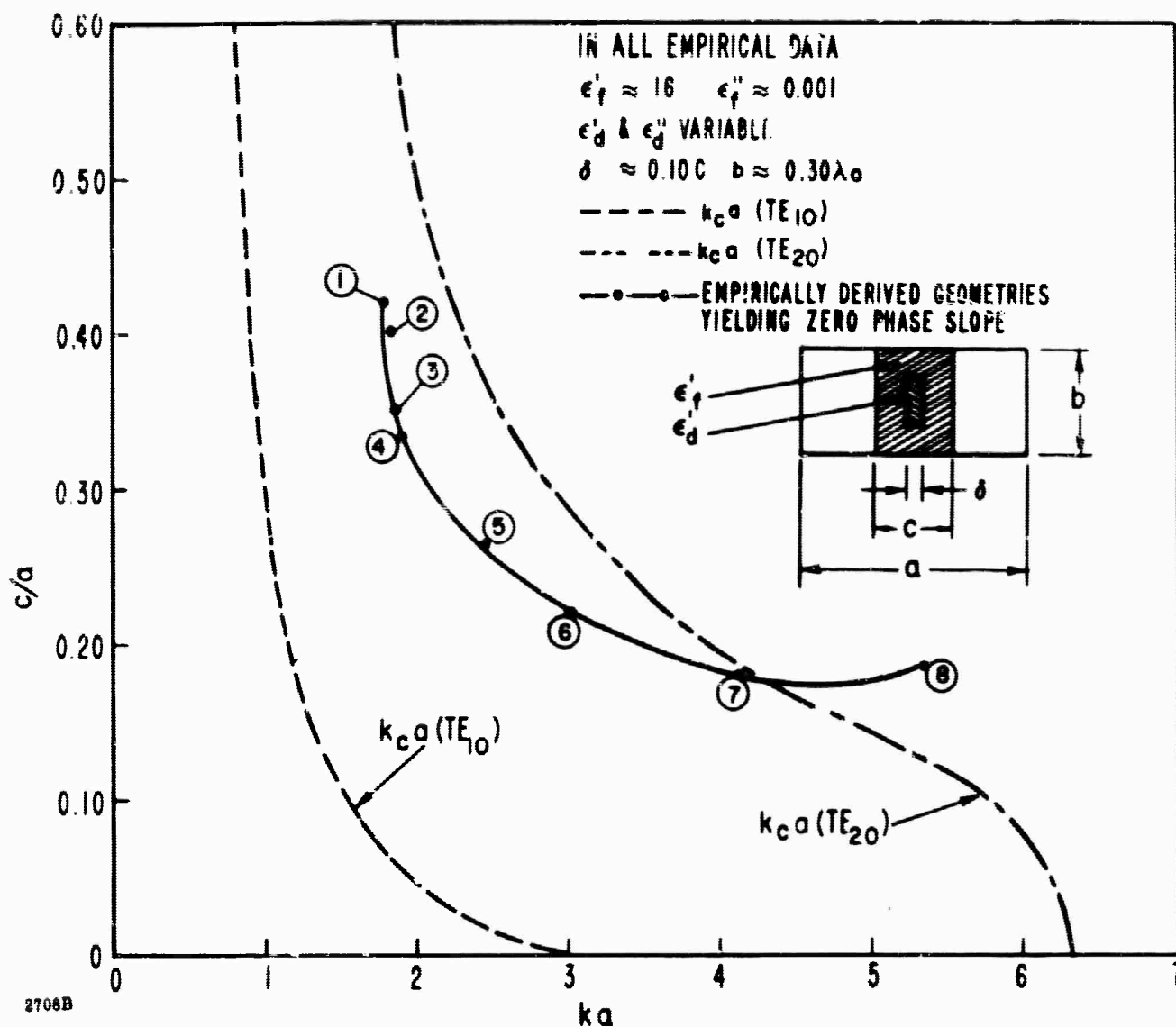
Figure 25. Toroid Width Versus Waveguide Width and Frequency (ka) Yielding Zero Phase Slope. Also Shown Are The TE_{10} and TE_{20} Mode Cutoff Frequencies.

Since $\beta_o a = 4.5$, then

$$\beta_1 a = 4.5/.704 = 6.40$$

$$\beta_2 a = 4.5/.355 = 12.70.$$

Therefore, at the center frequency (ka = 5.4), the lengths of the steps are to be $\ell = \lambda_g/4$ or

$$\ell_1 = \frac{\lambda_{g1}}{4} = \frac{\pi\, a}{2\beta_1 a} = 3.53/12.80 = 0.275"$$

$$\ell_2 = \frac{\pi\, a}{2\beta_2 a} = 3.53/25.40 = 0.139"$$

The thickness of the steps (c) are obtained, for aluminum oxide ceramic ($\epsilon' = 9.6$), from the graph of Figure 28. At $ka = 5.4$, $\beta_1 a = 6.40$ is obtained when $c_1/a = .029$ ($c = .031"$) and $\beta_2 a = 12.70$ is obtained when $c_2/a = .144$ ($c = .101"$).

(A) SYMMETRIC TWO-STAGE DIELECTRIC TRANSFORMER

(B) NONSYMMETRIC TWO-STAGE DIELECTRIC TRANSFORMER
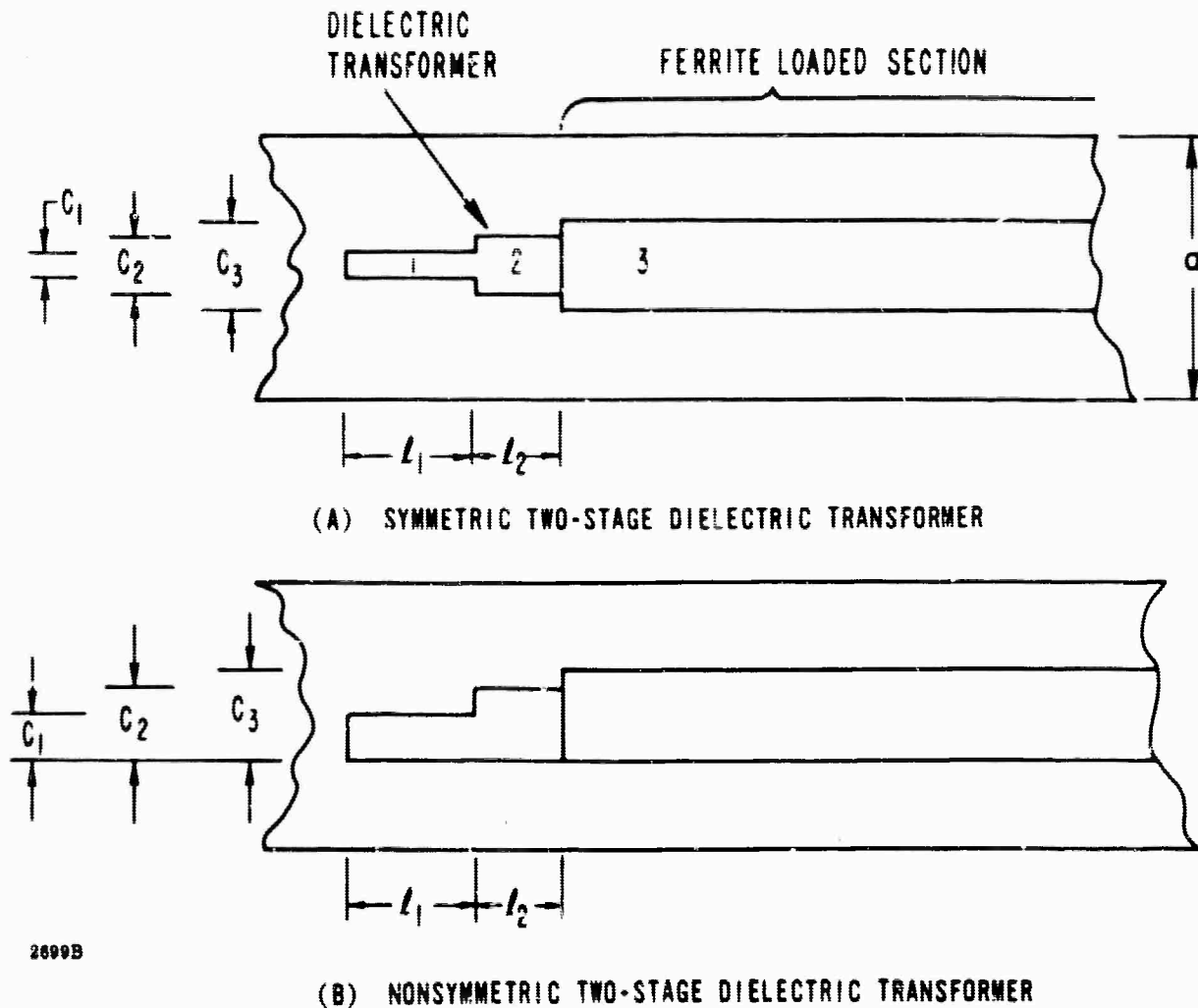
Figure 26. Cutaways Showing Symmetric And Non-symmetric Two-step Dielectric Transformers. The Steps Are Centrally-located, Full Height Slabs of Low Loss Dielectric of Lengths ℓ_1 and ℓ_2 and Thickness C_1 and C_2. The Load is Region 3 of Thickness C_3.

The steps could have been designed using $\epsilon' = 16$, of course, but at frequencies above 4 Ghz this usually leads to steps which are too thin to be practicable.

This design procedure leads to a set of symmetric steps as shown in Figure 26A. However, it is found that non-symmetric steps as shown in Figure 26B are easier to machine and give equivalent performance. The dimensions used are those calculated for the symmetric transformers.

4-34
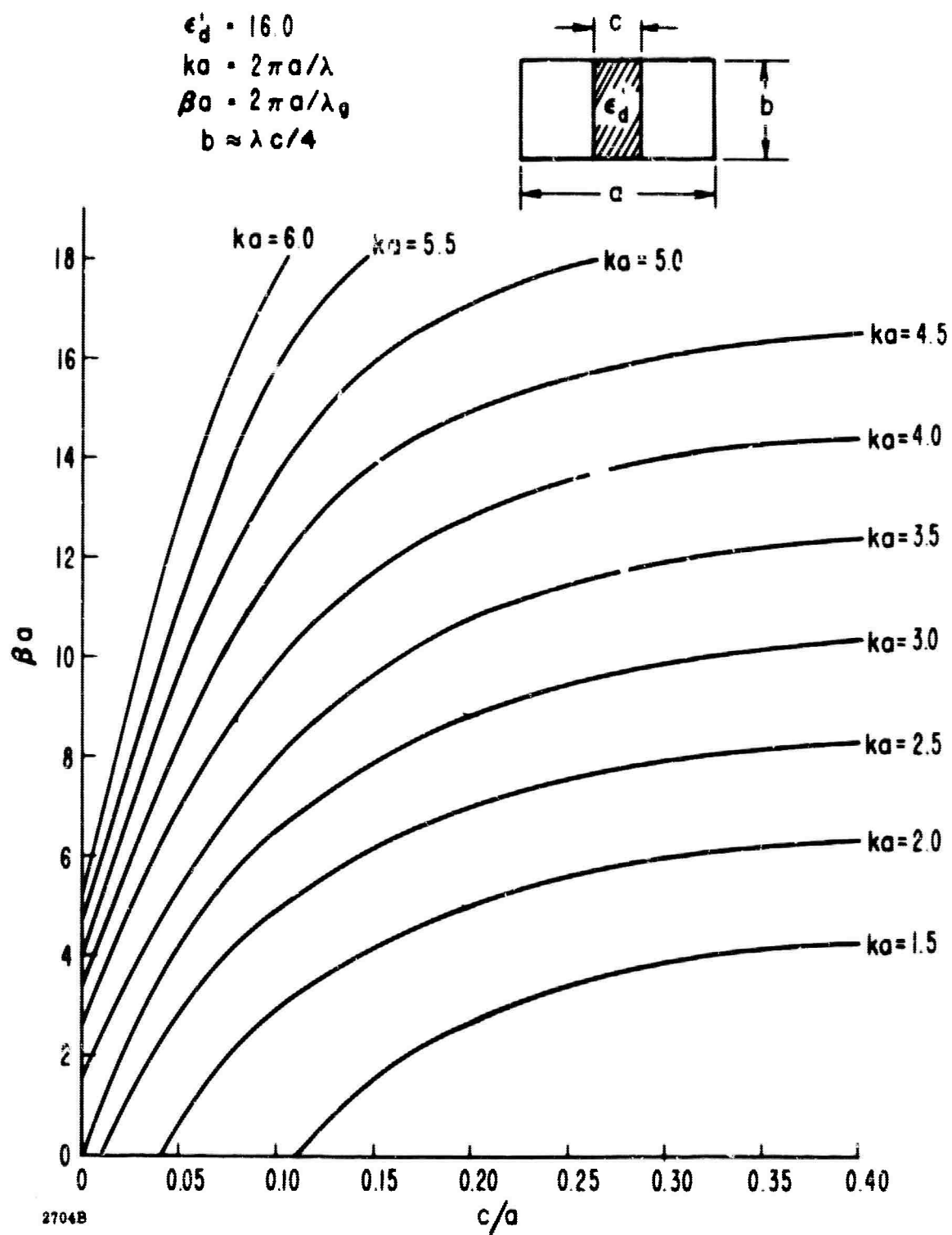
Figure 27. Phase Constant (βa) vs Loading Factor c/a With Frequency (ka) as Parameter For Dielectric Loaded Waveguide With $\epsilon'_d = 16$
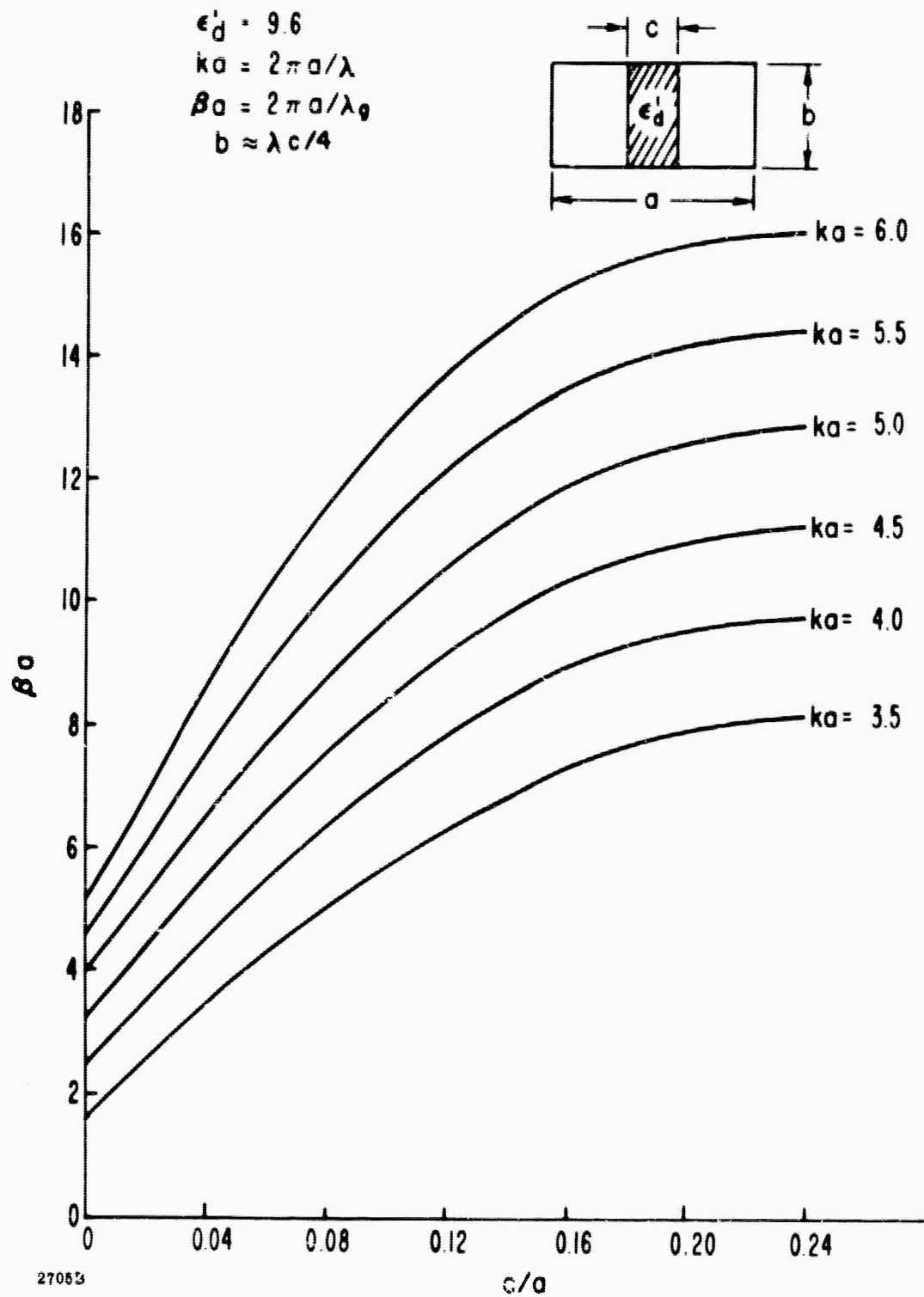
Figure 28. Phase Constant (βa) vs Loading Factor c/a With Frequency ka as Parameter For Dielectric Loaded Waveguide with $\epsilon'_d = 9.6$

4-36

Under ideal conditions, the VSWR of these steps is as given in Young's Tables (S ≤ 1.03). In ferrite loaded devices these conditions are never achieved and, in digital phase shifters, the actual conditions are far less than ideal. Among the more serious problems are gaps between the ferrite toroid and the waveguide walls, an rf permeability which changes with switching, rf interaction with the charging wires, bit-to-bit discontinuities, and so on. When the discontinuities due to these sources are minimized, it is common to obtain a total VSWR (reflections from both ends adding) of less than 1.15 across the band.

Figure 29 shows a cut-away view of the derived phase shifter test piece. The input and output are full width WR112 waveguide and two-step dielectric transformers are used for matching the empty waveguide to the ferrite-loaded portion. Polyiron sleeves are shown embedded in the waveguide walls around the charging wires to absorb any stray rf energy which would otherwise give rise to radiation problems.
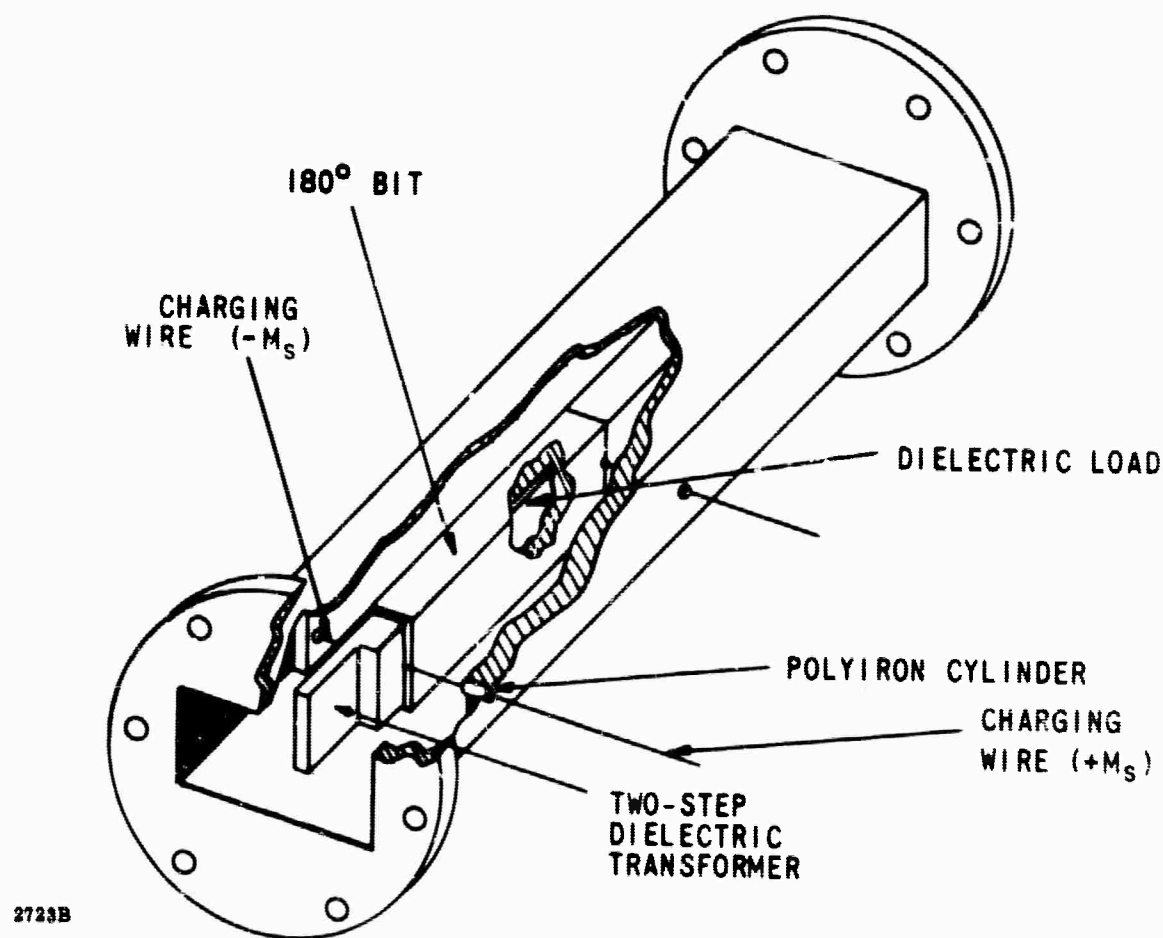
Figure 29. Cut-Away Illustration of the X-Band Nonreciprocal Digital Phase Shifter Structure

4.4.3 General Device Investigations

The basic test-piece depicted in Figure 29 was used to investigate the effects of the various structural parameters as well as frequency on phase shift, phase slope, losses, switching energy, and threshold power level.

The ratio c/a and waveguide width ka were varied experimentally to determine their influence on device performance. Three different "c" dimensions (.120", .135", .150") and five different "a" dimensions (.375", .500", .625", .875" and 1.125") were used. Three aluminum substituted yttrium iron garnets are a magnesium manganese ferrite were tested in these configurations. The properties of these materials are listed in Table VIII. The garnets have saturation magnetizations ranging from 960 to 1780 gauss, coercive fields of about .6 oersteds, and dielectric constants about 16. The ferrite has a $4\pi M_s$ of 2250, coercive field of 3.25, and a dielectric constant of 10. The remanent ratios $R_r = M_r/M_s$ varied.

Figure 30 shows a cross-sectional view of the basic phase shifter configuration depicted in Figure 29. The interior dimensions of the waveguide are "a" and "b"; the toroid has a height "b" throughout the measurements, variable width "c" and a slot of constant width "δ" filled with a low loss dielectric material with a dielectric constant of 15.

Figure 30 also shows the phase shift and slope of the G-243 garnet material with $4\pi M_r$ = 580 gauss. The curves are for "a" ranging from .375 to 1.125 inches and for c = .120, .135, and .150 inches.

It is seen that zero slope is obtained in the area of a = .400 inch, giving 67 degrees/inch, 87 degrees/inch and 79 degrees/inch for c = .120, .135, and .150 inches respectively. Note that the sample having the least slope gives the maximum phase shift. This is consistent with the theory (Section 3.4.2).

Figure 31 shows somewhat the same pattern and the same trends for the G-404 garnet with $4\pi M_r$ = 780 gauss. The maximum phase shift is about 120 degrees/inch and again, it is seen that the ferrite having the least slope gives the greatest amount of phase shift, except this time it is the sample with the largest width.

In Figure 32 the same trends are seen; here, maximum phase shift corresponds to the condition for minimum slope in the Sperry G-232 garnet with $4\pi M_r$ = 1040 gauss. The maximum phase shift is about 150 degrees/inch. As expected, this garnet, with a $4\pi M_r$ greater than G-243 by a factor of about 1.8, produces about 1.8 times as much phase shift (all other things equal).

TABLE VIII. PROPERTIES OF GARNET MATERIALS USED

$$3\left[(1.0-x)Y_2O_3 \cdot xRE_2O_3\right] \cdot 5\,(1.0-w)Fe_{1.925}O_3$$

SMEC NO.	COMPOSITION x	w	BATCH SIZE (gms)	WAXING TIME (HRS)	FIRING SCHEDULE °C/hr	SAMPLE SHAPE	DENSITY gms/cm³	PARTICLE SIZE (MICRONS)	DIELECTRIC LOSS TAN. (X BAND)	DIELECTRIC CONSTANT (X BAND)	g FACTOR	LINE WIDTH ΔH (oe) X BAND
G-289 S	0	0	750	16	1475/5	D	5.09	15	<0.0001	15.7	2.02	40
PG-232-61P	0	0	1450	24	1475/5	E	5.11	16	<0.0001	16.0	2.02	2
G-290N	0	0.03	750	16	1475/5	D	5.07	16	<0.0001	15.5	2.01	33
G-404-2C	0	0.05	750	16	1475/5	E	5.08	NM	<0.0001	15.8	2.01	30
G-404-2C	0	0.05	750	16	1475/5	D	5.07	9	<0.0001	15.7	2.01	31
G-291Q	0	0.08	750	16	1475/5	D	5.05	15	<0.0001	15.4	2.01	32
G-243-2C	0	0.10	750	16	1475/5	D	5.02	10	<0.0001	15.2	2.01	38
PG-243-5y	0	0.10	710	16	1475/5	E	5.02	NM	<0.0001	15.2	2.01	5
G-292-R	0	0.12	750	16	1475/5	D	5.04	10	<0.0001	15.3	2.01	30
G-293-U	0	0.15	750	16	1475/5	D	5.04	8	<0.0001	15.0	2.01	33
G-293-R	0	0.15	750	16	1500/5	D	5.04	14	<0.0001	15.0	2.01	30
G-238-5C	0	0.20	750	16	1500/5	D	4.99	10	<0.0001	14.9	2.02	36
G-250-4C	0	0.25	750	16	1500/5	D	4.98	9	<0.0001	14.6	2.03	50
G-345-K	0.01 Dy	0	750	16	1475/5	D	5.09	NM	<0.0001	15.6	NM	NM
G-129-2C	0.02 Dy	0	750	16	1475/5	D	5.13	NM	<0.0001	15.7	1.99	80
G-351-2D	0.05 Dy	0	750	16	1475/5	D	5.17	NM	<0.0001	15.6	1.94	165
G-351-2C	0.10 Dy	0	750	16	1475/5	D	5.26	NM	<0.0001	15.9	1.88	280
G-295-E	0.15 Gd	0	750	16	1475/5	B	5.30	NM	<0.0001	16.0	2.02	40
G-295-F	0.15 Gd	0	750	16	1475/5	A	5.30	NM	<0.0001	16.0	NM	NM
G-295-G	0.15 Gd	0	750	16	1475/5	C	5.30	NM	<0.0001	16.0	NM	NM
G-429-C	0.25 Gd	0	750	16	1475/5	D	5.42	NM	<0.0001	16.0	2.02	70
G-296-18G	0.30 Gd	0	3000	24	1475/5	A	5.45	NM	<0.0001	16.1	2.02	82
G-296-18J	0.30 Gd	0	3000	24	1475/5	C	5.45	NM	<0.0001	16.1	2.02	80
G-296-18H	0.30 Gd	0	3000	24	1475/5	B	5.44	NM	<0.0001	16.1	2.02	80
G-430-D	0.06 Dy	0.05	750	16	147./5	D	5.18	NM	<0.0001	15.3	1.91	195

A

MATERIALS USED IN DEVICE STRUCTURES

$$(1.0-w)Fe_{1.925}O_3 \cdot wAl_{1.925}O_3$$

DIELECTRIC CONSTANT (BAND)	g FACTOR	LINE WIDTH ΔH (oe) X BAND	$4\pi M_s$ (GAUSS)	DRIVE CURRENT I_D (AMPS RMS)	COERCIVE FIELD H_c (oe)(60~)	COERCIVE FIELD (H_g/H_c)	SQUARENESS S_D	$4\pi M_{RD}$ (GAUSS)	REMANENCE RATIO R_R
5.7	2.02	40	1780	3.3	0.28	10	0.84	1173	0.66
6.0	2.02	3	1780	4.7	0.5	10	0.90	1037	0.58
5.5	2.01	33	1650	4.65	0.39	10	0.86	1280	0.78
5.8	2.01	30	1375	4.30	0.55	10	0.83	780	0.57
5.7	2.01	31	1375	5.75	0.49	10	0.84	995	0.72
5.4	2.01	33	1200	4.90	0.42	10	0.83	793	0.66
5.2	2.01	38	960	7.20	0.61	10	0.81	720	0.75
5.2	2.01	35	960	6.10	0.70	10	0.87	581	0.61
5.3	2.01	30	900	7.05	0.60	10	0.84	660	0.73
5.0	2.01	33	675	7.75	0.66	10	0.80	490	0.73
5.0	2.01	30	675	4.60	0.39	10	0.78	470	0.70
4.9	2.02	36	380	4.30	0.37	10	0.87	305	0.80
4.6	2.03	50	180	6.25	0.51	10	0.77	135	0.75
5.6	NM	NM	1780	4.30	0.37	10	0.86	1200	0.67
5.7	1.99	80	1780	4.20	0.36	10	0.87	1320	0.74
5.6	1.94	165	1770	5.45	0.46	10	0.72	1005	0.57
4.9	1.88	280	1700	5.10	0.43	10	0.83	1155	0.68
5.0	2.02	40	1530	5.7	0.65	10	0.81	960	0.63
5.0	NM	NM	1530	5	0.60	10	0.87	950	0.62
5.0	NM	NM	1530	4.2	0.60	10	0.62	960	0.63
5.0	2.02	70	1300	7.50	0.65	10	0.60	590	0.45
5.1	2.02	82	1240	5.8	0.70	10	0.71	580	0.47
5.1	2.02	80	1240	4.8	0.70	10	0.58	635	0.51
5.1	2.02	80	1240	6.1	0.70	10	0.74	620	0.50
5.3	1.91	195	1300	5.35	0.45	10	0.85	950	0.73

*SAMPLE SHAPE

A 0.025 0.135 0.220 0.385

B 0.010 0.012 0.010 0.245

C 0.048

D .318 0.200 0.500 .025

E 0.245 0.385 0.135 0.012

4-39/40
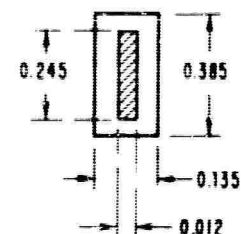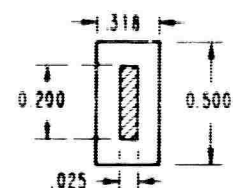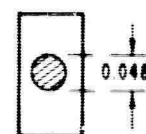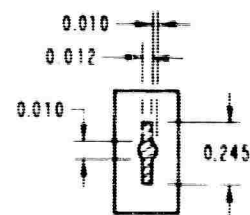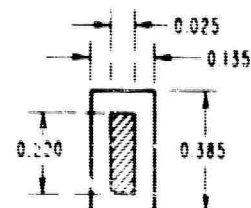
B
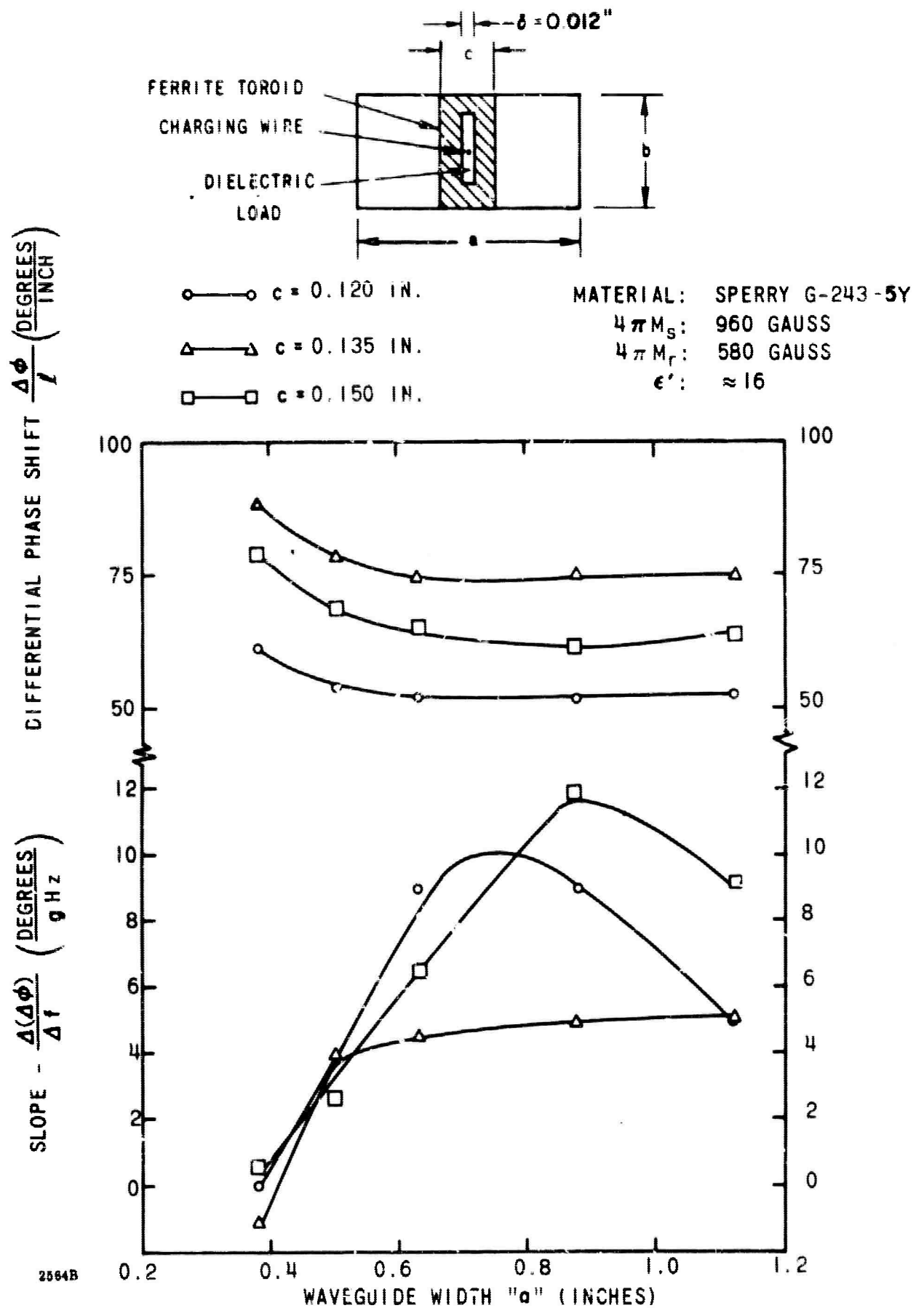
Figure 30. Differential Phase Shift and Slope vs (at 9 gHz) Waveguide Width "a" With Toroid Width "c" as Parameter for Sperry Garnet G-243
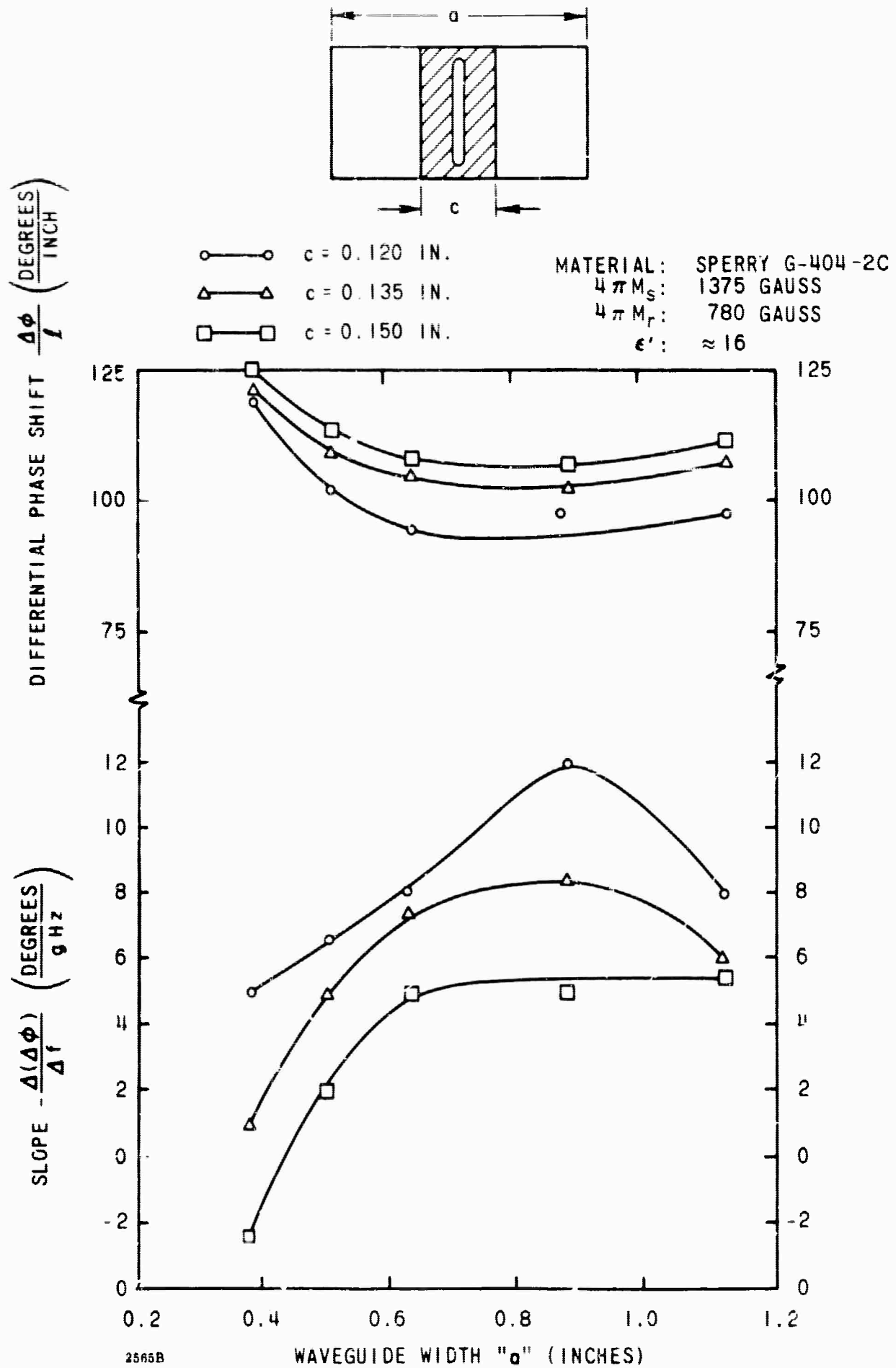
Figure 31. Differential Phase Shift and Slope (at gHz) vs Waveguide Width "a" With Toroid Width "c" as Parameter for Sperry Garret G-404
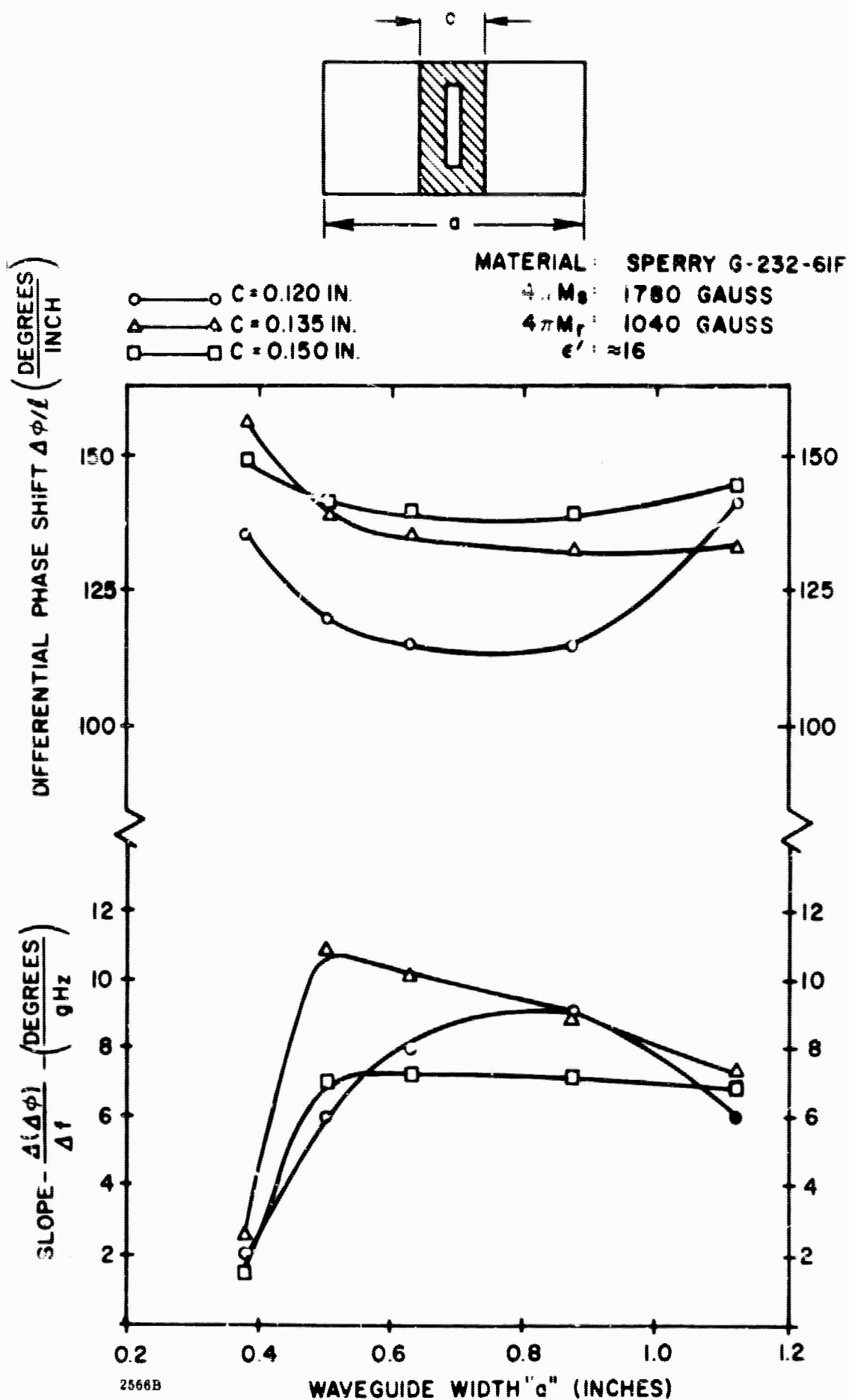
Figure 32. Differential Phase Shift and Slope (at 9 gHz) vs Waveguide Width "a" With Toroid Width "c" as Parameter for Sperry Garnet G-232

Figure 33 shows the phase shift and slope curves for the Sperry F-118 ferrite. The slope again goes to zero at about a = .400 inch for the toroid with c = .150 inch. Although the $4\pi M_s$ = 2250 gauss, the $4\pi M_r$ is only 570 gauss so that the maximum phase shift is about 70 degrees/inch. This low $4\pi M_r$ is now attributed primarily to the high coercive force.

The losses of the garnet materials used in these tests are shown in Figure 34. While these curves are somewhat erratic, it is possible to draw some tentative conclusions. It appears that the loss increases little, if any, with increasing $4\pi M_s$ for these narrow linewidth materials operating far from resonance. Thus, since phase shift goes directly as $4\pi M_s$, the figure of merit for these materials is also proportional to $4\pi M_s$. It further appears that maximum loss corresponds to the smallest waveguide width "a" but is not least for the largest "a". Thus it seems that some intermediate value of "a", as near to .375" as losses permit, would give not only an optimum figure of merit but also small phase slope. It is also seen that, over the range of "c" dimensions tested, the .150" value gives the least loss. The .135" value also gives less loss than the .120". This is interesting because it indicates that both from a loss and phase shift standpoint the wider toroids will have better figures of merit.

The switching energies of the toroids used were calculated by the method of section 4.4.1. Dividing the energy values thus obtained by the measured phase shift at 9 gHz for the foregoing conditions, we are able to plot the curves shown in Figure 35. These are curves of total switching energy per degree of phase shift versus toroid width "c" and waveguide width "a". It is seen that, in all materials, for a = .375 inch and c = .135 inch, less energy is required. Also as expected, the higher $4\pi M_s$ materials require less energy per degree of phase shift (except for the ferrite). Thus, a 360 degree phase shifter with a = .375", c = .135" using pure YIG with $4\pi M_r$ = 1040 gauss would consume 360 x .60 = 216 microjoules total energy (including wire and toroid energy losses) during each switching event at 9 gHz. Using G-243 ($4\pi M_r$ = 580) a total energy of 360 x .67 = 315 microjoules would be consumed. Note that the coercive fields of all three of these garnet materials are about the same. This comparison points up another good reason for choosing high $4\pi M_r$ materials where other requirements permit.

Figure 36 shows the threshold power level of five garnet materials versus ω_m/ω where $\omega_m = \gamma 4\pi M_s$ and ω is the operating frequency. For all data points except the lower right, a = .375 inch, b = .385 inch. For the lower right point, a = 1.000 inch and b = .372 inch. The curve on the left shows a strong dependence on ω_m/ω;
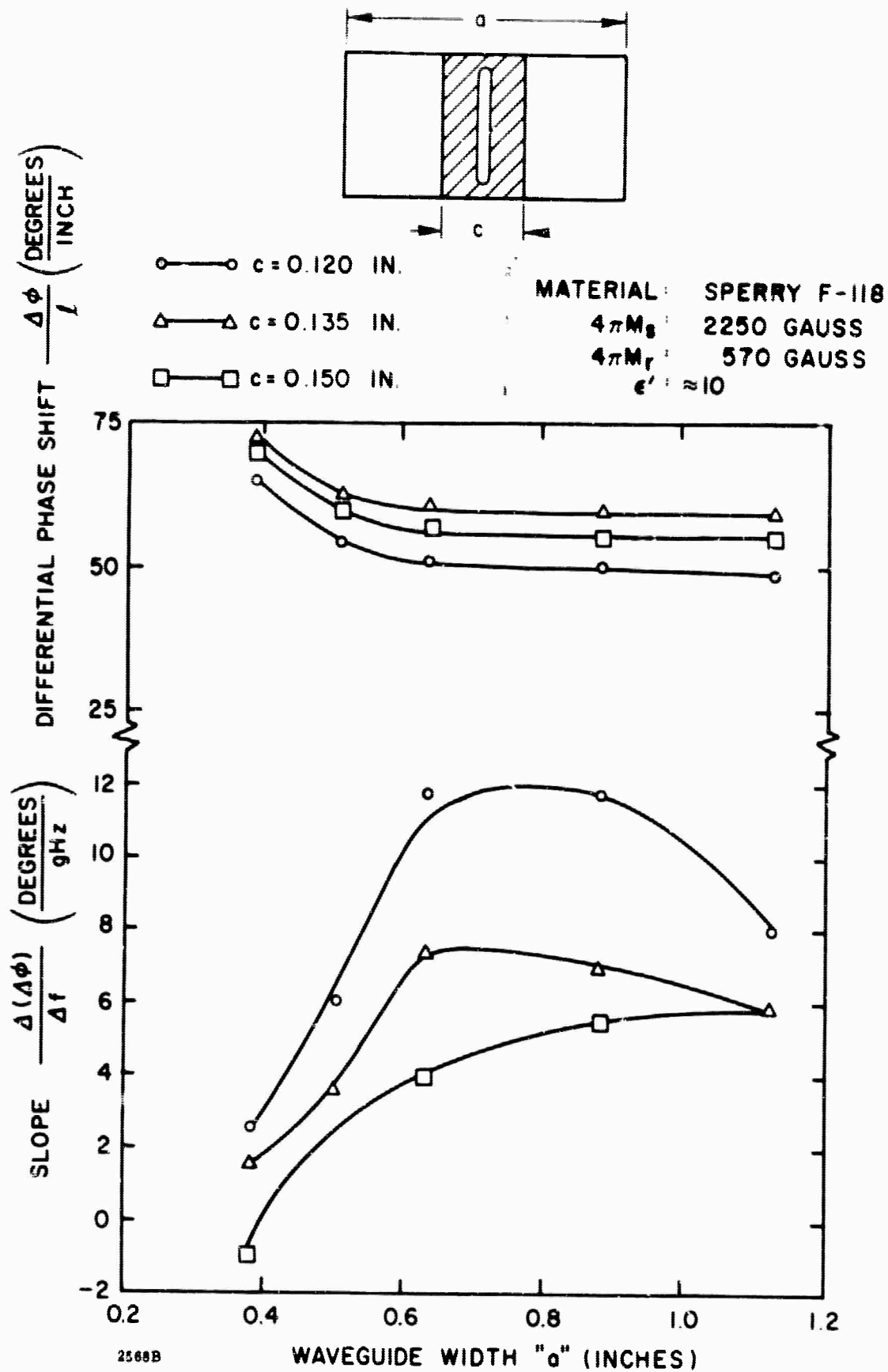
Figure 33. Differential Phase Shift and Slope (at 9 gHz) vs Waveguide Width "a" With Toroid Width "c" as Parameter for Sperry Ferrite F-118
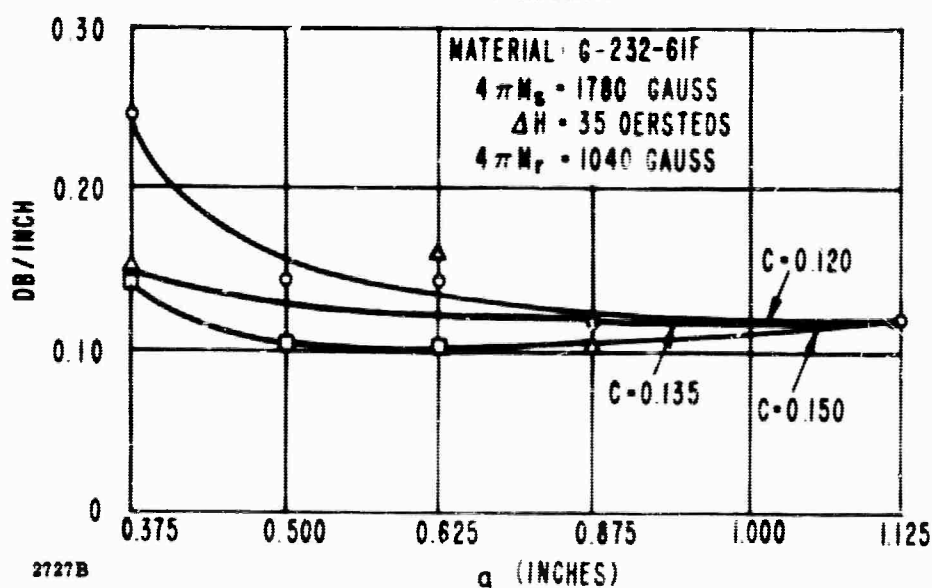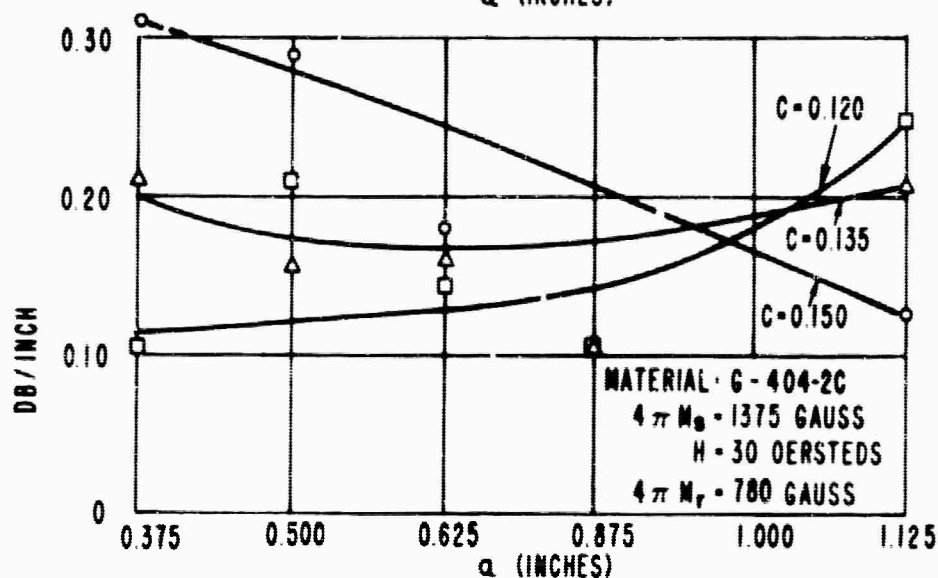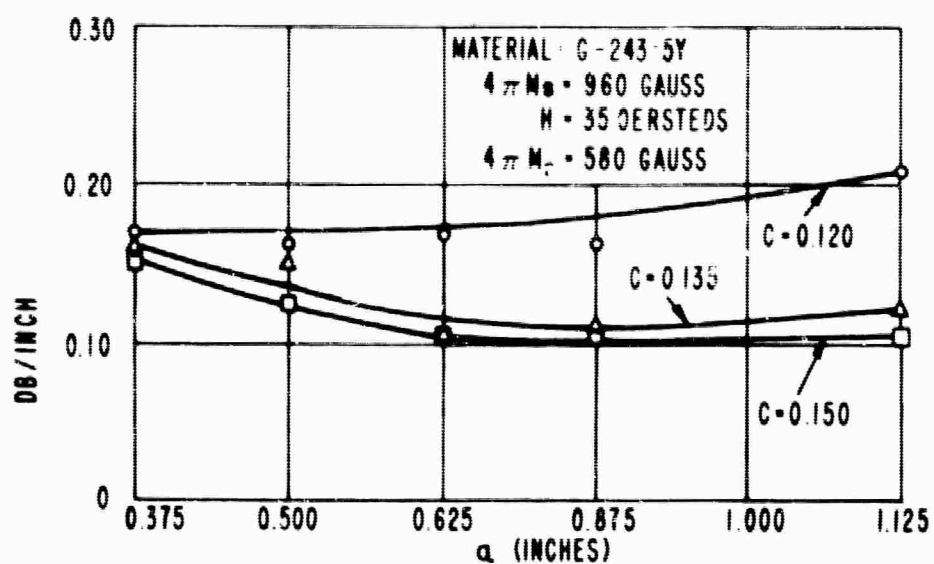
Figure 34. Loss Per Unit Length (at 9 gHz) vs Waveguide Width (a) and the Toroid Width (c)
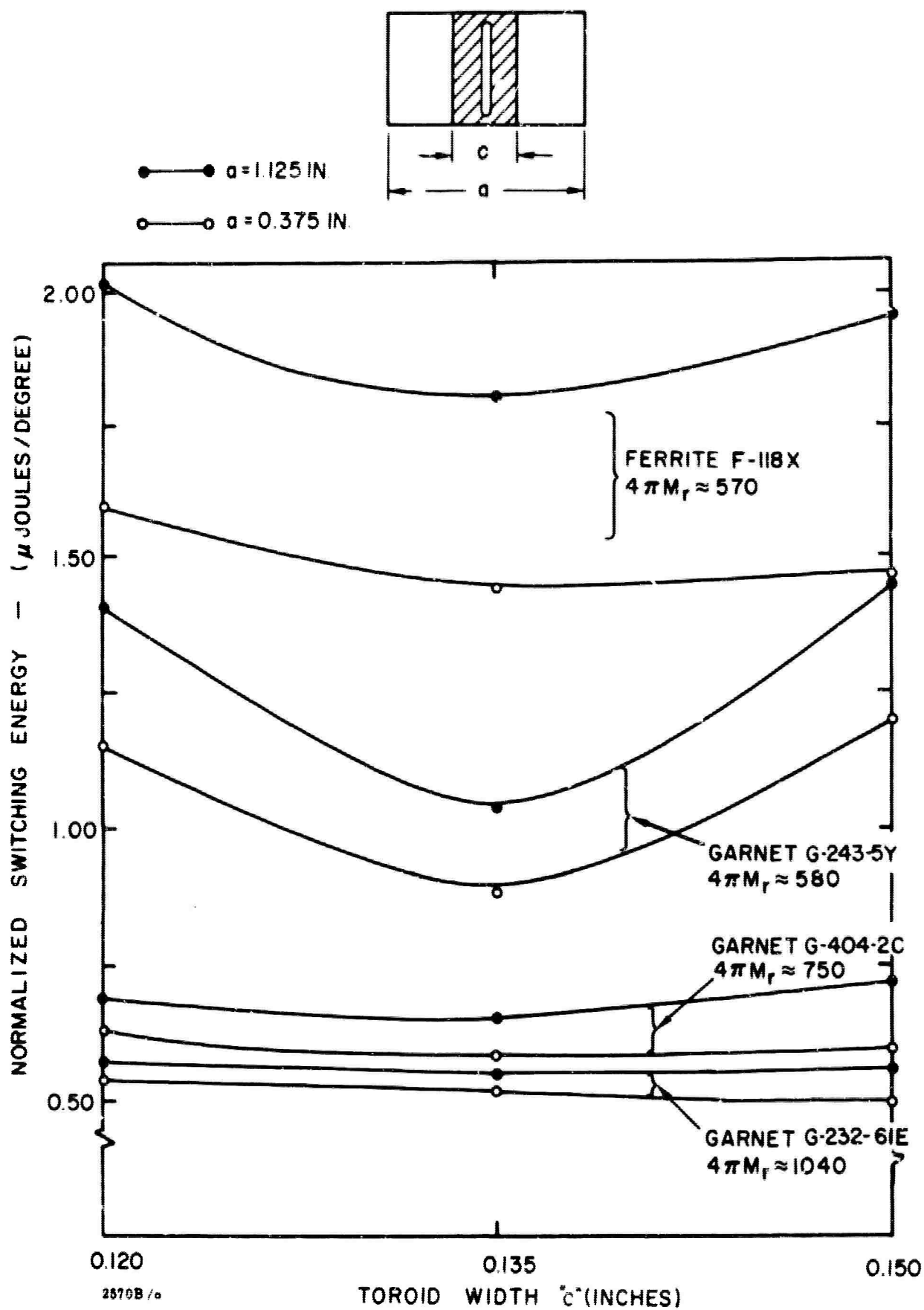
Figure 35. Total Switching Energy Per Degree Phase Shift vs
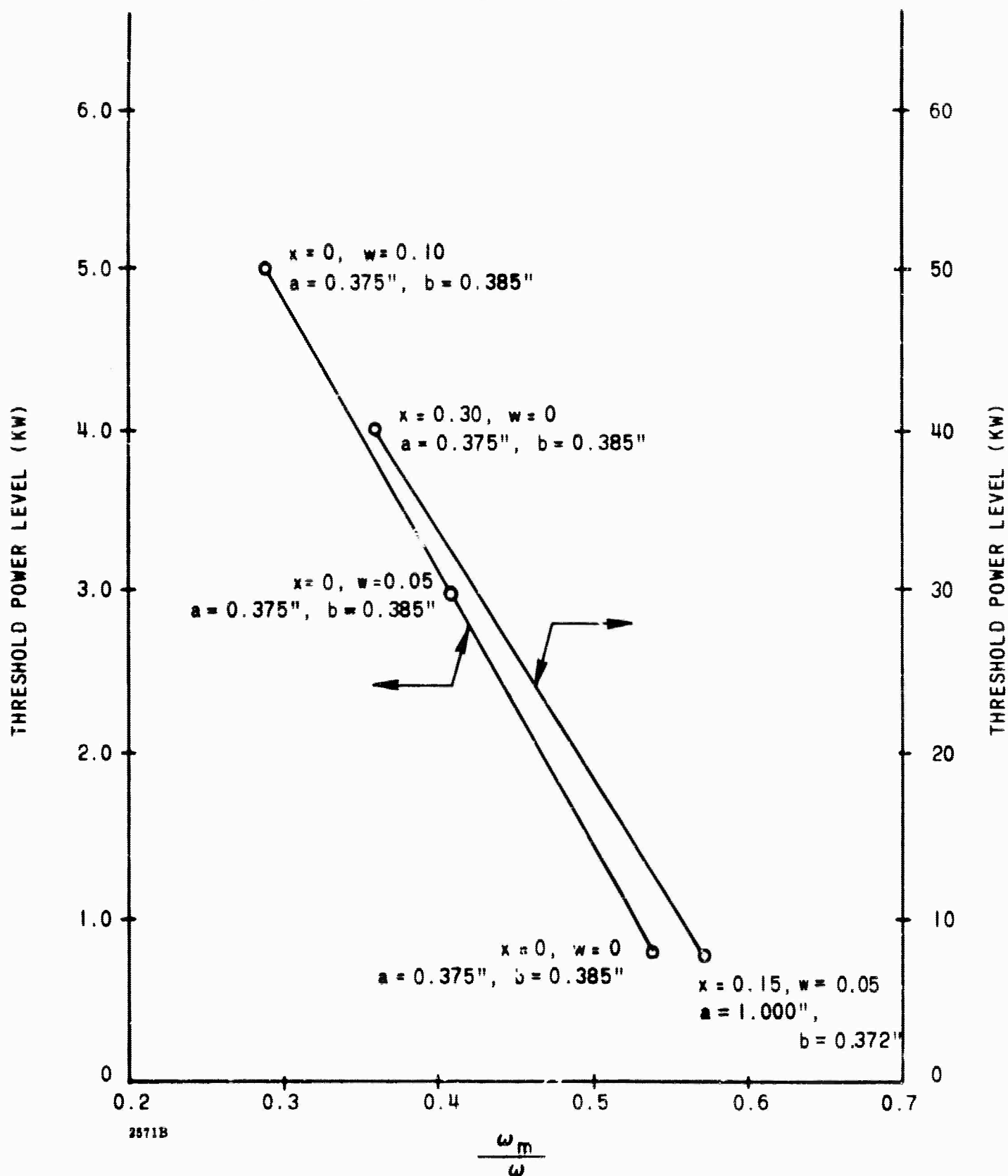Toroid Width "c" and Waveguide Width "a" at 9 gHz

$$3\left[(1-x)\ Y_2O_3 \cdot xGd_2O_3\right] \cdot 5\left[(1-w)\ Fe_2O_3 \cdot wAl_2O_3\right]$$

Figure 36. Threshold Power Level Variation with Saturation Magnetization for Five Garnet Materials

the linewidths of these three materials are approximately the same. The linewidths of the materials in the right hand curve are 82 oersteds and 65 oersteds for the top and bottom, respectively. These latter two materials are temperature compensated materials containing gadolinium and were therefore expected to have much higher threshold power levels.

Figures 37 and 38 show differential phase shift and loss at 9 Gh_z versus dielectric constant ϵ_d' of the dielectric load for three different slot geometries and two different garnet materials. The waveguide dimensions are a = .500 inch and b = .385 inch. The exterior dimensions of the toroids are c = .135 inch and b = .385 inch. The measurements of phase shift and loss were made from 8.0 to 10.0 Gh_z but since both were virtually constant across the band, only the data at 9.0 Gh_z are presented in an attempt at consolidation.
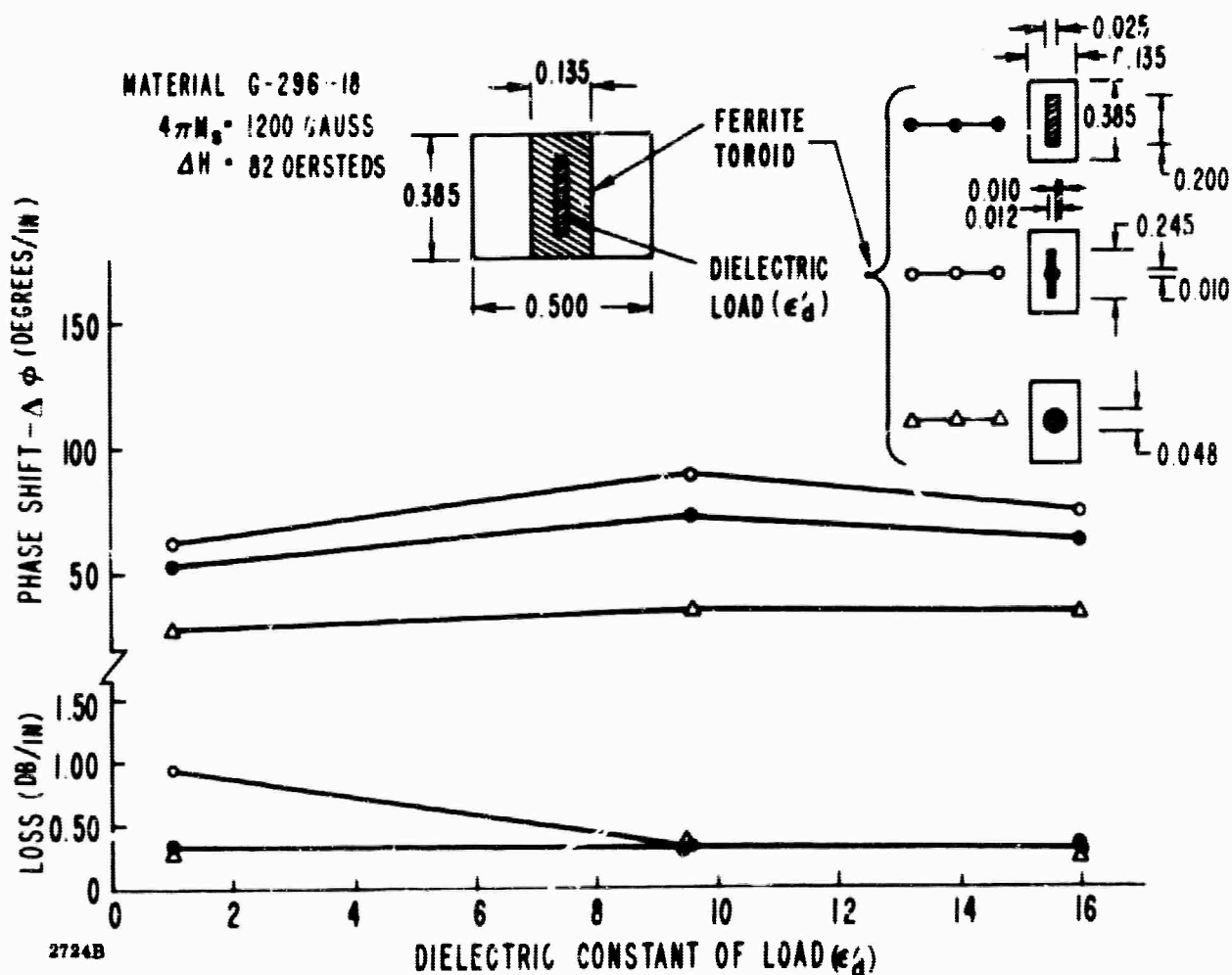
Figure 37. Phase Shift and Loss Vs Dielectric Constant and Geometry of Dielectric Load for G-296-18. Properties of Toroids Listed in Table VIII
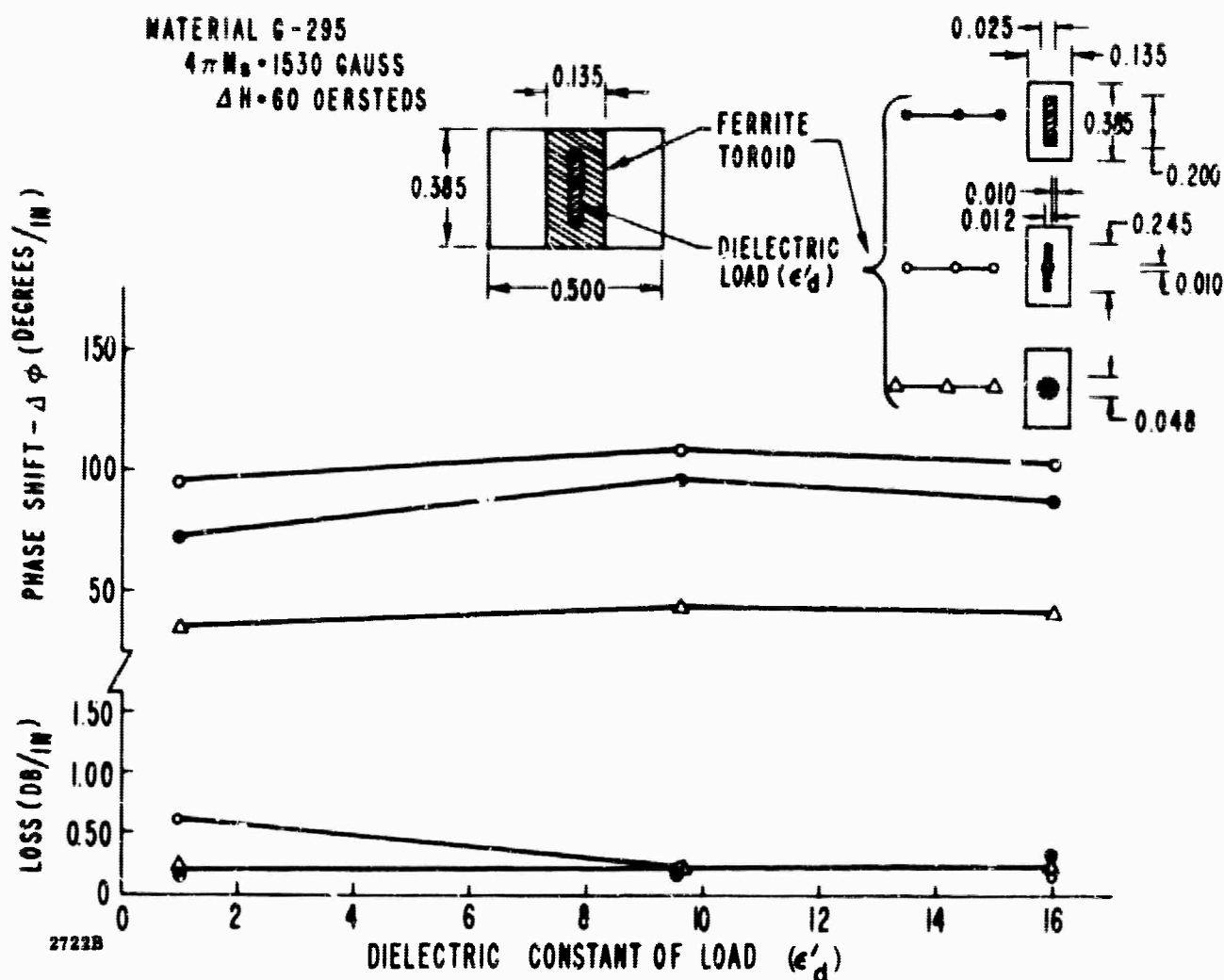
Figure 38 . Phase Shift and Loss Vs Dielectric Constant and
Geometry of the Dielectric Load for G-295. Proper-
ties of Toroids Listed in Table VIII

In both materials, maximum differential phase shift is obtained with the cruci-
form shaped slot while the round slot configuration gave the least phase shift. This
variation is probably due to the variation in the volume and magnetization of the active
portion of the material; that is, the material which contributes to the differential
phase shift. This would, of course, be the regions containing components of magne-
tization normal to the circularly polarized components of rf magnetic field.

It is also seen that $\epsilon'_d = 9.6$ gives the maximum phase shift in all cases. It
is not clear at this time why $\epsilon'_d = 9.6$ should give more phase shift than when $\epsilon'_d = 16$.
However, the difference is not great and may possibly be the result of a difference in
the fit between the dielectrics and the slots. The air-filled ($\epsilon'_d = 1$) cruciform con-
figuration was substantially more lossy than the other configurations and the G-295
material is less lossy than the G-296-18. This may be due to differences in the loss
tangents even though the measured loss tangent of both samples was < 0.0001.

4-50

The following comments are offered as a summary of the observed relationships between the operating characteristics and the material and structural parameters:

1. Phase shift is directly proportional to $4\pi M_r$, γ, and the volume of material containing components of circularly polarized rf magnetic fields orthogonal to the magnetization. This volume increases with dielectric constant and size of the toroid as well as the dielectric constant of the dielectric load. The geometry of the dielectric load should be consistent with the requirement for maximum volume. While phase shift increases drastically for sufficiently small waveguide widths, for larger widths it is relatively insensitive to width.

2. Phase slope is primarily a function of the waveguide width "a" and toroid width "c" and the dielectric constant of the toroid ϵ_f. For small waveguide widths, it a strong function of "a" and a weak function of $c\sqrt{\epsilon'}_f$. For large waveguide widths it is a weak function of "a" and a strong function of $c\sqrt{\epsilon_f}$. Minimum slope and maximum phase shift are obtained under the same conditions.

3. Switching energy increases with the volume and coercive field of the toroid and decreases with increased switching time.

4. Peak power threshold increases as the transverse component of the rf magnetic field and ω_m/ω decrease, and ΔH, ΔH_k increase, where $\omega_m = \gamma 4\pi M_s$, ΔH and ΔH_k are the linewidths of the material and $k\underline{th}$ spin wave, respectively.

5. Rf losses are dependent on virtually every feature of the structure: impedance mismatches, radiation, wall and dielectric losses, and magnetic loss. Properly designed impedance transformers effectively eliminate mismatches while radiation loss can be virtually eliminated by controlling the field patterns so as to assure minimum interaction between the rf electric field and the charging wires. Wall and dielectric losses depend essentially on the sizes of the waveguide and toroid as well as the conductivity of the waveguide and dielectric constant and loss tangent of the toroid. Assuming good conductivity and low loss toroid material, the optimum configuration is obtained by adjusting "a" and $c\sqrt{\epsilon_f}$ for minimum loss and zero phase slope. If the toroid loss tangent is not low then losses can be reduced by increasing the size and/or dielectric constant of the dielectric load provided it's loss tangent then the question of how close to ω_c can ω be is taken up in more detail in the following section.

4.4.4 Magnetic Losses

The usual methods of measuring magnetic loss in ferrite samples cannot be used here because of the demagnetizing field associated with the toroid geometry -- especially the requirement of zero applied field. Other workers have measured this loss previously [26,27] in shorted sections of coaxial line. The ferrite ring under test was placed against the short and the loss was related to the attenuation of the reflected wave. They observed a loss which decreased continuously with increasing frequency for a given material or, conversely, increased continuously with increasing saturation magnetization at a given frequency. In such a structure the rf magnetic field interacts only with the non-aligned components of the magnetization since it is parallel to the aligned components. The resultant loss is reciprocal.

Design of the Test Piece. In the structure shown in Figure 39, the losses result principally from interaction between the rf magnetic field and the alignment components of the magnetization M_r. The main advantages of this (waveguide) structure are that it more nearly represents the configurations used in actual phase shifters, and interaction is much stronger and the effect of reversing the toroid magnetization is not hidden. The main disadvantages are that the strength of the interaction varies somewhat as the volume of ferrite material experiencing circularly polarized rf fields changes, and it is not intrinsically broadband such as the coaxial structure. In the design of the test structure a special effort was made to minimize these disadvantages.

Defining bandwidth here as the ratio of the cutoff frequencies of the TE_{20} mode to the dominant TE_{10} mode*, then $B = \dfrac{F_c (TE_{20})}{F_c (TE_{10})} = \dfrac{k_c (TE_{20})}{k_c (TE_{10})}$. For air-filled waveguide, of course, $B = 2$. When a dielectric of thickness c is placed in the waveguide, B takes on higher values (see, for example, Figure 25) and, for the configuration shown in Figure 40, $B = 3.85$. Figure 40 also shows the variation of the ratio of the rf magnetic field components h_x and h_y, called the ellipticity $\left|h_x/h_y\right|$, with frequency at three different points in the dielectric. The values of $\left|h_x/h_y\right|$ shown were calculated using the expression

$$\left|h_x/h_y\right| = \frac{\beta a}{(16k^2 a^2 - \beta^2 a^2)^{\frac{1}{2}}} \cot (16 k^2 a^2 - \beta^2 a^2)^{\frac{1}{2}} X \qquad (52)$$

[26] H. Hair, "Development of Helical Phase Shifters", Final Report, Prepared by General Electric for MIT Lincoln Laboratory under Subcontract 250 (December 1964).

[27] D. H. Temme, "Progress and Problems in High Power Phasers for Array Radar", NEREM Record, 1964.

* P. H. Vartanian - ibid.

4-52

where

$$\beta a \;=\; 2\pi a/\lambda_g$$

$$ka \;=\; 2\pi a/\lambda$$

$$X \;=\; X_1,\; X_2,\; X_3. \;=\; /050a,\; .020a,\; .010a$$

a = the waveguide width

λg = the waveguide wavelength

λ = the free space wavelength

The appropriate values for βa can be found in Figure 27. The rf permeability was assumed equal to 1.

Referring again to Figure 40 it is seen that if $a = 2.66$ inches the TE_{10} mode cuts off at $ka = 1.4$ (1 Ghz) while the TE_{20} mode cuts off at $ka = 5.4$ (3.8 Ghz). Over the range $ka = 2.0$ to $ka = 5.4$, very little variation is observed in the ellipticity of the rf magnetic field components. Near the center of the dielectric the ratio gets large and its variation is more noticeable. In the actual phase shifter configurations, however, that portion comprises the slot of the toroid and, so, does not contribute to the magnetic losses. The assumption of unity for the rf permeability is misleading to the extent that in one direction of propagation the fields are slightly displaced relative to their positions for the other direction of propagation*, neither direction yielding exactly the same field configuration as the case in which the permeability was taken as unity. However, the variation of this factor with frequency is not expected to be substantially different in either direction of propagation.

The final important consideration in the design of the test piece is that of matching and launching the TE_{10} mode in the toroid loaded section. Since empty waveguide cannot propagate this wide range of frequencies it was necessary to enter the structure via a dielectric-loaded stripline configuration.[28] The width of the strip (see Figure 39) was tapered linearly from its value at the unloaded portion ($w/b = 1.2$) to a point ($w/b = 0$) and the pointed end was attached electrically to one of the ground planes. The strip thickness ($t/b \approx .01$) was made very small. The dielectric ($\epsilon' = 15$) was tapered from zero height at the point where $w/b = 1.2$ to full height at $w/b = 0$. Referring to Figure 41 it is seen that where $w/b = 1.2$ the impedance is about 50 ohms and, if displacing the strip does not appreciably alter the impedance[29], then, in the vicinity of $w/b = 0$, the impedance is $Z_o \approx \dfrac{190}{\sqrt{15}} \approx 50$ ohms. Using a dielectric constant of 15 here is only approximate since the wave is probably not contained entirely in the dielectric.

---

[28] J. Parks, L. Lavedan, B. Savage, "Miniaturized Ferrite Digital Phase Shifter for Phased Array Application" - to be published -

[29] S. B. Cohn, "Characteristic Impedance of Shielded Strip Transmission Line", IRE TRANSACTIONS of the PGMTT, April, 1954.
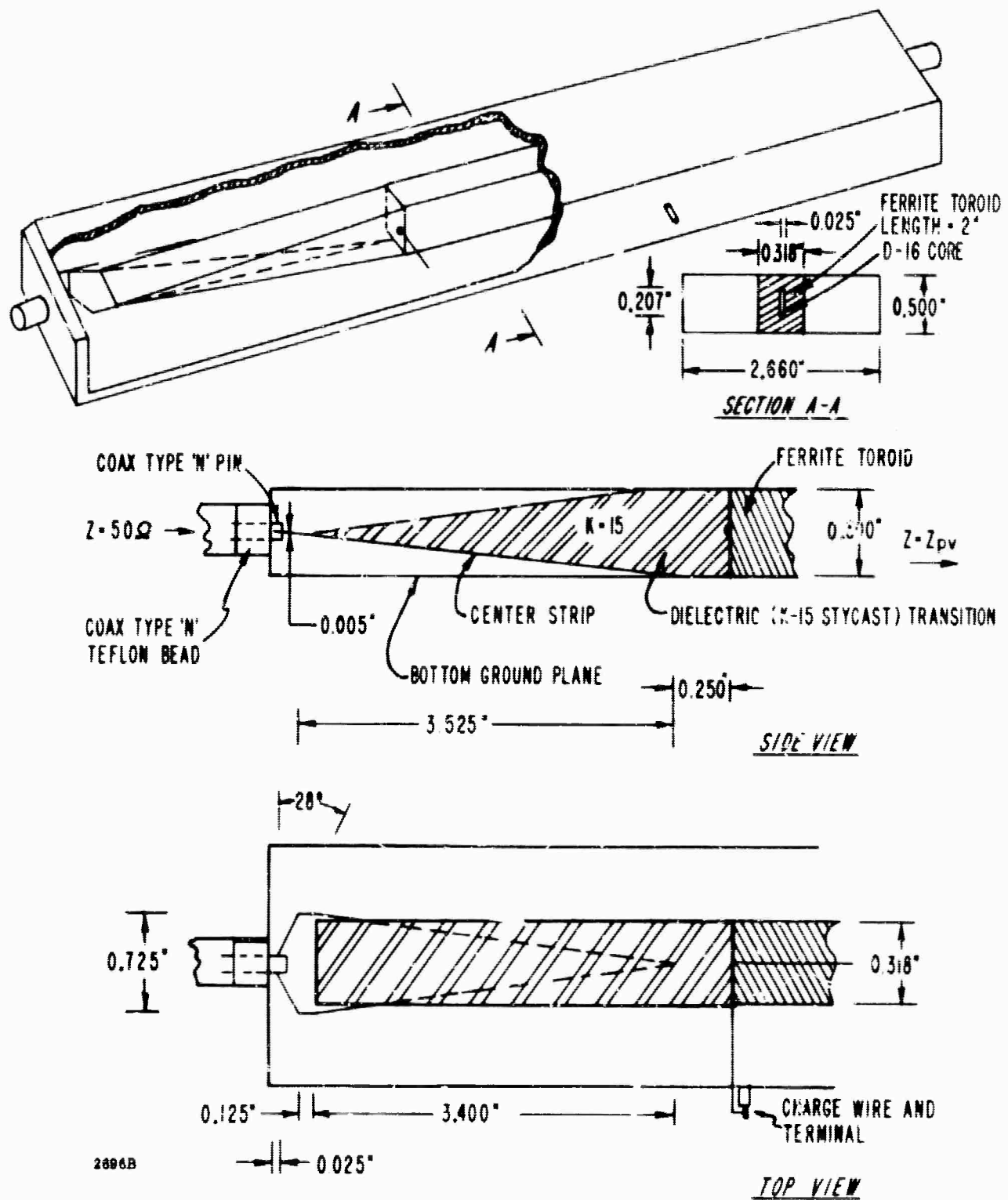
*W. Ince and E. Stern - Ibid.

FERRITE TOROID
LENGTH = 2"
D-16 CORE

SECTION A-A

COAX TYPE 'N' PIN

COAX TYPE 'N'
TEFLON BEAD

CENTER STRIP

BOTTOM GROUND PLANE

DIELECTRIC (K-15 STYCAST) TRANSITION

FERRITE TOROID

SIDE VIEW

CHARGE WIRE AND
TERMINAL

TOP VIEW

2696B

Figure 39. Test Piece For Magnetic Loss Measurements

4-54

$\epsilon' = 16$

$\mu' = 1$ (ASSUMED VALUE)

X = DISTANCE FROM WAVEGUIDE CENTER LINE TO POINT IN MATERIAL

$c/a = 0.12 \quad \dfrac{k_c (TE_{20})}{k_c (TE_{10})} = 3.85$

If a = 2.660 INCHES, THEN:

ka	FREQUENCY (Ghz)
2.5	1.770
3.0	2.125
3.5	2.480
4.0	2.830
4.5	3.185
5.0	3.549
5.5	3.893

ELLIPTICITY — $|h_x/hy|$

$X_3 = 0.010\,a$

$X_2 = 0.020\,a$

$X_1 = 0.050\,a$

TE_{10} MODE CUTOFF

TE_{2n} MODE CUTOFF

ka

2709B
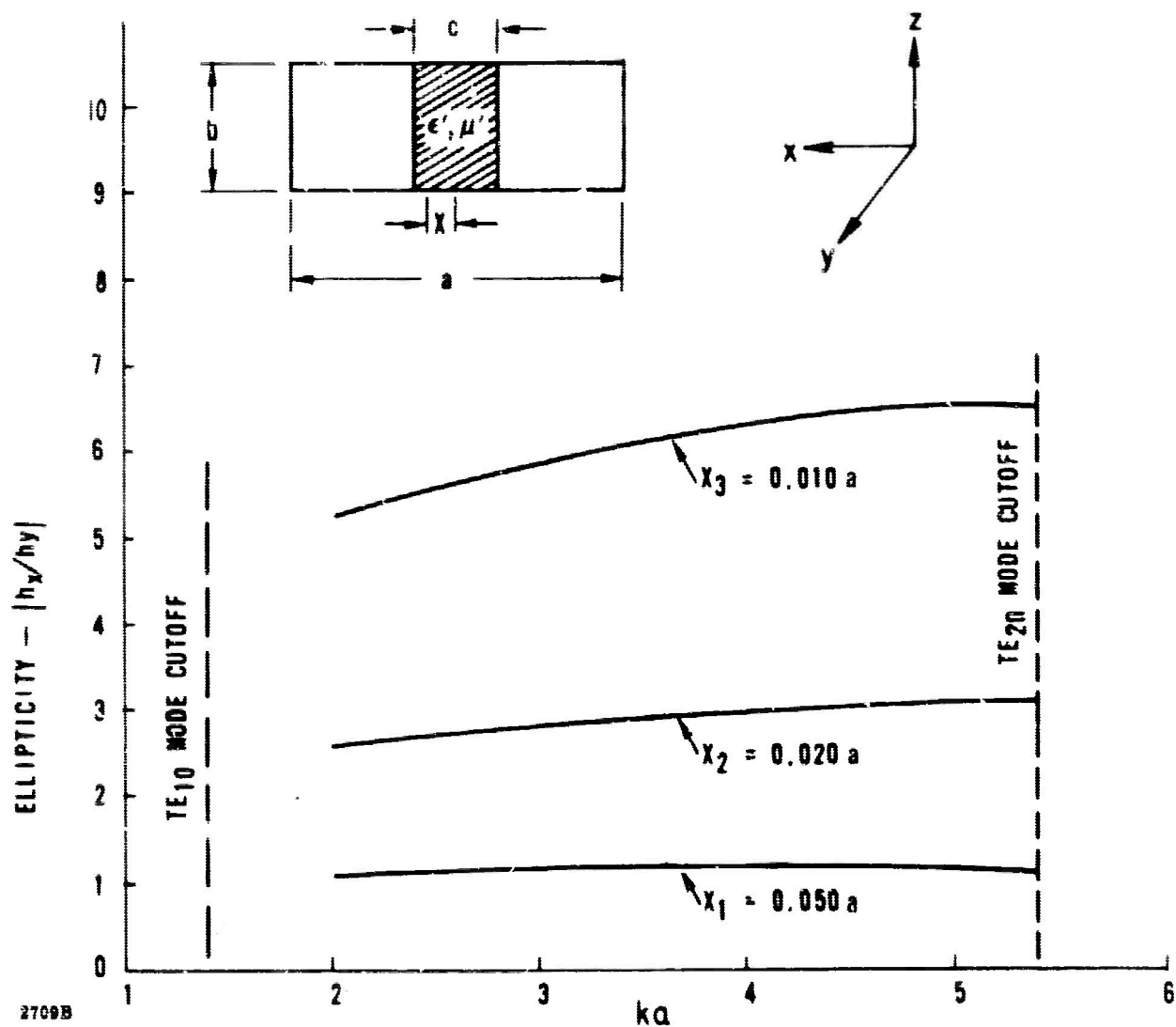
Figure 40. Variation of Ellipticity $|h_x/hy|$ with Frequency at these different points within a Dielectric ($\epsilon' = 16$) of width C = 0.12a

4-55

Beyond the point where $w/b = 0$ the TEM wave can no longer propagate but because of the dielectric loading, higher order modes are possible. The most likely higher order mode at any point in the TEM line is the TE_{11} mode which has a field configuration very much like the dominant TE_{10} mode in rectangular waveguide. Such a mode is able to propagate in the dielectr. loaded portion of the stripline and it remains only to provide an electrical discontinuity capable of exciting this mode. The reason for displacing the strip off the center line and shorting it to the ground plane is to provide a vertical assymetry which was found to be necessary in order to change the orientation of the rf magnetic field. The transition from the TE_{11} to the TE_{10} is natural and is probably completed at the point where $w/b = 0$.

The impedance of the waveguide portion of the structure was calculated in the following way. The power-voltage impedance of empty rectangular waveguide is given by [30]

$$Z_{pv1} = \frac{754 b_1}{a} \left(\frac{\lambda_{g1}}{\lambda} \right) = \frac{754 b_1}{a_1} \left(\frac{ka_1}{\beta_1 a_1} \right) \tag{53}$$

where $\beta_1 = 2\pi/\lambda_{g1}$, $k = 2\pi/\lambda$

and λ_{g1} = the guide wavelength in the air-filled waveguide Section 1. (See Figure 42.) If waveguide Section 2 is dielectrically loaded, then the ratio of the wave impedances of the two sections will be given by $Zw_2/Zw_1 = \beta_1 a_1/\beta_2 a_2$. It was assumed that if $a_1 = a_2$ and $b_1 = b_2$ then the power voltage impedance of section 2 will be

$$Z_{pv2} = \frac{754 b_1}{a_1} \left(\frac{ka_1}{\beta_1 a_1} \right) \left(\beta_1 a_1/\beta_2 a_2 \right) \tag{54}$$

or $\qquad Z_{pv2} = \frac{754 b}{a} \left(\frac{ka}{\beta_2 a} \right).$

The impedance Z_{pv2} was then set equal to 50 ohms at the anticipated center frequency of the operating band (3 Ghz) and the equation solved for b using a = 2.660 inches, and the appropriate values of $\beta_2 a$ obtained from Figure 27. This yielded

$$b = .1765 \, \frac{11.7}{4.25} = .487 \text{ inches.}$$

A value of b = .500 inches was chosen. Across the Frequency band of 2 to 4 Ghz, Z_{pv2} varies from a high of 62 ohms at 2 Ghz to 42 ohms at 4 Ghz. This is shown in Figure 42.

[x]G. Southworth, "Principles and Applications of Waveguide Transmission," D. Van Nostrand Publishing Co., December 1956, P 105.
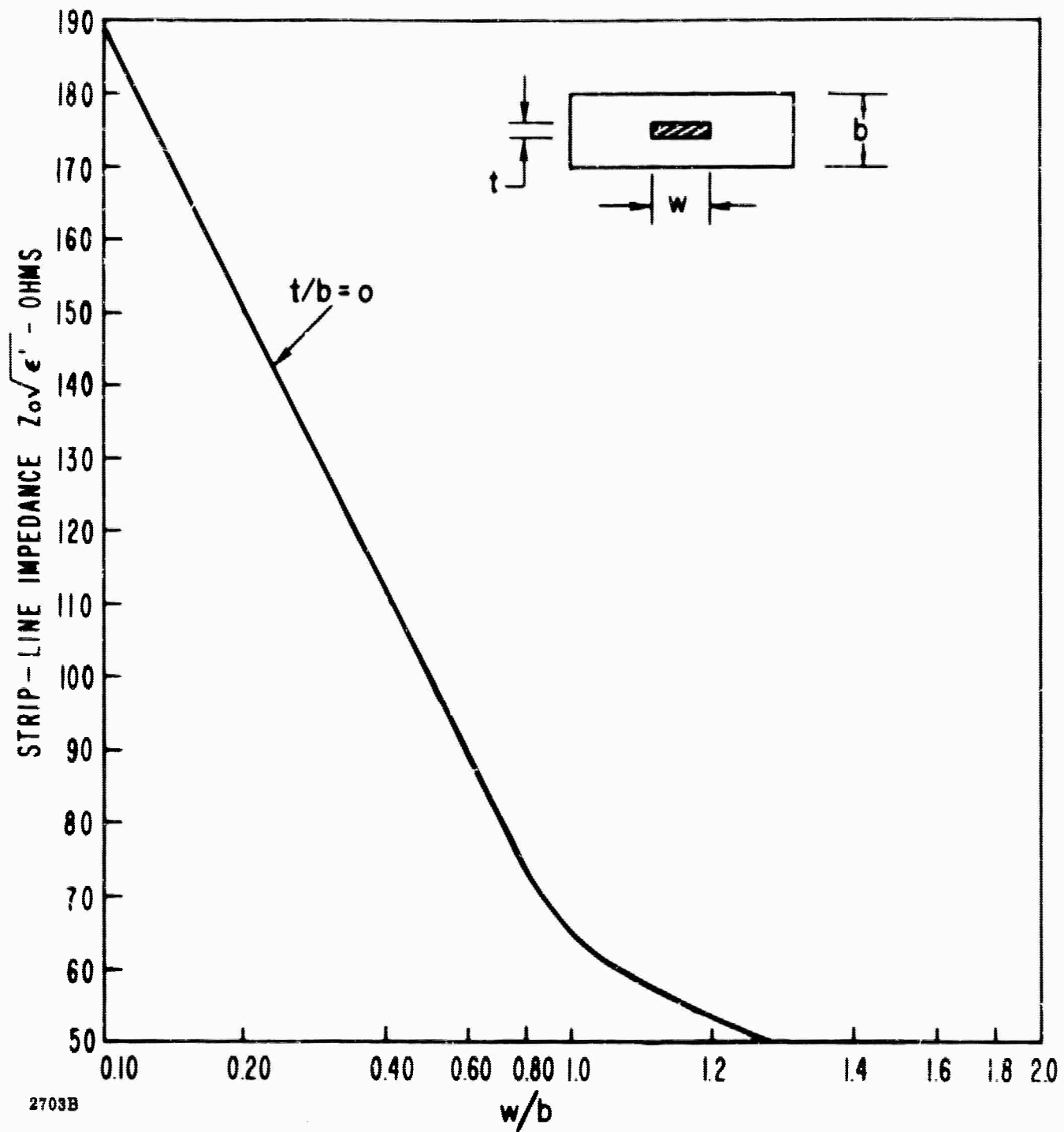
4-56

Figure 41. Stripline Impedance Varations With Strip Width W for Strip Thickness
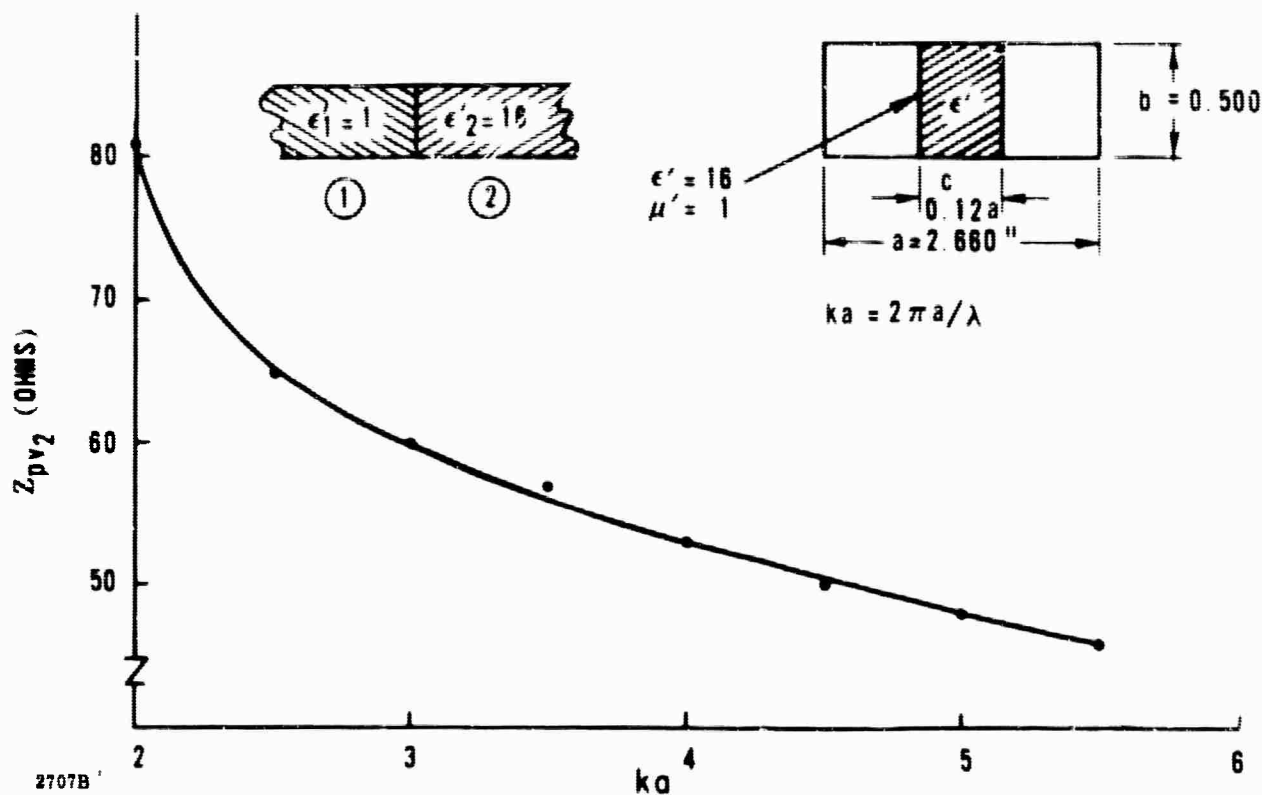
BLANK PAGE

Figure 42. Power Voltage Impedance of The Dielectric-loaded Waveguide as Calculated by Equation (54).

The complete structure is shown in Figure 39. It has type N female coaxial line connectors followed by a short section of air filled strip line, then the dielectric-loaded tapered strip portion leading into the dielectric loaded section of waveguide. While the impedance of the stripline portion should not vary with frequency, $Z_{pv\,2}$ does and this, combined with other reflections, yielded a total VSWR as shown in Figure 43 when the dielectric used in the waveguide was Trans-Tech's D-16. The loss of the structure is also shown in Figure 43.

The setup used for measuring magnetic loss was the same as that shown in Figure 23A with the exception that the couplers were Narda Model 3022 coaxial line couplers. Structural losses and dielectric losses were accounted for in the magnetic loss measurements by subtracting the loss due to VSWR and the measured loss of the D-16 from that of the ferrite toroids. Since the dielectric loss tangents and dielectric constants of the ferrites are very nearly the same as the D-16 the remainder was felt to closely represent the magnetic loss of the ferrite.
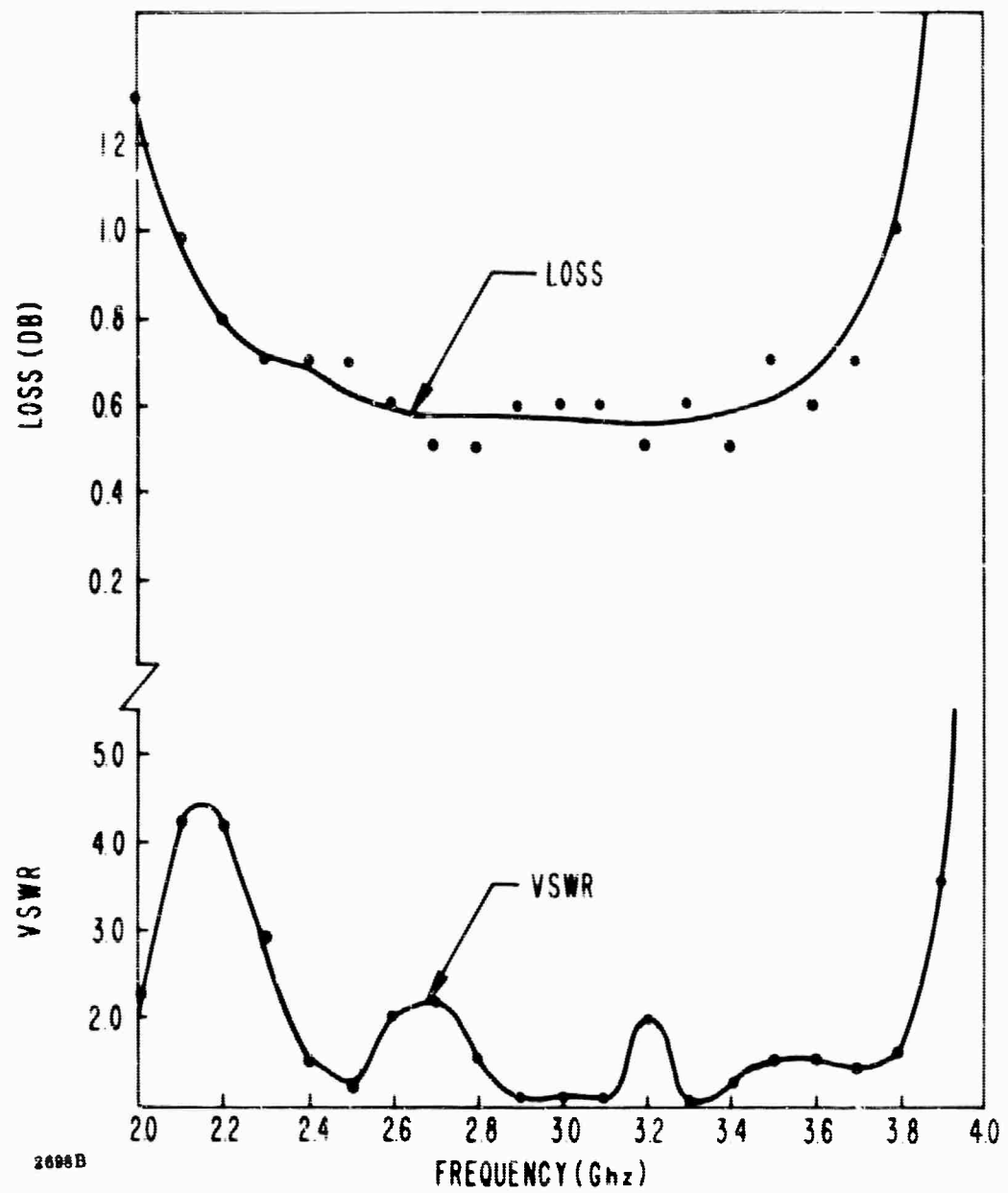
Figure 43. Loss and VSWR of the Derived S-Band Test Structure using D-16 Dielectric in place of the Ferrite Toroids

Magnetic Loss Measurements. Nine aluminum and a 1% dysprosium sub-stituted YIG toroids have been tested in the S-Band apparatus described above. Losses were measured for both the positive (CP+) and negative (CP-) circularly polarized waves by reversing the magnetization. The toroids were magnetized using a 500 microfarad, 50 volt capacitor which was allowed to freely discharge through the charging wire of the toroid (see Figure 44).

Figure 44 shows the loss of G-292-R (YIG, 12% Al) with $4\pi M_s$ = 900 gauss and ΔH = 25 oersteds. The capacitor was charged to 45 volts. The loss appears to reach a peak somewhere below 2 Ghz and is virtually the same as that of the D-16 dielectric at 2.5 Ghz. Defining a quantity ω_c as the frequency at which the toroid loss is indestinguishable from that of the D-16, then $\omega_c \approx 2.6$ Ghz.
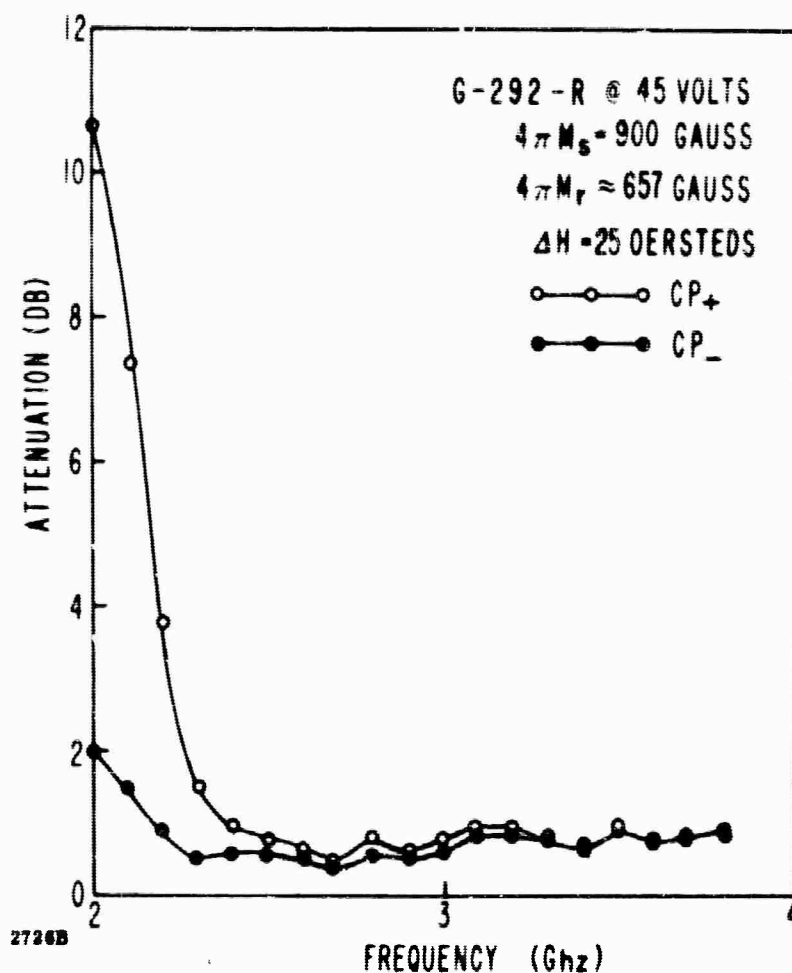
Figure 44. Magnetic Loss vs Frequency for 12% Aluminum Substituted YIG. See Table VIII for Material Properties.

Figure 45 shows the loss of G-243-2c (YIG, 10% Al) with $4\pi M_S$ = 960 gauss and ΔH=35 oersteds. Again the frequency at which the loss peaks up (ω_r) is below 2 Ghz but $\omega_c \approx 2.9$ Ghz.

Figure 46 shows the loss of G-291-Q with $4\pi M_S$ = 1200 gauss and ΔH = 30 oersteds. For this material $\omega_r < 2$ Gh$_z$ and $\omega_c \approx 3.1$ Gh$_z$.
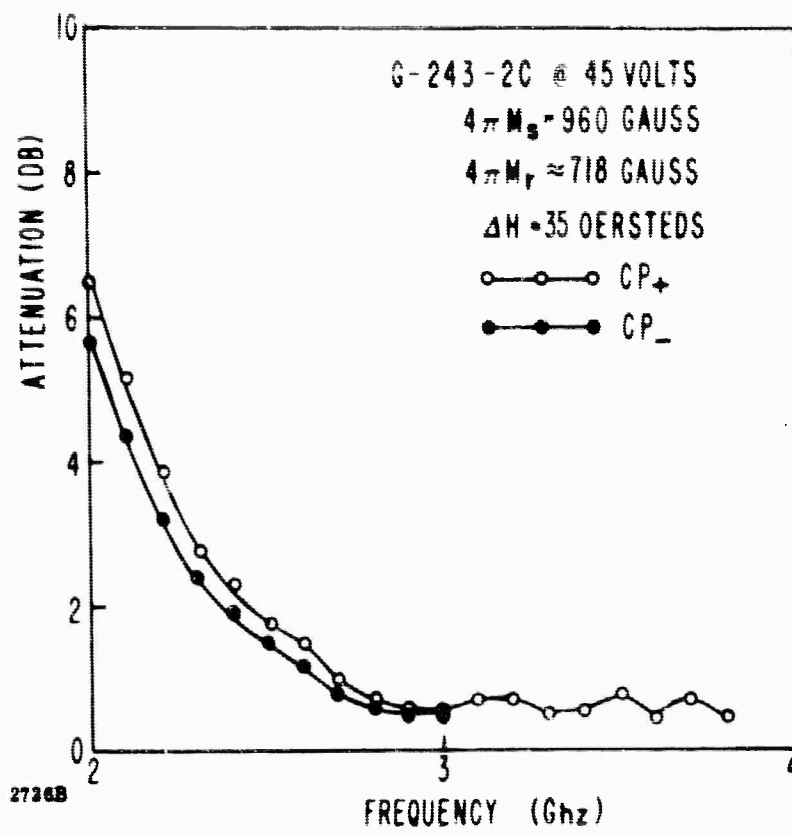
Figure 45. Magnetic Loss vs Frequency for 10% Aluminum Substituted YIG. See Table VIII for Material Properties.
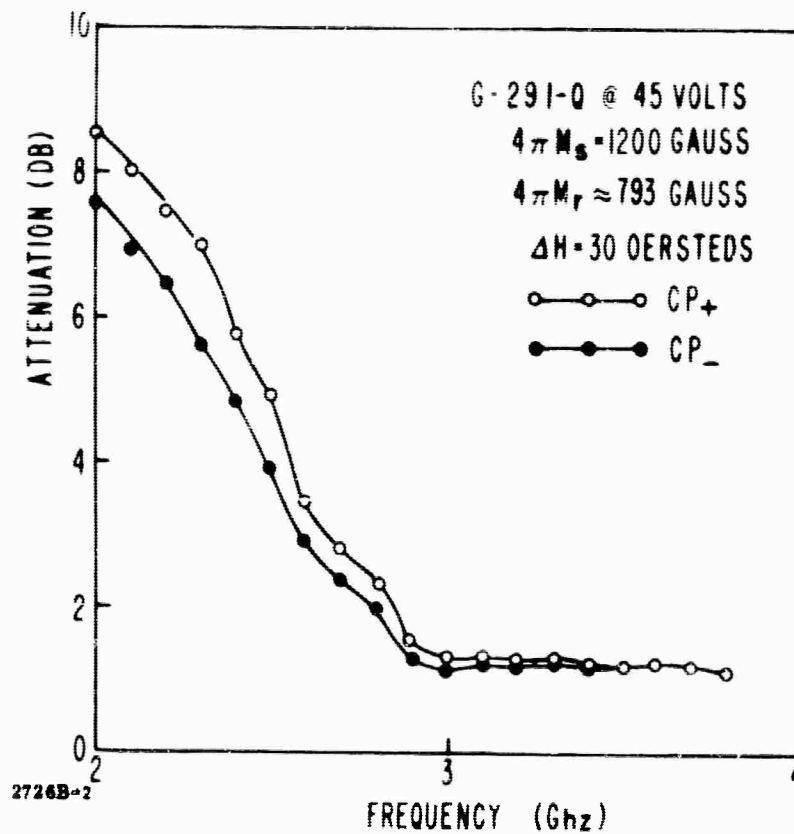

Figure 46. Magnetic Loss vs Frequency for 8% Aluminum Substituted YIG. See Table VIII for Material Properties.

4-60

In Figure 47, G-290-N (YIG, 3% Al), with $4\pi M_S = 1650$ gauss and $\Delta H = 34$ oersteds, peaks up at about $\omega_r \approx 2.7$ Gh$_z$ and $\omega_c > 3.8$ Gh$_z$.
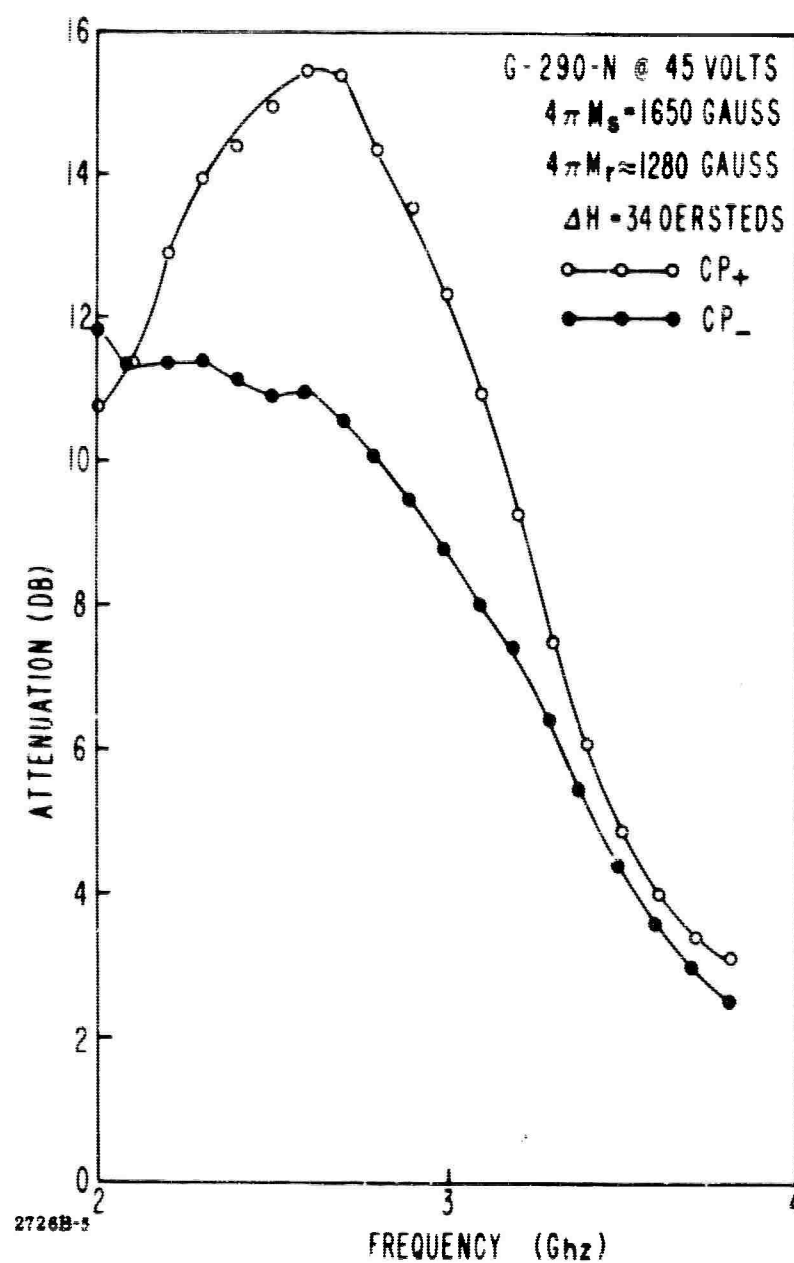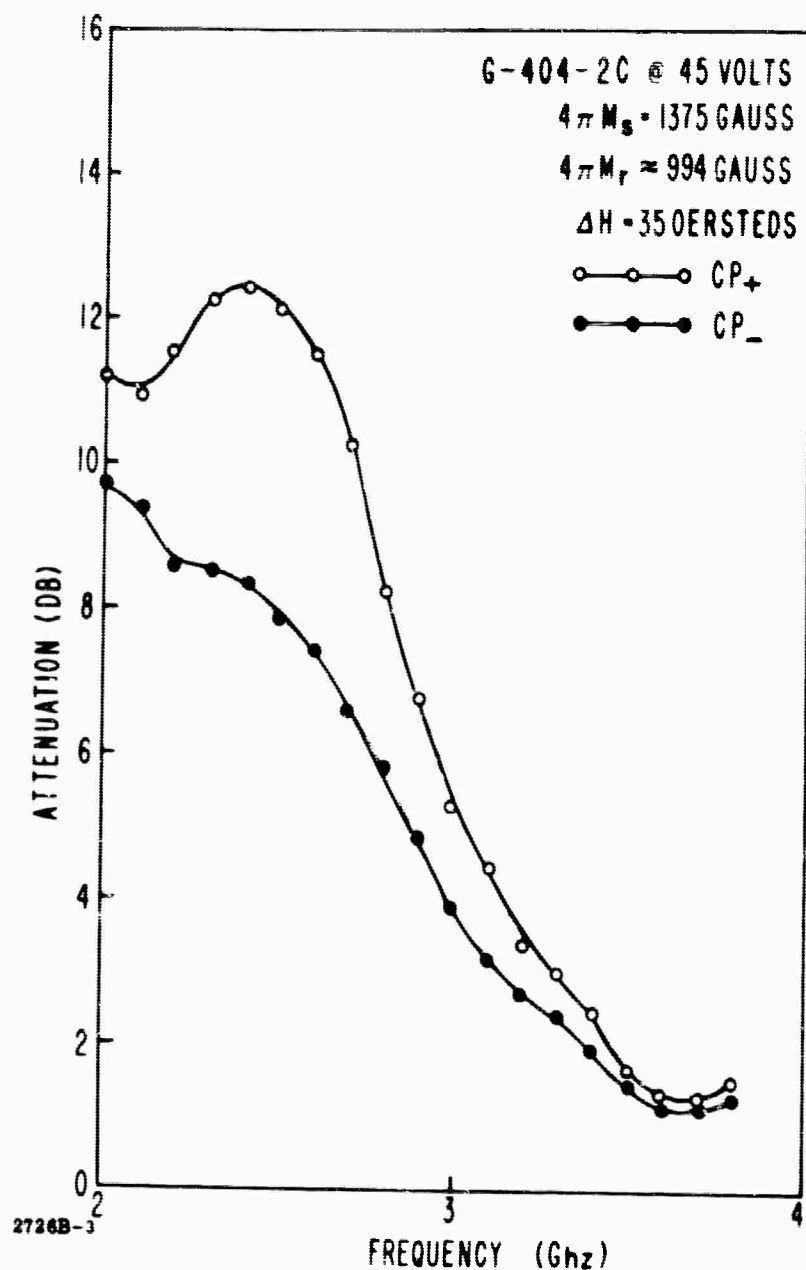

Figure 47. Magnetic Loss Versus Frequency for 3% Aluminum Substituted YIG. See Table VIII for Material Properties

In Figure 48, G-404 -2c (YIG, 5% Al), with $4\pi M_S = 1375$ gauss and $\Delta H = 35$ oersteds, a loss peak is seen at 2.4 Ghz. Whether or not this is the main resonance loss is not certain since the loss appears to be increasing again at 2.0 Ghz. For this material $\omega_c \approx 3.8$ Ghz.

Figure 48. Magnetic Loss vs Frequency for 5% Aluminum Substituted YIG. See Table VIII for Material Properties.

4-62

In Figure 49, G-289-S (YIG) with $4\pi M_s = 1780$ gauss and $\Delta H = 37$ oersteds is seen to peak up at $\omega_r = 3.0$ Ghz.

Thus, as $4\pi M_s$ increases the magnetude of the losses and ω_r increase.
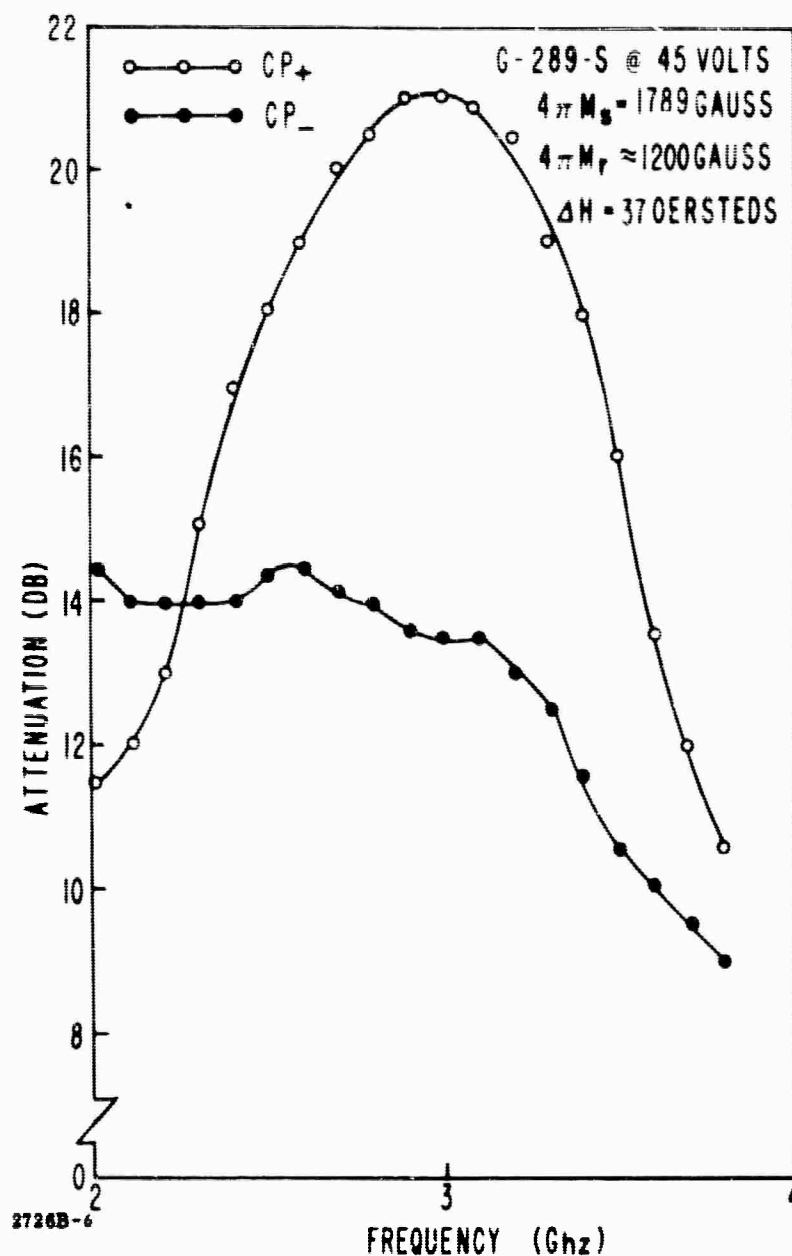
Figure 49. Magnet Loss Versus Frequency for YIG. See Table VIII for Material Properties

Figure 50 shows the (CP+) loss of the ten garnets plotted as a function of ω_m/ω. The graph clearly shows that for these narrow linewidth materials and for this geometry and charging voltage $\omega_r = \dfrac{\omega_m}{1.75}$ and $\omega_c \approx \omega_m$.

Figure 51 shows the CP+ and CP- loss of G-345 (1% D_y + YIG), at charge voltages of 45, 4 and 2 volts. As the charging voltage is decreased ω_r increases. At these charging voltages the loss peaks up at 2.9, 3.1 and 3.6 Gh_z, respectively. It is further seen that as the charging voltage is decreased the difference in loss between CP+ and CP- decreases.

Figure 52 shows the loss of the same sample after annealing at 1000°C to assure a virgin state. The loss of the uncharged toroid was measured and CP+ and CP- losses are represented by the single 0 volt curve of the figure. The sample was then magnetized by a 1 volt charge on the capacitor which resulted in the CP+ loss peak of 21 db and a CP- loss of 14 db.
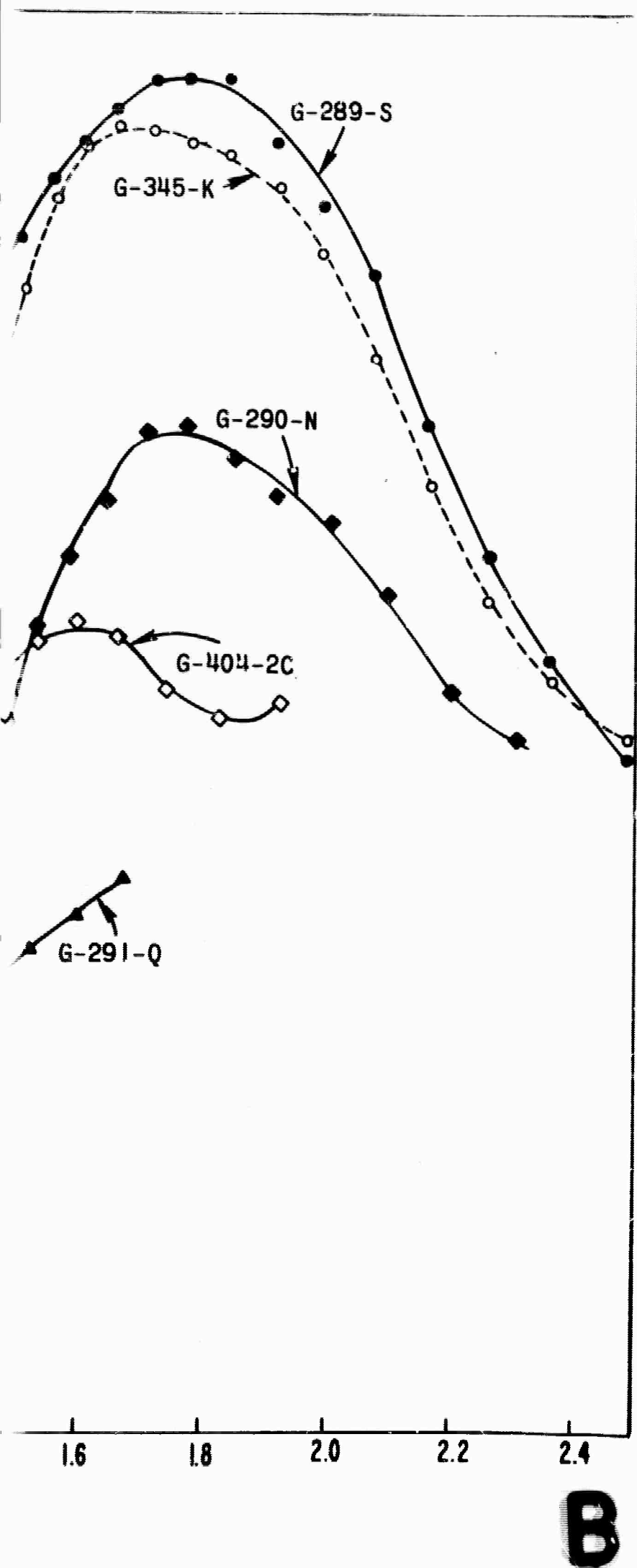
Attenuation (DB) versus $\omega m/\omega$ for various garnet samples.

	$4\pi M_S$	$4\pi M_R$
G-292-R	900	657
G-243-2C	960	718
G-291-Q	1200	793
G-345-K	1780	1197
G-289-S	1780	1200
G-290-N	1650	1280
G-404-2C	1375	994
G-293-R	675	490
G-238-5C	380	305
G-250-4C	200	135

$$\omega m/\omega = \gamma 4\pi M_S/\omega$$

2772B

A
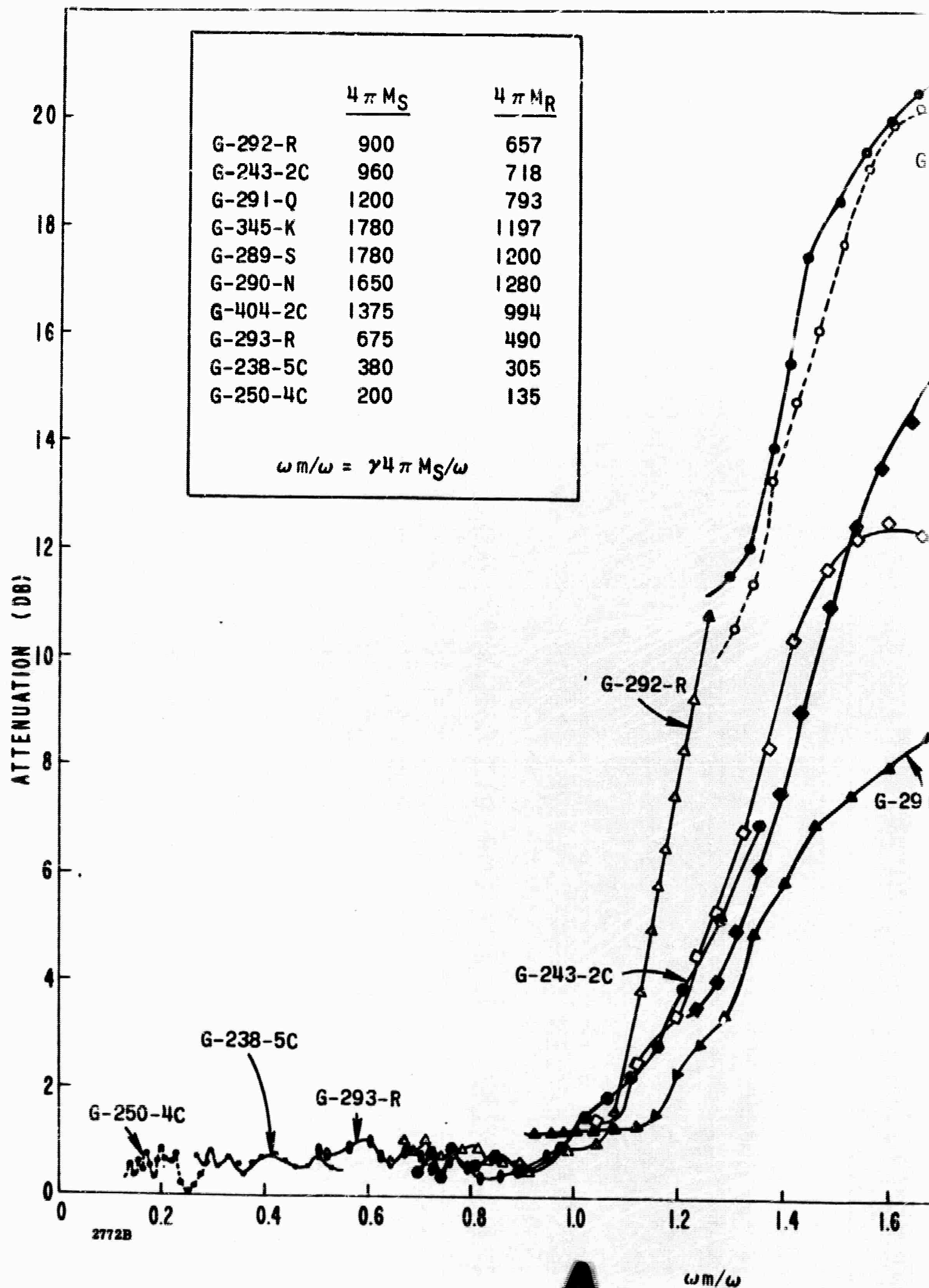
Figure 50. Magnetic Losses of Ten Garnet Materials
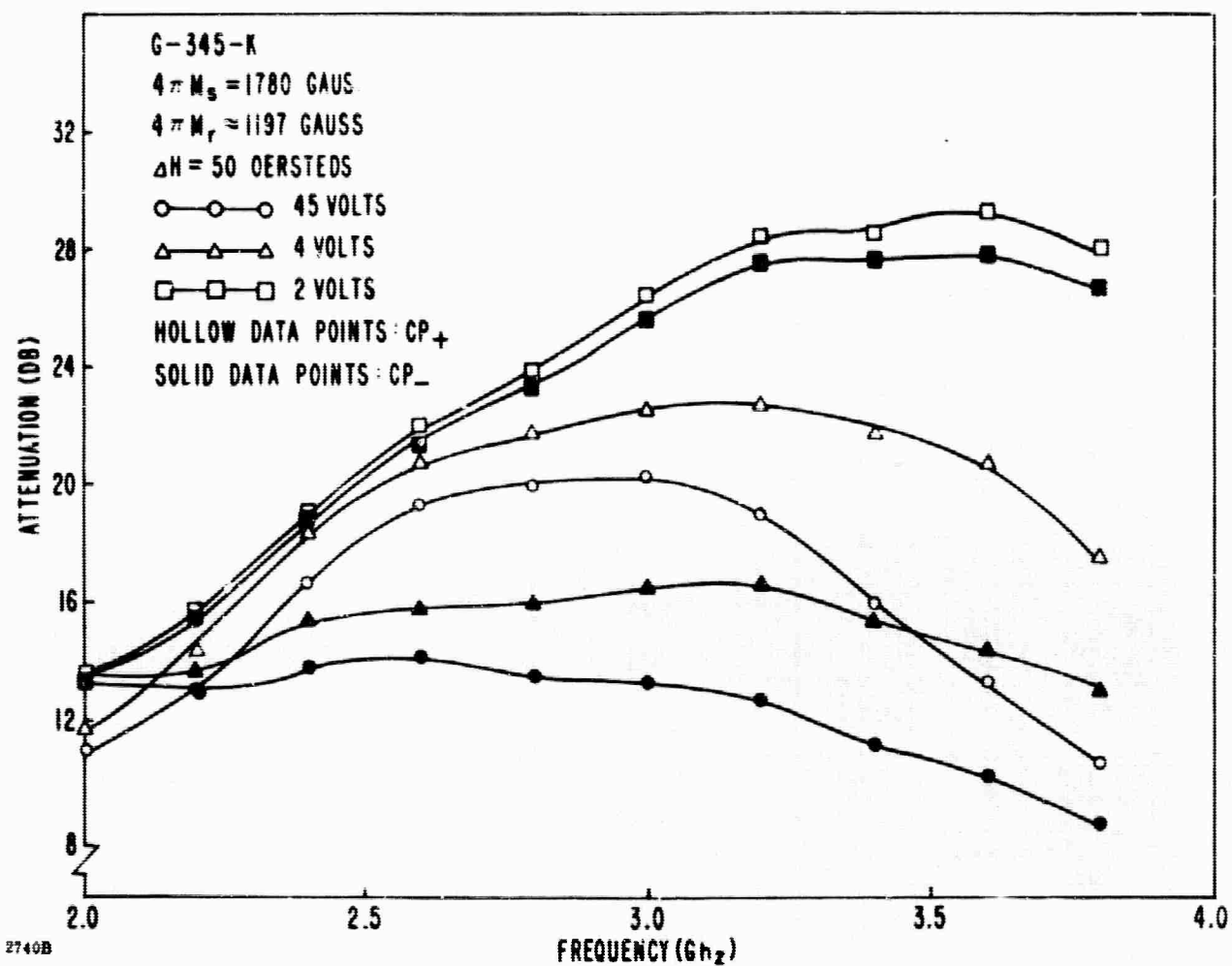
Figure 51. Magnetic Loss Versus Frequency of G-345-K at
3 Different Charging Voltages

2740B
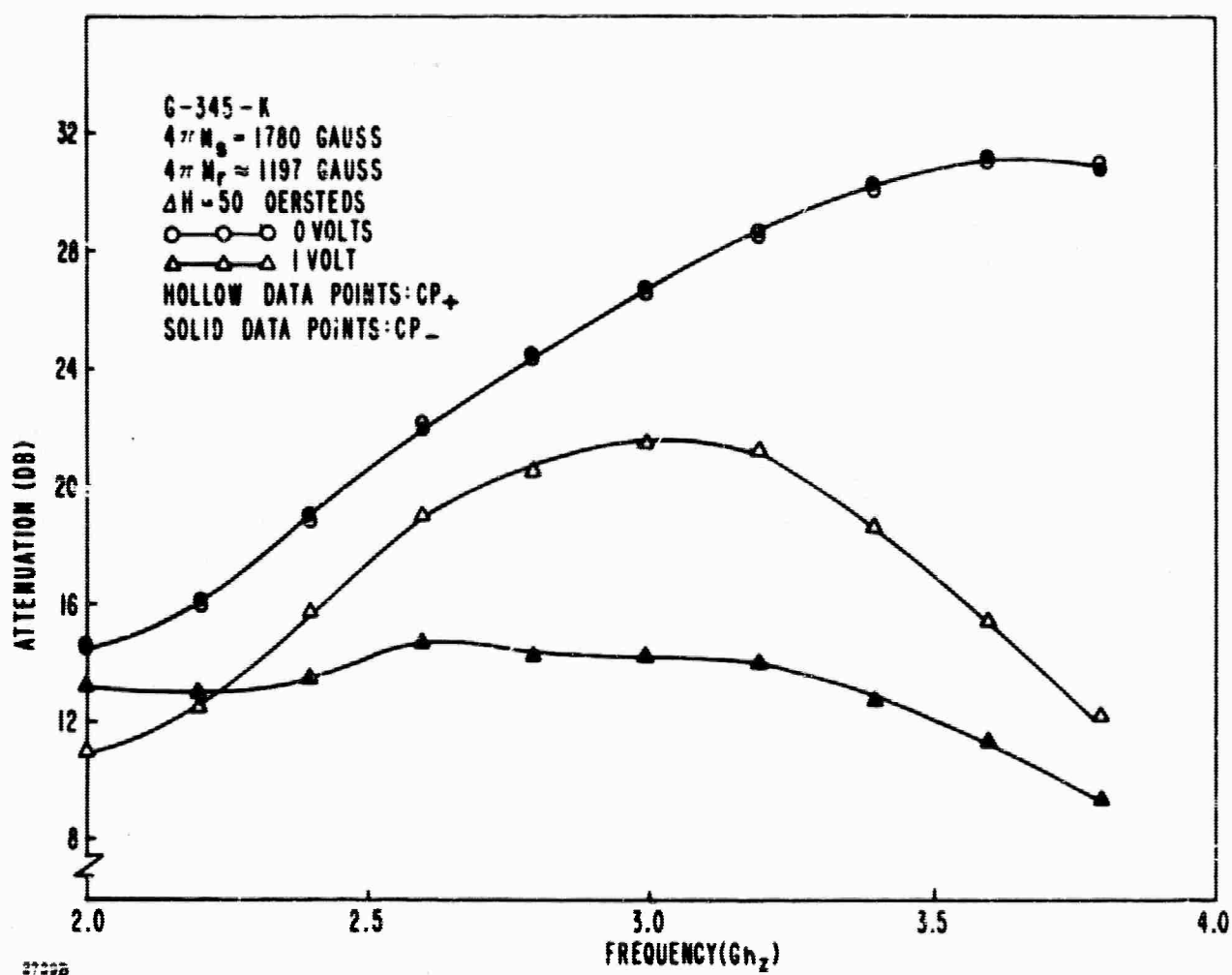
Figure 52. Magnetic Loss Versus Frequency of G-345-K after An-
nealing at 1000°C for 1 Hour. The Curves Apply to
Different Charge Voltage and for Positive (CP+) and
Negative (CP-) Circularly Polarized Waves

4.5 DEVICE CONFIGURATION AND PERFORMANCE

During this reporting period many improvements were made in device performance. These were made possible by the investigations reported in the previous sections. Further improvements are envisioned from these findings.

Figure 53 shows a cross-sectional view of the X-band phase shifter at its present stage of development. The toroid material is G-296 (30% gadolinium substituted YIG) rather than G-286 (2% dysprosium-substituted YIG) as previously used. The geometry of the toroid is smaller (.135" wide x .385" high with a .012" wide slot) and is dielectrically loaded with alumina (Western Gold and Platinum Co's. AL-995). In

addition .050" thick boron nitride heat sinks are shown intimately contacting the active regions of the toroid.
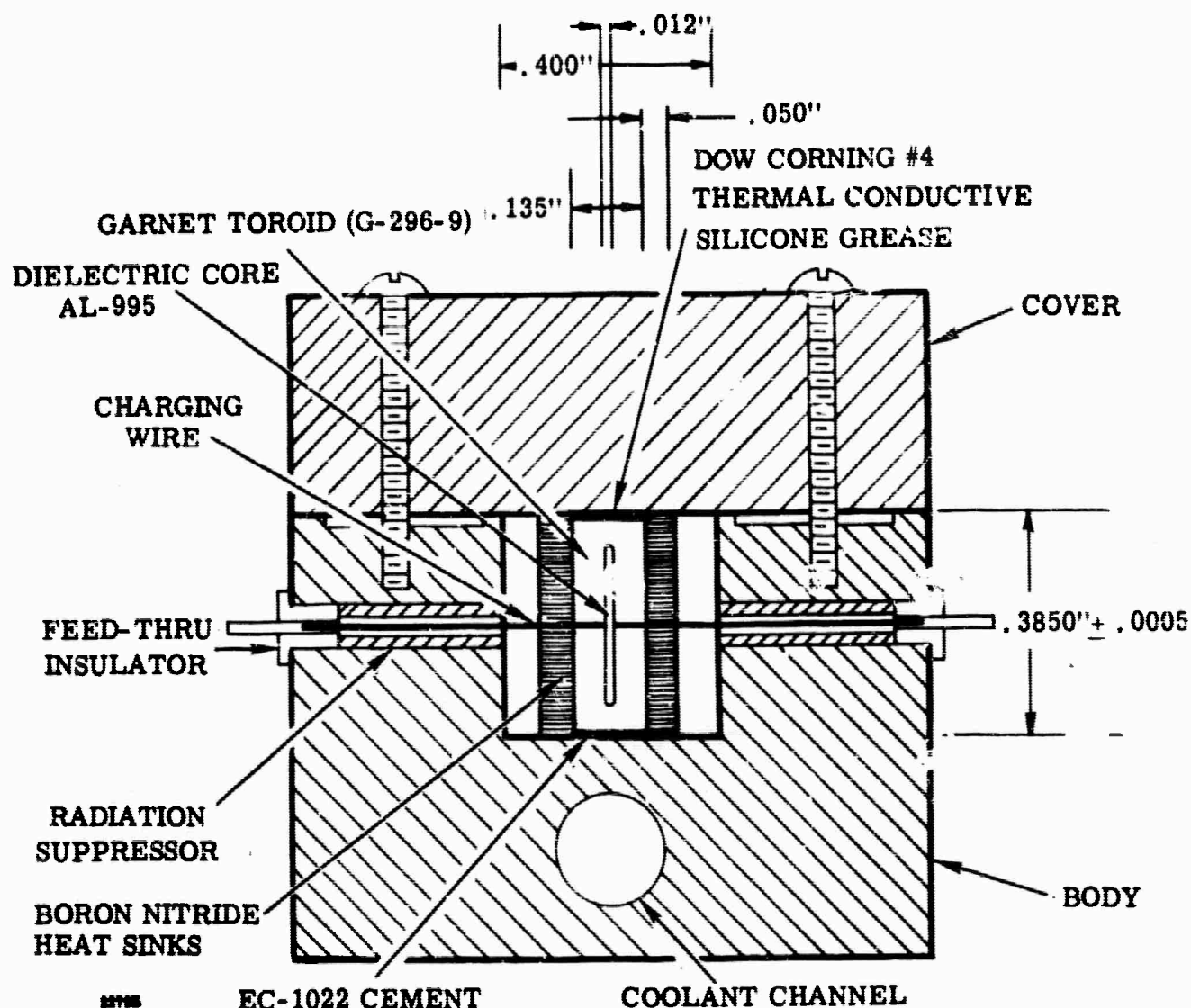

Figure 53. Cross Sectional View of Present X Band Digital Phase Shifter Configuration

The performance of this structure is shown in Figures 54, 55 and 56 where measurements show the phase shift to be flat within 2 percent for all bits, loss is less than 1.25 db and VSWR is less than 1.20. A major improvement can be seen in both these quantities over that previously reported.

The total switching energy for this configuration has been measured to be less than 100 microjoules per event for the 180° bit. The peak power threshold is 30 kilowatts as seen in Figure 56.
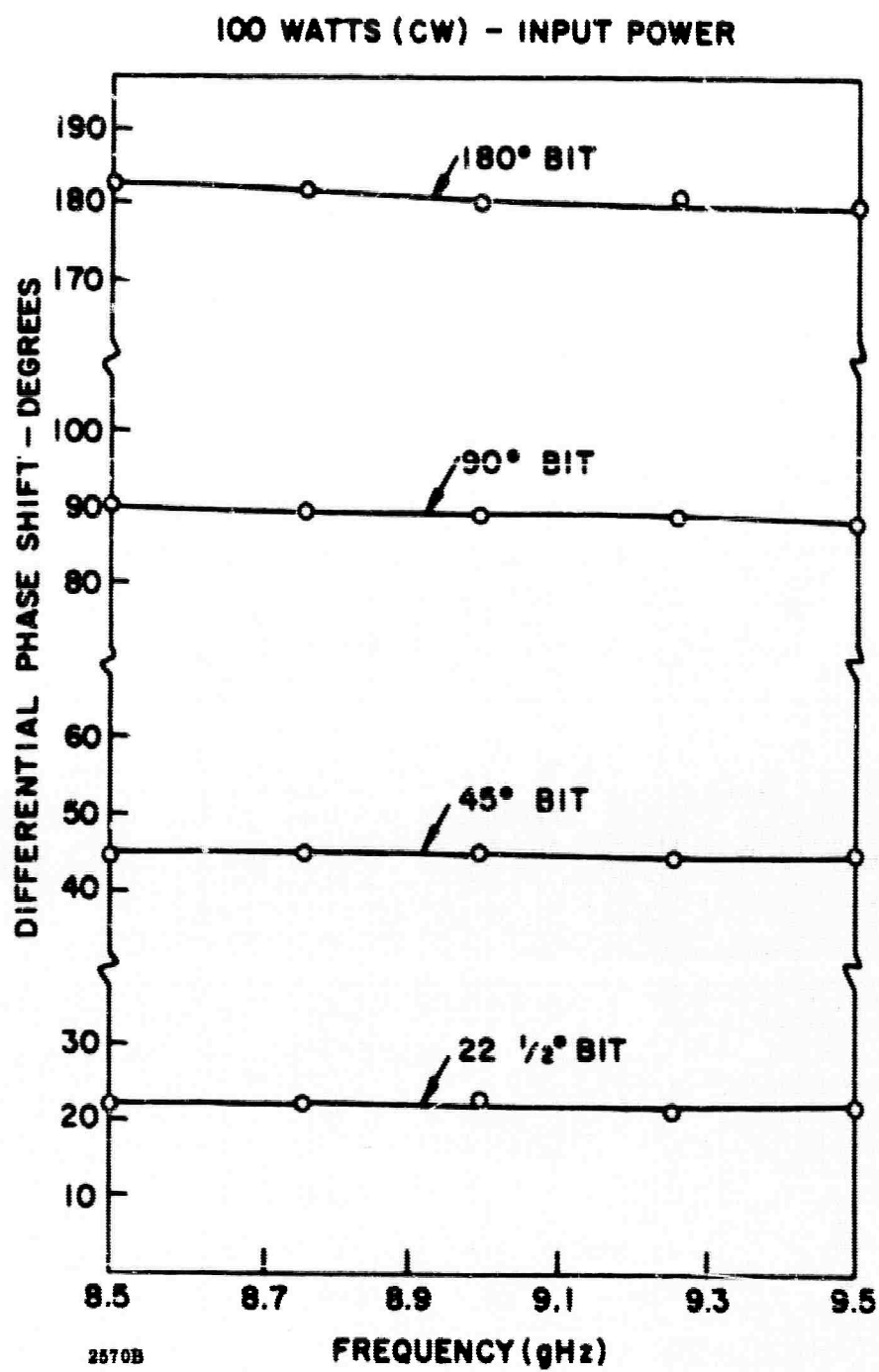
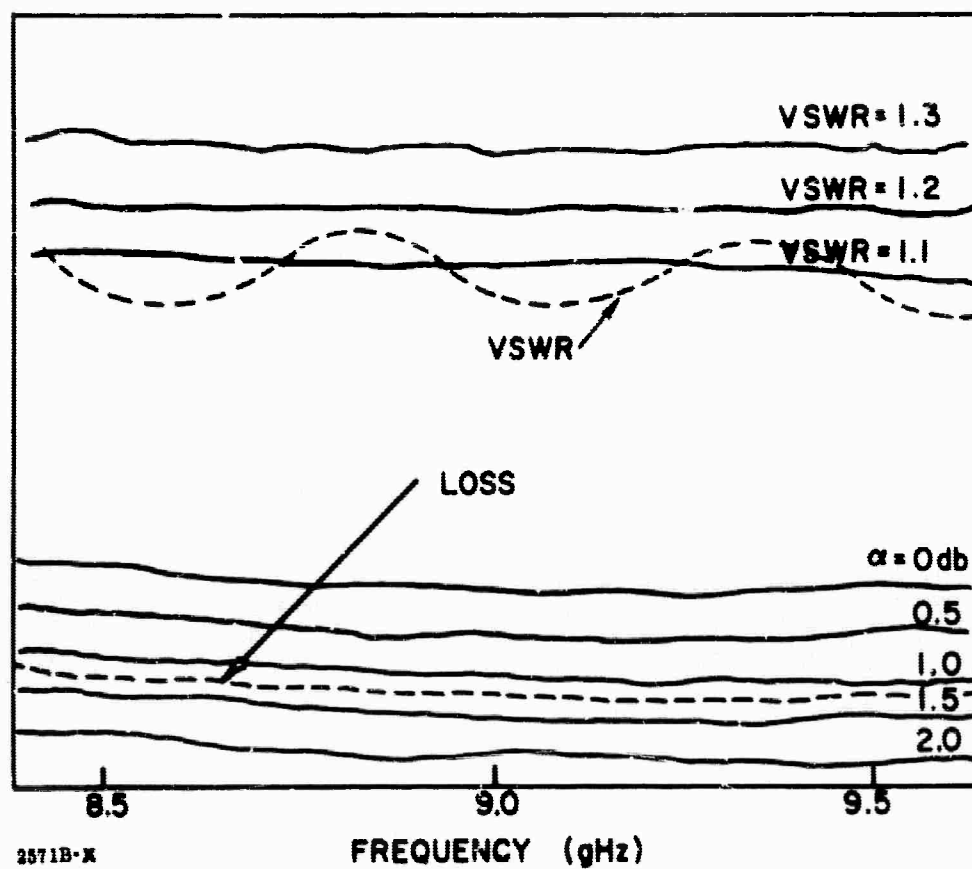Figure 54. Differential Phase Shift of the Configuration Shown in Figure 53

Figure 55. Loss and VSWR of the Digital Phase Shifter Configuration
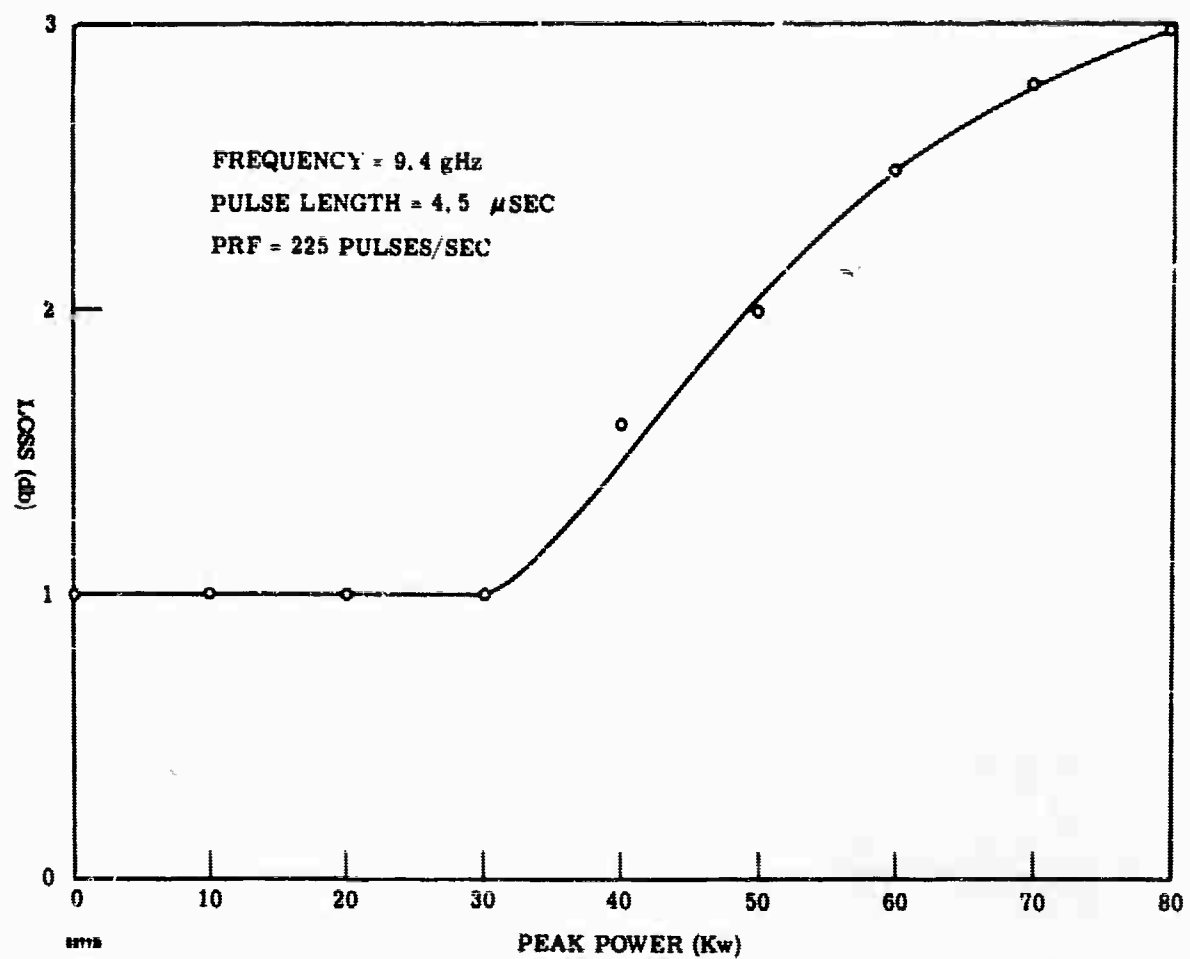Shown in Figure 53

FREQUENCY = 9.4 gHz
PULSE LENGTH = 4.5 μSEC
PRF = 225 PULSES/SEC

Figure 56. Loss Versus Peak Power Level Measurements on the Configuration of Figure 53, Showing a Threshold Power Level of 30 Kw

BLANK PAGE

5. PROGRAM PLANS FOR NEXT SEMIANNUAL PERIOD

The following investigations are planned for the next semiannual period:

1. Additional measurements on the remanent magnetizations of previously studied materials.

2. Study of the temperature stability of the remanent magnetization for selected materials.

3. Continue S-band investigations to obtain information on the influence of linewidth, magnetization anisotropy field, and toroidal shape on magnetic losses.

4. Investigate the possibility of adjusting the toroid geometry so as to reduce the upper frequency limit of magnetic losses for below resonance operation or, conversely, adjust the geometry to raise the resonance frequency to permit above resonance operation.

5. Study the effects of slot size and permittivity on device performance particularly threshold power level and switching energy.

6. Complete the X-band waveguide studies and fabricate the required phase shifters.

7. Select the most promising materials and geometry (based on the S-band studies) for the L-band coaxial r   se shifter and complete the design and test of the phase shifters required.

8. Study the possibility of using the temperature dependence of the coercive force as a method of stabilizing the remanent magnetization with temperature.

9. Investigate the feasibility of operating at a power level well above the threshold power level as an additional method of overcoming high power effects.